FINAL REPORT

on

POINT BEACH NUCLEAR PLANT UNIT NO. 1 PRESSURE VESSEL SURVEILLANCE PROGRAM: EVALUATION OF CAPSULE V

to

WISCONSIN ELECTRIC POWER COMPANY

June 15, 1973

by

J. S. Perrin, J. W. Sheckherd, D. R. Farmelo, and L. M. Lowry

Approved by V. G. Scotti

BATTELLE
Columbus Laboratories
505 King Avenue
Columbus, Ohio 43201

B/1

TABLE OF CONTENTS

POINT BEACH NUCLEAR PLANT UNIT NO. 1 PRESSURE VESSEL SURVEILLANCE PROGRAM: EVALUATION OF CAPSULE V

by

J. S. Perrin, J. W. Sheckherd, D. R. Farmelo, and L. M. Lowry

SUMMARY

The irradiation conditions and the irradiation-induced changes in mechanical properties of the Point Beach Nuclear Plant Unit No. 1 reactor pressure vessel (SA302 Grade B) have been determined from evaluation of specimens contained in surveillance Capsule V. This capsule contained base metal, heat-affected zone metal, and weld metal specimens. The capsule was removed after 1.49 equivalent full-power years of operation. The irradiation temperature did not exceed 590 F, and the capsule obtained a fluence of 3.58×10^{18} nvt (>1 Mev).

The measured changes in nil ductility transition temperature (NDTT) for the three materials were consistent with those observed for other surveillance programs involving similar materials and irradiation conditions. A relatively well defined trend band for change in NDTT with increasing exposure to fast neutrons was determined from the results of this program and those of the other programs. The upper-bound curve of this trend band indicates the projected 32 equivalent full power year (end of life) change in NDTT is in good agreement with the original predicted shift. The yield and ultimate tensile strengths of the materials examined increased as expected. The present investigation shows that the pressure vessel base metal, the weld metal, and the heat-affected zone metal mechanical properties are changing with irradiation in a manner in agreement with the changes expected when the pressure vessel was constructed.

INTRODUCTION

This report presents the results of the examination of Capsule V, the first capsule of the continuing surveillance program for monitoring the effects of neutron irradiation on the SA302 Grade B Point Beach Unit No. 1 reactor pressure-vessel material under actual operating conditions. This report contains experimental procedures, results, and discussion relating to the investigation.

Radiation damage studies initiated during the early days of nuclear power-reactor development revealed the deleterious effects of high energy neutrons upon the notch ductility of reactor vessel steels. The effect was characterized by a rapid rise in the nil ductility transition temperature (NDTT) with increasing neutron exposure. In addition, the tensile properties show a significant loss of uniform elongation and reduction of area with increasing neutron exposure.

Sufficient data on the effects of radiation on the mechanical properties of reactor pressure-vessel steel are now available to indicate the type and relative magnitude of property changes to be encountered during the expected lifetime of the reactor structure. This information is an integral part of the design basis for a nuclear reactor. At the time of startup of the Point Beach Unit No. 1 reactor, the pressure-vessel materials were of sufficient quality to ensure that the expected radiation-induced changes in mechanical properties would permit continued safe operation of the reactor even at the projected end-of-life period of 40 years of operation at an 80 percent load factor (32 equivalent full power years). During this period the reactor operating limitation curves (i.e., pressure and temperature) will be periodically adjusted to incorporate the projected changes in mechanical properties.

To further ensure the continued safe operations of the plant, a reactor-vessel radiation-surveillance program is being conducted. The primary purpose of this program is to evaluate the specific changes in the mechanical properties of the pressure-vessel materials under the actual service conditions (neutron fluence, time, and temperature) of the reactor plant. It is known that the magnitude and relationships of the property changes are functions of the specific material composition and metallurgical condition; the amount, rate, and energy spectrum of the radiation;

and the exposure temperature[1-7]*. The surveillance program is designed to provide information for determining whether the reactor pressure-vessel operating limitations are indeed conservative, as is expected.

The surveillance program for the Point Beach Nuclear Plant Unit No. 1 was designed and recommended by the Westinghouse Electric Corporation and is based on ASTM E 185, "Surveillance Tests on Structural Materials in Nuclear Reactors"[8]. The details of this program and the preirradiation mechanical properties of the materials are presented in Reference (9). Prior to startup, six capsules containing tensile, Charpy V-notch, and WOL fracture-mechanics specimens of the pressure-vessel materials were installed in the reactor. The capsules were located between the thermal shield and the vessel wall. In addition to these mechanical-property test specimens, the capsules contain thermal-monitor and neutron-fluence specimens for evaluation of the specific temperature and radiation exposure conditions of the specimens.

The particular exposure condition variables evaluated are the total integrated fast fluence of the capsule and the maximum temperature encountered by the specimens during the exposure period. The temperature history of the surveillance capsule is fairly representative of that encountered by the pressure-vessel wall. However, the capsule is a finite distance from the reactor pressure-vessel wall and, therefore, the capsule received an accelerated fluence as compared to the vessel wall.

The most essential mechanical properties evaluated by the test specimens in the surveillance capsule are the ductile-to-brittle fracture transition temperature and the conventional tensile-strength and ductility values. In this context, essential refers to those requirements of the current methods for establishing pressure-temperature operating limitations of the reactor pressure vessel and not necessarily the more advanced and/or sophisticated methods for setting safe operating limitations of a structure.

---

*References at end of text.

An essential requirement of the mechanical property measurements is that they be made on representative material. For this surveillance program, the capsules contain test specimens of the SA302 Grade B reactor-vessel steel from two 6-3/4 in. thick shell plates from the vessel intermediate and lower shell courses adjacent to the core region, and also weld metal and heat-affected zone (HAZ) metal. The thermal history of the material used to fabricate test specimens is as identical as possible to that received by the reactor pressure vessel during fabrication, with the exception that the specimen post-weld heat treatment has been simulated. In addition to the reactor materials, test specimens of a specially prepared correlation material (SA302 Grade B) made available by Subcommittee II of ASTM Committee E10 were also contained in the capsule. The data obtained from evaluations of the correlation material provide a valuable link with the surveillance programs of other nuclear-reactor pressure vessels.

An advanced materials-evaluation technique was used during the course of this examination. This advanced technique was instrumentation of the Charpy test to obtain additional data during Charpy testing. The additional information obtained during this testing is presented in Appendix C, "Instrumented Charpy Examination".

BACKGROUND

The purpose of this section is to supply background information on the general features of radiation damage and the current requirements for assessment of the fracture-safe operating criteria for reactor pressure-vessel steel.

The overall effects of fast neutron irradiation on the mechanical properties of low-alloy ferritic pressure-vessel steel are well documented in the literature [1-6]. The minimum integrated fast neutron exposure necessary to produce changes in the mechanical properties of this class of steel is somewhat dependent on the reactor operating temperature. In general, a fluence greater than 10^{17} nvt (>1 Mev) is required for temperatures between 400 and 500 F, and for temperatures greater than 500 F a fluence greater than 10^{18} nvt (>1 Mev) is required to produce a measurable change in mechanical properties. The operating temperature of the Point Beach Unit No. 1 reactor pressure vessel is approximately 550 F, and this temperature is in the range where large exposure times are required to produce measurable mechanical-property changes. The amount of radiation damage is also strongly dependent on minor changes in the chemical composition of these ferritic steels [10,11]. This is very important when comparisons are made between the properties of base metal and weld metal. The chemical composition of the base metal is well controlled and characterized. However, the current industry practice is such that the composition of the heat-affected-zone and weld metal is not as well characterized as the base metal.

Since irradiation increases the yield and tensile strength values (at the expense of a reduction in ductility), the major emphasis in a surveillance program is devoted to considerations of the ductile-to-brittle transition temperature. This property is usually determined by tests with notched specimens impact loaded to fracture using the Charpy V-notch impact test. The general effect of fast neutron irradiation is to produce an increase in this transition temperature. There is considerable documentation of the effects of neutron irradiation on the notch ductility properties of common structural materials [1-7, 12-14].

Investigations at the Naval Research Laboratory are responsible for the development of the widely used nil ductility transition temperature concept for establishing fracture-safe operating limits of ferritic steel structures. The NDTT is a function of the fundamental deformation and fracture properties of the material and is defined by the Drop-Weight Test, as discussed in ASTM E208, "Conducting Drop-Weight Test to Determine Nil-Ductility Transition Temperature of Ferritic Steels"[15]. In this test, the NDTT is defined as the temperature at which the drop-weight specimen is broken in a series of tests in which duplicate no-break refers to the type of specimen fracture where the crack is arrested before traversing the width of the specimen. Therefore, at temperatures above the NDTT the specimens are ductile and at temperatures below the NDTT the specimens are brittle. This NDTT concept was developed by Pellini[16] and has proven a good qualitative tool for avoiding brittle fracture of ferritic steel structures. The NDTT is used as a primary index temperature for the Fracture Analysis Diagram (FAD) interpretive approach to brittle fracture prevention on which the "NDTT +60F" criterion is based[16].

The standard drop-weight test specimen is prohibitively large for inclusion in most radiation-surveillance programs. The Charpy V-notch specimen is relatively small and widely used; therefore, it has been adopted as a primary specimen for radiation-surveillance studies. To be consistent with the concepts required for the FAD, a Charpy correlation energy or "fix" is normally determined for a particular steel to index the NDTT. For the SA302 Grade B steel the "fix" temperature which corresponds to the NDTT is that at which a correlation energy of 30 ft-lb occurs for the standard Charpy V-notch impact test[9]. When referring to an NDTT measured by Charpy V-notch test techniques, it is understood that this implies a prior knowledge of the correlation energy.

Fracture orientation is another concept that should be considered when assessing the fracture-safe operating criteria for a reactor pressure vessel from the results of surveillance-specimen evaluations. There are weak and strong fracture directions in most ferritic materials. In this context, direction refers to the plane and path of the crack. The transition energy curves for these two directions will have different upper-shelf energy values,

with that for the weak direction being the lower. At the 30 ft-lb fix temperature it is difficult to discriminate between different fracture directions. Therefore, the interest in difference in fracture directions is directed toward considerations of the upper-shelf energy values.

The reactor environment may alter the pressure-vessel material properties to a condition where NDTT concepts of fracture-safe operation no longer apply, by causing the upper shelf energy to drop to a sufficiently low value. This type of behavior is known as low-energy tear fracture, where only a relatively small amount of energy (i.e., usually comparable to that associated with brittle low-temperature fractures) is required for extensive propagation of a ductile fracture. This behavior is typical of some high-strength steels, and the radiation damage caused by the reactor environment can be regarded as promoting a strength transition of fracture properties.

The point at which NDTT concepts no longer apply is not well defined. However, some investigators[17] identify this point as that where the upper-shelf energy is equal to or less than 50 ft lb for a transition temperature curve determined by Charpy impact tests. In addition to a shifting of the transition energy curve upward in temperature, radiation damage decreases the difference between the upper and lower shelves by essentially lowering the upper-shelf energy.

The reactor pressure vessel under consideration was designed and fabricated so that the operating stresses imposed upon the weak direction of the material are lower than those for the strong direction. In addition, the design is such that vessel penetrations having complex stress states are not subjected to radiation levels which would appreciably alter the material properties.

In addition to the transition temperature approach, there is the fracture-mechanics approach to studying the problem of brittle material failure[18]. The fracture-mechanics approach relates the stress field at the tip of a crack to the requirements for brittle fracture. Here, the conditions for brittle fracture are defined from knowledge of the stress at the crack tip caused by stress on the bulk structure, the resistance of the material to crack propagation, and the size and severity of a defect capable of initiating fracture.

The stress field in the material near the crack tip is defined by a single parameter known as the stress intensity factor K. This parameter is a function of the geometry of the bulk structure, the geometry and location of the crack, and the distribution and magnitude of external loads on the bulk structure. Therefore, if a component is designed so that the geometries of the structure and defect are known, the stress intensity at the crack tip can be obtained from the applied stress and the size of the defect. The value of K has been determined for many practical laboratory configurations. The wedge open loading or WOL specimen design used in this work has been evaluated to the point where the relation between applied load and stress intensity is well defined.

The brittle fracture of a material occurs when the magnitude of the stresses at the crack tip exceeds some critical value. When the material is loaded in tension with the flaw perpendicular to the direction of the load and there is limited local plasticity, then this critical value of K is the plane-strain fracture toughness, K_{Ic}. The value of K_{Ic} at a particular load rate and temperature can be considered an intrinsic material property which is a measure of the resistance of a material to brittle failure in the presence of a stressed crack.

The value of K_{Ic} for a material is affected by metallurgical and mechanical variables. In addition to the effects of load rate and temperature, previously mentioned, the measurement of K_{Ic} is hindered by the effects of specimen size. The condition of plane strain is essential, for the assumptions of elastic behavior are inherent in the fracture-mechanics approach. If there is a great deal of local plastic deformation around the crack, the measured critical value of K is not one of plane strain and therefore it is not a valid K_{Ic} measurement. There is a maximum plastic-zone size that can be tolerated without affecting the validity of the measured value of K_{Ic}. For the specimen geometry used in this work, the plastic-zone size can be calculated from the measured value of K_{Ic} and yield strength. The thickness (B) of the WOL specimen used must be $\geq 2.5\ (K_{Ic}/\sigma_{ys})^2$, where σ_{ys} is the yield stress. This is termed the ASTM validity criterion for WOL fracture-toughness specimens[19].

From a consideration of this criterion it can be seen that once a specimen size is determined (fixing B) the test temperature alone will determine whether a valid K_{Ic} can be measured. Thus, the results must be anticipated before the test temperature is selected, and the yield strength must be known as a function of temperature.

It can be seen from the validity requirements that evaluation of materials having high K_{Ic} values and low yield strengths requires very thick specimens. When the use of large specimens is not practical, the test temperature must be decreased so that an adequate reduction in K_{Ic} and attendant increase in yield strength will permit satisfaction of the validity requirements.

CAPSULE RECOVERY AND DISASSEMBLY

Battelle's Columbus Laboratories (BCL) personnel went to the Point Beach Nuclear Plant Unit No. 1 to pick up the surveillance capsule assembly. They brought a pool-side jib crane, a specialized underwater cutting tool, and a shipping cask. The cutting head of the underwater cutting tool is a mild steel casting. The head had been sand blasted, copper plated, and then nickel plated to prevent it from rusting and thereby contaminating the pool water. To further avoid contamination, pool water was used in the line leading from the pump intensifier unit to the cutting head. The specialized underwater cutting tool is shown in Figure 1. The tool is shown positioned on top of the shipping cask in Figure 2.

The capsule assembly had an overall length of 131 inches. Point Beach personnel removed the capsule assembly from the pressure vessel and transferred it underwater in a canal to the spent fuel pool. The upper lid and lower drain lid were removed from the shipping cask. Using an overhead crane, the cask was then raised from the receiving area, moved to a position over the spent fuel pool, and lowered into the pool so that the bottom end of the cask was resting on the floor of the pool. The bridge crane was then used to position the capsule and attached lead tube such that the capsule was in the cask except for the lead tube and about six inches of the capsule.

The cutting tool was lowered into the pool using a stainless steel cable attached to the pool-side jib crane. The cutter was guided into position using the stainless steel pipe line leading to the cutting head. Binoculars were used to determine the position of the cutting head. The lead tube was separated from the capsule assembly by making a cut about 2 inches above the top end of the capsule. The lead tube was placed into the cask along side the capsule.

The cask was raised from the pool and its exterior was thoroughly rinsed with water. The water inside the cask was allowed to drain into the pool. The overhead crane was then used to lower the cask to the decontamination area. The cask was decontaminated to the level of removable

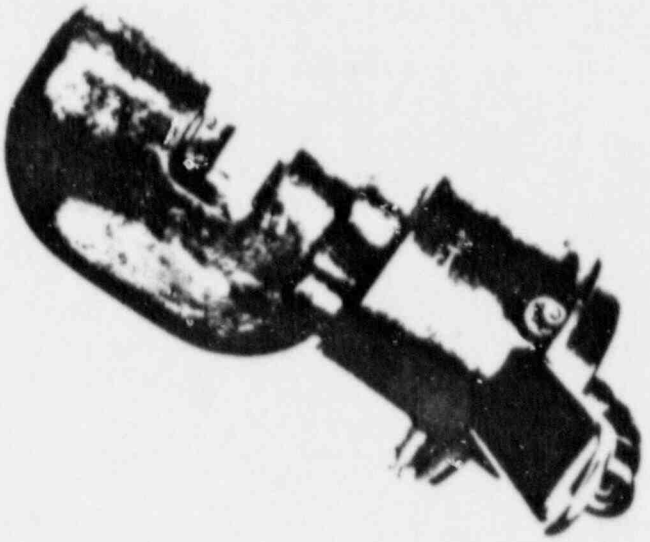

TE02016

FIGURE 1. SPECIALIZED UNDERWATER CUTTING TOOL. This tool is used to cut the capsule lead tube to separate it from the capsule.

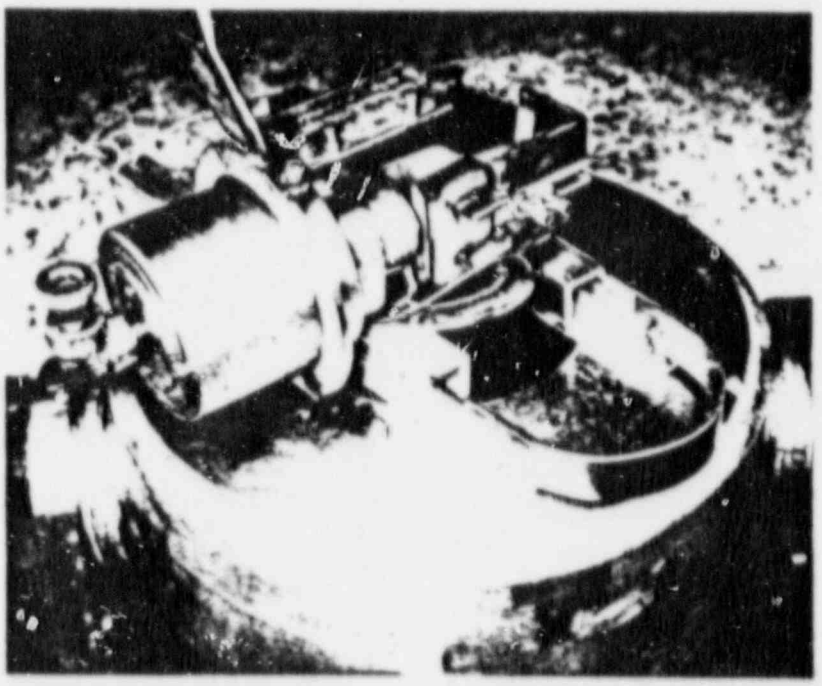

TE01916

FIGURE 2. CUTTING TOOL PLACED ON TOP OF SHIPPING CASK

contamination required for shipping, 2200 disintegrations/100 cm^2/min $\beta\gamma$ and 220 disintegrations/100 cm^2/min α. The cask was then shipped to the BCL Hot Laboratory Facility by commercial carrier.

Upon arrival at BCL, the cask was placed in a hot cell. The capsule and lead tube sections were then removed from the cask. The capsule was examined to confirm the cut separating the lead tube from the capsule was in the lead tube, thereby maintaining the water-tight integrity of the capsule. Visual examination showed the capsule to be a dark gray color. The capsule had a slight bow, but subsequent examination showed that the bowing had not damaged the specimens in the capsule.

The specimens were removed from the capsule and inventoried. The appearance of the specimens was a dark gray color. Before testing, the mechanical property specimens were cleaned in the following manner: washed in Chlorothene, washed in Radiacwash and distilled water, rinsed twice in distilled water, and rinsed in reagent grade alcohol.

SAMPLE PREPARATION

Pressure Vessel Material

Babcock and Wilcox supplied the SA302 Grade B reactor pressure vessel material from plates C1423 and A9811. These two plates were used in the lower and intermediate shell courses of the vessel. Babcock and Wilcox also supplied a weldment which joined the two shell plates. Appendix A contains the chemical analyses and thermal treatment history of the plate materials.

material from each shell plate was heat-treated with the shells. All test specimens were machined from the 1/4 thickness location of the plate after performing a simulated stress-relieving treatment. The test specimens represent material taken at least one plate thickness (6-3/4 inches) from the quenched edges of the plate. Specimens were machined from weld and heat-affected zone metal from a stress-relieved weldment joining the two shell plate materials. All heat-affected zone specimens were obtained from the weld-heat-affected zone of plate A9811.

The axis of the notch of the Charpy V-notch impact specimens was machined perpendicular to the major surfaces of the plate. The longitudinal axis of the impact specimens was parallel to the rolling direction of the plate. All tensile specimens were machined with the longitudinal axis of the specimen parallel to the rolling direction of the plate. All WOL test specimens were machined with the simulated crack in the specimen perpendicular to the rolling direction and the major surfaces of the plate.

Correlation Monitor Material

The SA302 Grade B material for the correlation monitors was supplied by the U.S. Steel Corporation from 6-inch-thick plate. Appendix B contains the chemical analyses and thermal treatment history of the correlation monitor materials.

EXPERIMENTAL PROCEDURES

This section describes the procedures employed in the testing of the impact, tensile, and WOL specimens. Also included are the procedures used to examine the dosimeters and thermal monitors. All testing and evaluations were performed at Battelle's Columbus Laboratories.

Dosimeter and Thermal Monitor Examination

The capsule contained two kinds of low-melting-point eutectic alloy thermal monitor wires for determination of the maximum temperature attained by the test specimens during irradiation. These thermal-monitor wires were sealed in Pyrex tubes and inserted in spacers in the capsule. During capsule disassembly the thermal monitor wires were removed from the spacers and Pyrex tubes for visual examination.

The capsule contained dosimeters of copper, nickel, cadmium-shielded aluminum-cobalt alloy, unshielded aluminum-cobalt alloy, neptunium 237 and uranium 238. In addition, the mechanical test specimens provided material for iron dosimeters. The reactions used for the dosimetry calculations were as follows:

Iron:	$^{54}Fe\ (n,p)\ ^{54}Mn$
Nickel:	$^{58}Ni\ (n,p)\ ^{58}Co$
Copper:	$^{63}Cu\ (n,\alpha)\ ^{60}Co$
Cobalt:	$^{59}Co\ (n,\gamma)\ ^{60}Co$
Uranium:	$^{238}U\ (n,f)\ ^{137}Cs$
Neptunium:	$^{237}Np\ (n,f)\ ^{137}Cs$

All dosimeter samples were analyzed except two. One bare cobalt wire was not recovered during capsule disassembly, and one cadmium-shielded cobalt wire was not analyzed due to difficulty in removing the wire from the cadmium shield.

After removal from the capsule, the individual samples were placed in vials for transfer to the radiochemistry laboratory. Radiation readings at 1 meter and on contact were recorded. The nickel, copper, and cobalt wires were decontaminated by wiping with dilute acid, distilled water, and reagent grade acetone. The iron samples, and ^{238}U and ^{237}Np capsules were wiped with dilute acid and distilled water to remove major contamination and then cleaned ultrasonically in a solution of Radiac and water.

The pure copper wires were weighed to ±0.0001 g, and the activation product (^{60}Co) intensity was determined directly by gamma ray spectrometry without dissolving the samples. The iron, nickel, and cobalt (Al-0.15 percent Co) samples were weighed, dissolved in a solution of HCl and HNO_3, diluted to appropriate volumes, and 1 ml samples were taken for gamma counting.

^{238}U and ^{237}Np capsules were opened in an alpha radiation containment box by specially prepared tools used to grip the small 1/4 in. diameter x 3/8 in. long cylinders and cut off the tops. The tool used for cutting off the tops was a modified tubing cutter. The ^{238}U and ^{237}Np were present in the form of oxide powders. The two samples were poured into small tared primary containment vials and then into clean tared secondary vials for weighing to ±0.0001 g on an analytical balance. They were dissolved in 8M HNO_3 (U_3O_8) and 8M H_2SO_4-0.1M $NaBrO_3$ (NpO_2), and diluted to appropriate volumes. ^{137}Cs analyses were performed in duplicate after purification by the chloroplatinate method. For assurance of complete fission product decontamination, Zr and Ru holdback carriers were employed, and an extra scavenge precipitation step was performed.

All the activation products were analyzed by gamma-ray spectrometry utilizing a 3 in. diameter x 3 in. long NaI (Tl) scintillation crystal detector and model ST 400 K Tullamore transistorized 400 channel analyzer (Victoreen Instrument Co.) capable of 8.5 percent resolution FWHM (full width half maximum) at the 0.663 Mev ^{137}Cs-^{137m}Ba gamma ray energy level. The ^{60}Co and ^{137}Cs samples were counted directly against NBS standards. The ^{54}Mn and ^{58}Co activities were obtained from comparison with theoretical efficiency curves prepared from NBS standards.

The procedures used in the evaluation of the dosimetry samples followed the appropriate ASTM recommendations[20-26].

Impact Tests

The impact tests were performed on a standard Wiedemann-Baldwin testing machine in accordance with the recommendations of the pertinent ASTM standard[27]. The accuracy of the machine was verified on November 23, 1972 with standards purchased from the U.S. Army Materials Research Agency. The results are given in Table 1.

TABLE 1. CALIBRATION DATA FOR THE BCL HOT LABORATORY CHARPY IMPACT MACHINE TESTED ON NOVEMBER 23, 1972

Group	Average BCL Energy, ft-lb	Standard Energy[a] ft-lb	Variation	
			Actual	Allowed
Low Energy	13.0	12.8	+0.2 ft-lb	±1.0 ft-lb
Medium Energy	41.7	42.6	-2.1 percent	±5.0 percent
High Energy	68.1	69.4	-1.9 percent	±5.0 percent

(a) Established by U.S. Army Materials and Mechanics Research Center

The design for the specimens used for all impact tests is shown in Figure 3. ASTM test procedures for specimen temperature control were utilized. The low temperature bath consisted of agitated methyl alcohol cooled with additions of liquid nitrogen. The container was a Dewar flask which contained a grid to keep the specimens at least 1 in. from the bottom. The height of the bath was enough to keep a minimum of 1 in. of liquid over the specimens. The Charpy specimens were held at temperature for a minimum of at least the ASTM recommended time.

The tests above room temperature were conducted in a similar manner except that a metal container with a liquid bath was used. The bath used for temperatures from 70 to 212 F was water, and the bath used for temperatures above 212 F was oil. The baths were heated to temperature using a hot plate.

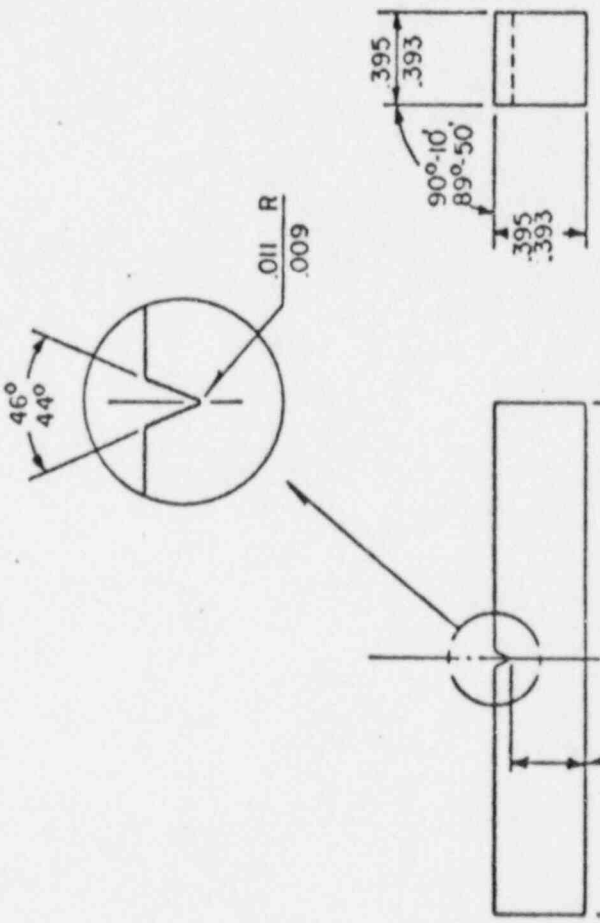

63/ ALL OVER UNLESS OTHERWISE SPECIFIED

FIGURE 3. CHARPY V-NOTCH IMPACT SPECIMEN

The specimens were manually transferred from the temperature bath to the anvil of the impact machine by means of tongs that had also been brought to temperature in the bath. The specimens were removed from the bath and impacted in less than 5 sec. The energy required to break the specimens was recorded and plotted as a function of test temperature as the testing proceeded. Selection of the test temperatures was based primarily on finding the temperature corresponding to a specimen absorbed energy of 30 ft-lb. The correlation between Charpy V-notch test results and the nil ductility transition temperature (NDTT)* for SA302 Grade B steel has been shown to be 30 ft-lb[9].

Lateral expansion was determined from measurements made with a vernier caliper. Fracture appearance was estimated from observation of the fracture surface, and comparing the appearance of the specimen to an ASTM fracture appearance chart[28].

The capsule contained a total of 48 Charpy V-notch specimens. Base metal specimens were from plates C1423 and A9811, which were used in the lower and intermediate shell courses of the vessel. Heat-affected zone and weld metal specimens were from a weldment which joined the two shell plates. Correlation monitor Charpy specimens were from material furnished by the U.S. Steel Corporation through Subcommittee II of ASTM Committee E10 on Radioisotopes and Radiation Effects.

*The NDTT is defined by the drop weight test and is described in ASTM E208-69[16].

Tensile Tests

The design of the tensile specimens is shown in Figure 4; the gage section has a nominal 0.250-in. diameter and a nominal 1.000-in. length. The tensile tests were conducted on a screw-driven Instron testing machine having a 20,000-lb capacity. A crosshead speed of 0.02 in. per min was used. The deformation of the specimen was measured using a strain gage extensometer. The strain gage unit senses the differential movement of two extensometer extension arms attached to the specimen gage length 1 in. apart. The extension arms are required for thermal protection of the strain gage unit during the elevated temperature tests. Figure 5 shows the extensometer extension arms and strain gage assembly used for tensile testing. A tensile specimen is shown at the top of the figure next to the region of the extension arms where the specimen is loaded for testing. The strain gage unit is shown at the bottom of the figure next to the region of the extensometer arms where the unit is attached during testing. The extensometer was calibrated before testing using an Instron high-magnification drum-type extensometer calibrator.

Elevated temperature tensile tests were conducted using a three-zone split furnace. An unirradiated tensile specimen with several thermocouples directly attached to the gage section was used to determine the optimum power input to each furnace zone before testing irradiated specimens. The irradiated tensile specimens were tested at 550 F. The specimens were held at temperature before testing to stabilize the temperature. Temperature was monitored using a Chromel-Alumel thermocouple in direct contact with the gage section of the specimen. Temperature was controlled within ±3 F.

Low temperature tests were made using a liquid nitrogen spray cryostat. The cryostat was of a split clamshell type. Liquid-nitrogen vapor was used to cool the specimen and the containment chambers. The liquid nitrogen flow rate was adjusted by means of a valve in the gas line, which allowed the specimen temperature to be closely controlled during testing. Tests were run at -180 F and -110 F, with temperature controlled within ±2 F during testing. Temperature was measured using a copper-constantan thermocouple in contact with the specimen gage section.

The load-extension data were recorded on the testing machine strip chart. The yield strength, ultimate tensile strength, and total elongation were determined from these charts. The reduction in area was determined from specimen measurements made using a vernier caliper.

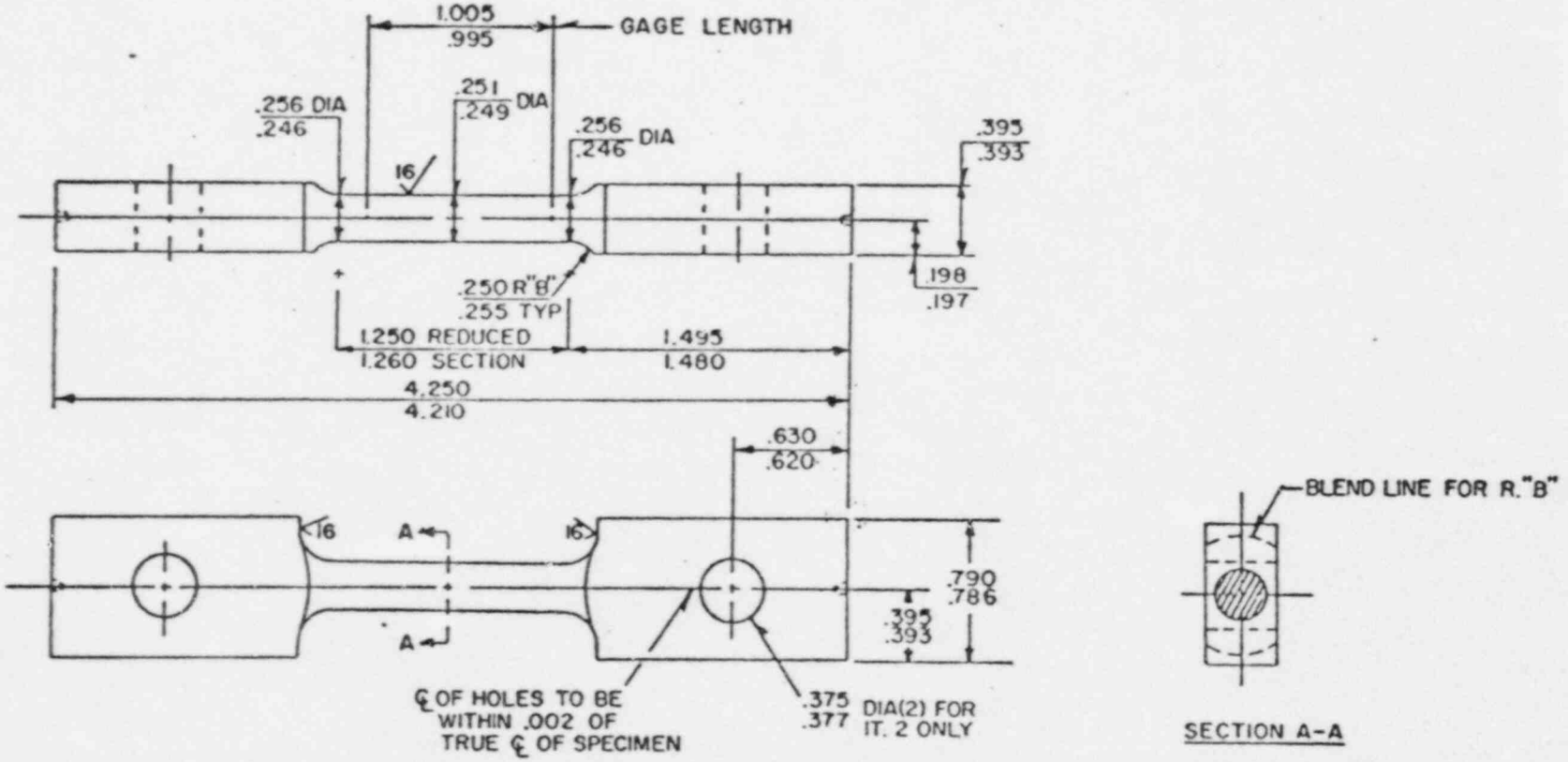

NOTES:
1-LATHE CENTERS REQUIRED.
2-125/ ALL OVER UNLESS OTHERWISE SPECIFIED.

FIGURE 4. TENSILE SPECIMEN

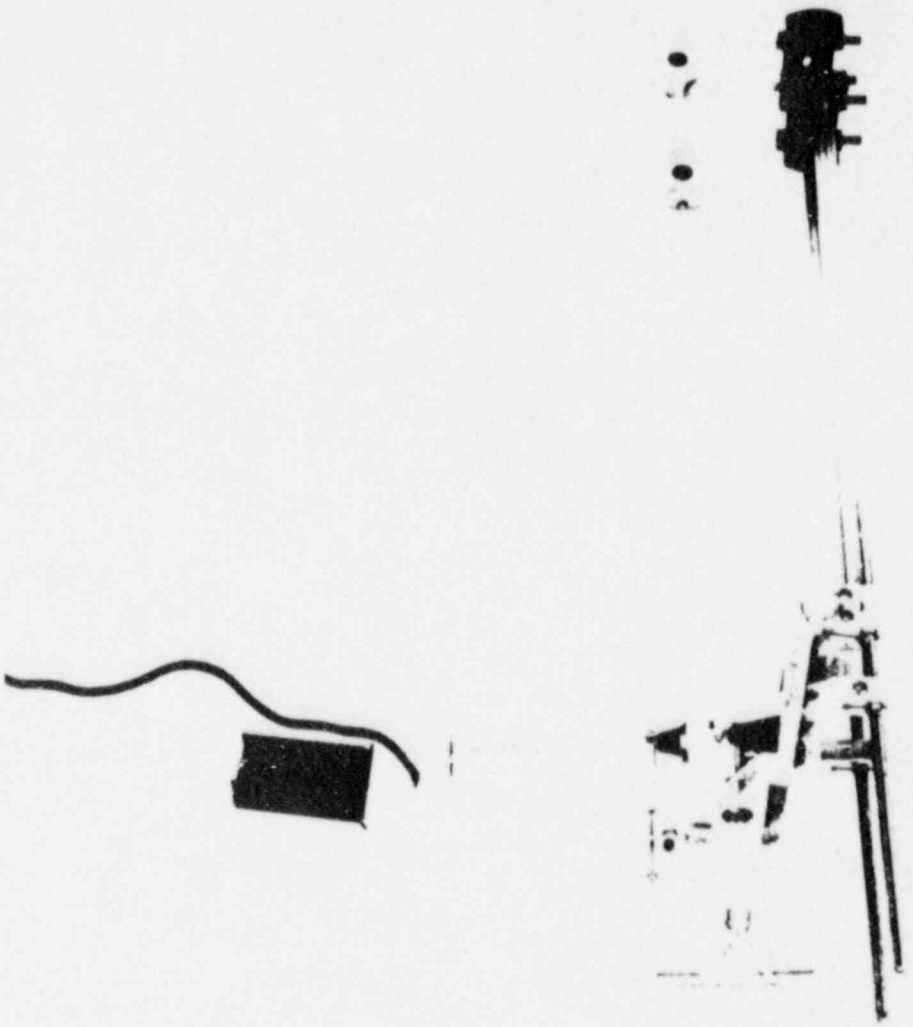

P4973

FIGURE 5. EXTENSOMETER EXTENSION ARMS AND STRAIN GAGE ASSEMBLY USED FOR TENSILE TESTING

Fracture Toughness Tests

The WOL specimens were tested according to the recommendations of ASTM E399, "Plane-Strain Fracture Toughness of Metallic Materials".[19] The procedures for testing the WOL type of fracture specimen are similar to those employed for conventional tensile specimens. The specimen, pulled in tension, is equipped with an extensometer device (COD gage). The COD gage is attached to two positions on the end of the specimen, such that the two arms span the crack notch. The resultant load-displacement record obtained during the test is then used to confirm that the specimen behaves elastically until unstable fracture occurs. The WOL specimen design is shown in Figure 6. As can be seen in the figure, a notch is machined into the specimen. After final machining and before irradiation, a crack was introduced into the specimen extending from the base of this notch. This precracking was done by fatigue loading the specimen in tension, which normally produces a "sharp crack" condition at the tip of the fatigue crack. The test parameters used to calculate the plain-strain fracture toughness K_{Ic} are load at unstable fracture, initial crack size, and the specimen dimensions. The equations employed in this type of K_{Ic} calculation and the procedural requirements are discussed in Reference (19).

An essential part of the testing procedure is the selection of a test temperature that will be likely to permit the occurrence of unstable fracture before gross yielding of the specimen. The latter is essentially controlled by the relationship of K_{Ic} to yield strength. The temperatures required for evaluation of K_{Ic} values for these irradiated specimens are substantially below room temperature and therefore a cryostat was employed. This device is used in much the same manner as the furnace is used in elevated-temperature tensile tests. The cryostat was of the split clamshell type; liquid-nitrogen vapor was used to cool the specimen and containment chamber. The liquid-nitrogen flow rate was adjusted by means of a valve in the gas line. In this manner the nitrogen flow rate and therefore temperature was controlled very accurately during testing. The temperature drift during testing was ±2 F of the test temperature. The COD gage and recorder were calibrated before

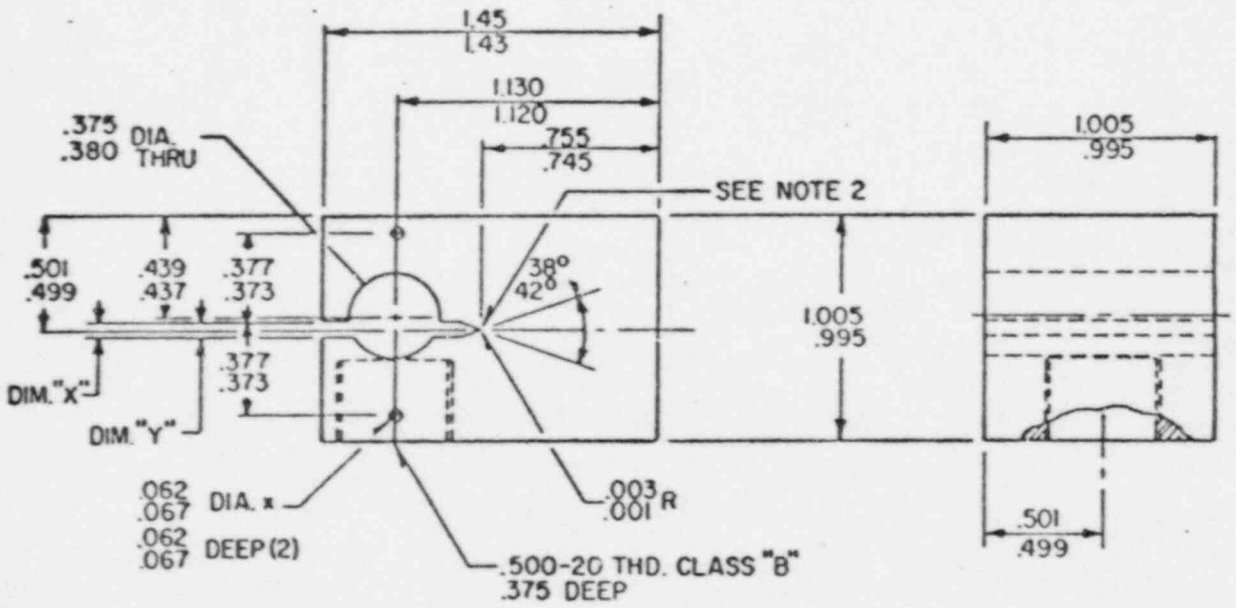

NOTES:

1. $\sqrt{32}$ ALL OVER
2. NOTCH DEPTH TO BE EXTENDED BY FATIGUE CRACKING

ITEM	DIM."X"	DIM."Y"
1	.0463 .0473	.0231 .0236
2	.0620 .0630	.0310 .0315

FIGURE 6. WEDGE OPEN LOADING SPECIMEN

testing with a knife-edge micrometer. All tests were conducted in an Instron run at a crosshead speed of 0.06 in. per min. The WOL specimen, pull rods, clip gage, and open cryostat are shown in Figure 7. Figure 8 shows a closeup view of the WOL specimen with attached clip gage.

In addition to the temperature measurements taken during each test, continuous load-time and load-displacement curves were recorded.

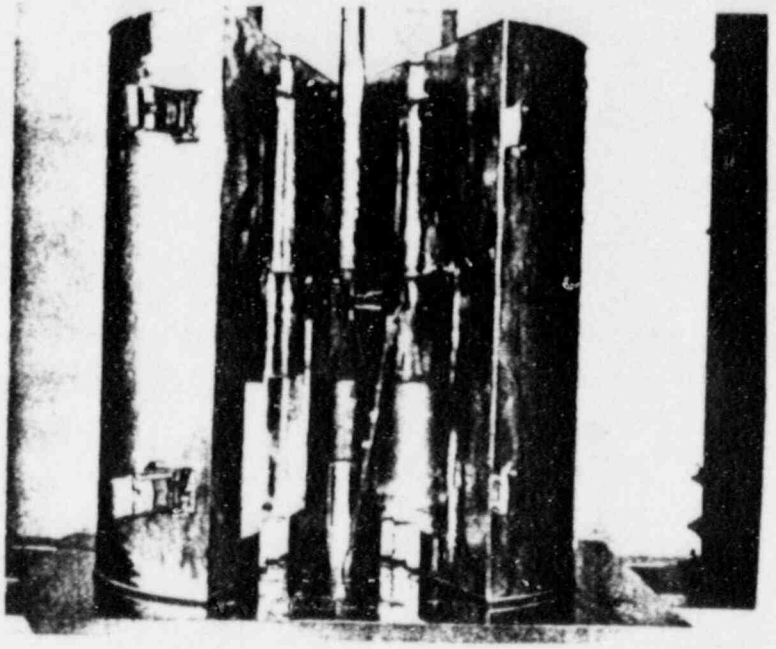

P4879A

FIGURE 7. OPEN CRYOSTAT SHOWING WOL SPECIMEN WITH ATTACHED CLIP GAGE

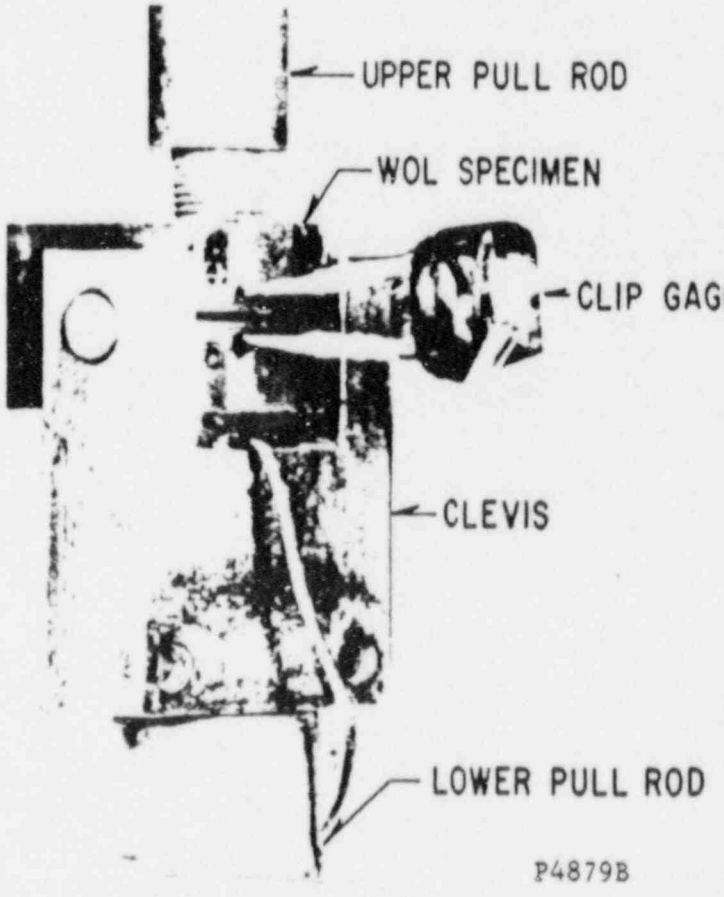

P4879B

FIGURE 8. CLOSEUP VIEW OF WOL SPECIMEN AND CLIP GAGE

RESULTS AND DISCUSSION

Dosimeter and Thermal Monitor Examination

The capsule contained three 579 F (2.5 percent Ag, 97.5 percent Pb) and two 590 F (1.75 percent Ag, 0.75 percent Sn, 97.5 percent Pb) thermal monitors. The monitors were in the form of wire with a square or rectangular cross section. The 579 F monitors were located in the top, middle, and bottom regions of the capsule. The 590 F monitors were located in the top-middle and bottom-middle regions of the capsule. (The top-middle region is the region located between the top and middle capsule regions, and the bottom-middle region is the region located between the bottom and middle capsule regions.) The 579 F bottom, the 579 F middle, the 590 F top-middle, and the 590 F bottom-middle thermal monitors were recovered for examination.

Monitors were examined at a magnification of 4X in a stereomicroscope. Figures 9 through 12 show the four specimens after removal from their Pyrex tubes. The slight bends seen in two of them were introduced when the Pyrex tubes were broken to remove the wires.

None of the 579 F or 590 F thermal monitors show any evidence of melting except the 590 F top-middle monitor. The latter monitor is shown in Figure 12; the right end shows slight evidence of incipient melting. However, there is no evidence of any general melting along the length of the monitor. This melting is believed to have occurred during sealing of the temperature monitor in the Pyrex tube.

Based on the examination of the thermal monitor wires, it appears that the capsule was not above 579 F during irradiation for any period of time long enough to cause appreciable melting of the thermal monitors.

Results of the fast and thermal neutron dosimetry analyses are shown in Tables 2 and 3, respectively. Of the five iron samples located at different positions, no significant variation in results was noted so that an average total neutron fluence (>1 Mev) of 3.58×10^{18} n/cm^2 was selected as most representative of the results. Excellent agreement was obtained with the nickel dosimeter at 3.57×10^{18} n/cm^2. The remaining results obtained from the copper, ^{238}U and ^{237}Np, ranged from 50 to 100 percent higher. A plot of the results of the five dosimeters versus location is shown in Figure 13.

4X P4765

FIGURE 9. 579 F BOTTOM THERMAL MONITOR

4X P4762

FIGURE 10. 590 F BOTTOM-MIDDLE THERMAL MONITOR

4X P4764

FIGURE 11. 579 F MIDDLE THERMAL MONITOR

4X P4767

FIGURE 12. 590 F TOP-MIDDLE THERMAL MONITOR

TABLE 2. FAST NEUTRON DOSIMETRY RESULTS (>1 Mev)

Dosimeter	Location in Capsule	ϕ >1 Mev n/cm^2-sec	nvt >1 Mev n/cm^2
^{54}Fe	Top	8.02×10^{10}	3.77×10^{18}
^{54}Fe	Mid Top	7.09×10^{10}	3.33×10^{18}
^{54}Fe	Middle	6.98×10^{10}	3.28×10^{18}
^{54}Fe	Mid Bottom	8.55×10^{10}	4.01×10^{18}
^{54}Fe	Bottom	7.52×10^{10}	3.53×10^{18}
^{54}Fe		Avg 7.63×10^{10}	Avg 3.58×10^{18}
^{58}Ni	Middle	7.60×10^{10}	3.57×10^{18}
^{63}Cu	Top	1.28×10^{11}	6.03×10^{18}
^{63}Cu	Mid Top	1.19×10^{11}	5.59×10^{18}
^{63}Cu	Mid Bottom	1.28×10^{11}	6.02×10^{18}
^{63}Cu	Bottom	1.30×110^{11}	6.12×10^{18}
^{63}Cu		Avg 1.26×10^{11}	Avg 5.94×10^{18}
^{238}U	Middle	1.12×10^{11}	5.27×10^{18}
^{237}Np	Middle	1.51×10^{11}	7.12×10^{18}

TABLE 3. THERMAL NEUTRON DOSIMETRY RESULTS

Dosimeter	Location in Capsule	ϕ, n/cm^2-sec	nvt, n/cm^2
$^{59}Co_{BARE}$	Top	2.68×10^{11}	1.26×10^{19}
	Mid Top	2.70×10^{11}	1.26×10^{19}
	Mid Bottom	2.58×10^{11}	1.21×10^{19}
	Bottom	2.62×10^{11}	1.23×10^{19}
		Avg 2.65×10^{11}	1.24×10^{19}
$^{59}Co_{CADMIUM}$	Top	9.47×10^{10}	4.46×10^{18}
	Mid Top	9.65×10^{10}	4.52×10^{18}
	Middle	10.6×10^{10}	5.00×10^{18}
	Mid Bottom	9.20×10^{10}	4.33×10^{18}
		Avg 9.73×10^{10}	4.58×10^{18}
$^{59}Co_{TRUE\ THERMAL\ FLUX}$*		1.67×10^{11}	7.84×10^{18}

*Corrected for cadmium ratio $R = Co_{BARE}/Co_{CADMIUM}$

$R = 1.24 \times 10^{19}/4.58 \times 10^{18} = 2.72$

$nvt_{th} = Co_{BARE} \times (R-1)/R = Co_{BARE} \times 0.632$

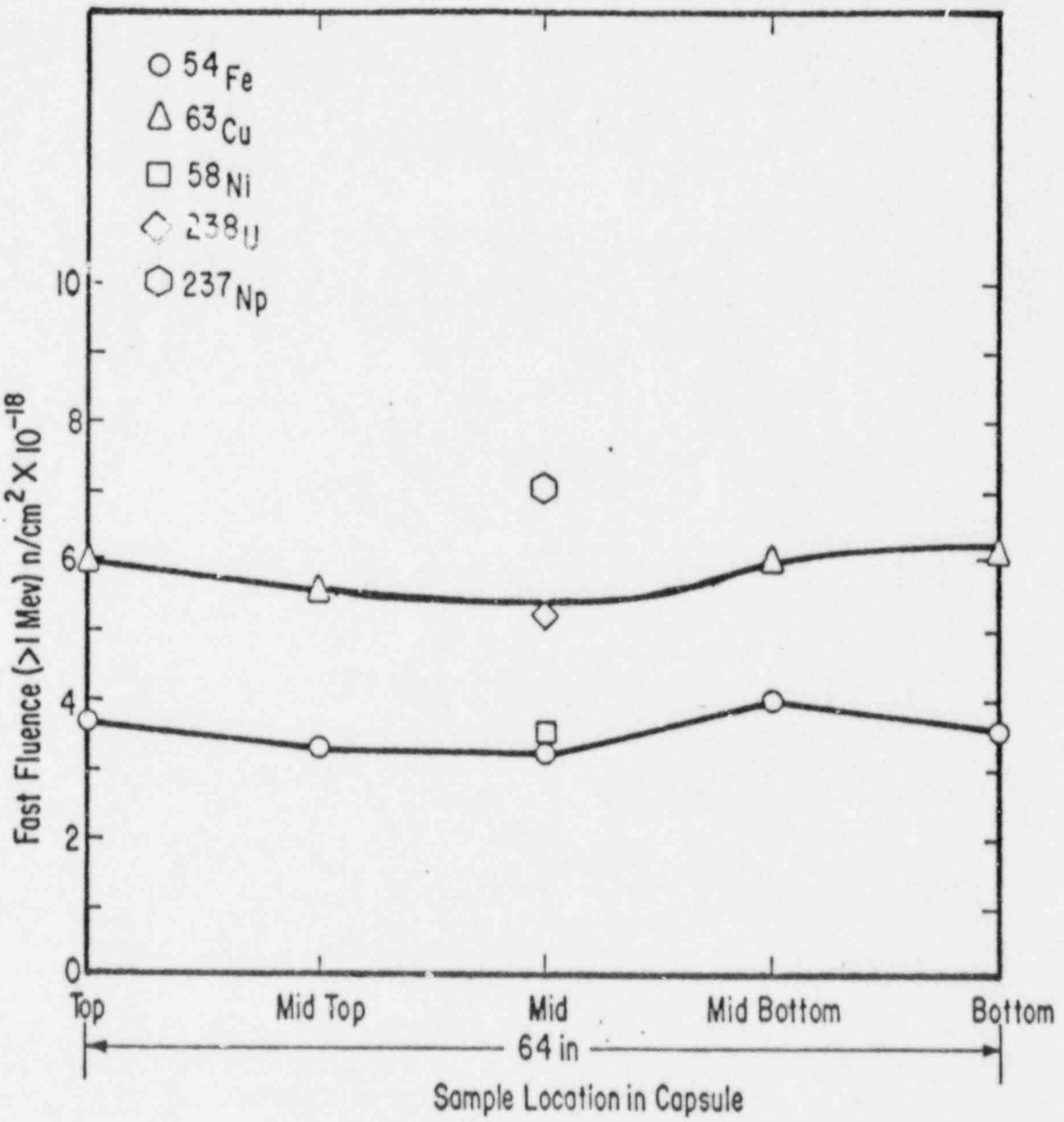

FIGURE 13. FAST NEUTRON FLUENCE PROFILES

Several factors enter into the analyses and calculations such as knowledge of the neutron energy spectrum at the surveillance capsule location, effective cross section for each reaction as a function of the neutron energy distribution, purity of certain materials, uncertainty of fission yields, and experimental error.

Thermal neutron dosimetry results from the ^{59}Co (n,γ) ^{60}Co reaction are given in Table 3. Correcting for the cadmium ratio, R = 2.72, true thermal neutron flux and total fluence values obtained were 1.67×10^{11} n/cm^2-sec and 7.84×10^{18} n/cm^2, respectively. A profile of the bare and cadmium shielded wires in Figure 14 shows very little fluctuation.

Constants used in the six different reactions are summarized in Table 4. Irradiation time of the capsule was 543.6 equivalent full power days and the time of removal from the reactor was September 30, 1972.

The fast neutron cross section values listed are the effective neutron cross sections for neutrons >1 Mev. There is no constant factor applied to the ASTM E261-70 fission spectrum values due to variation in threshold energy of the reaction, which is seen to vary from 0.4 Mev to 1.5 Mev and 3-4 Mev for ^{63}Cu (n,α) ^{60}Co, and the neutron energy distribution at the capsule location.

To calculate the effective cross section, a one-dimensional transport code, ANISN, was utilized. Twenty-seven energy groups were analyzed. Plots of the fission spectrum assumed at the core edge and the calculated spectrum at the reactor vessel inner surface are illustrated in Figure 15. Also shown is the ^{54}Fe (n,p) ^{54}Mn cross section as a function of neutron energy. The spectrum at the capsule location is at a lower energy range due to neutron travel through about 16 cm of steel and 10 cm of water. The most representative location of the samples was selected as 2.0 cm outside the thermal shield. This value would represent a conservative figure in that the effective cross section would be slightly smaller (higher resultant flux). However, a shift of 1 cm would only affect the resultant fluence by about 10 percent.

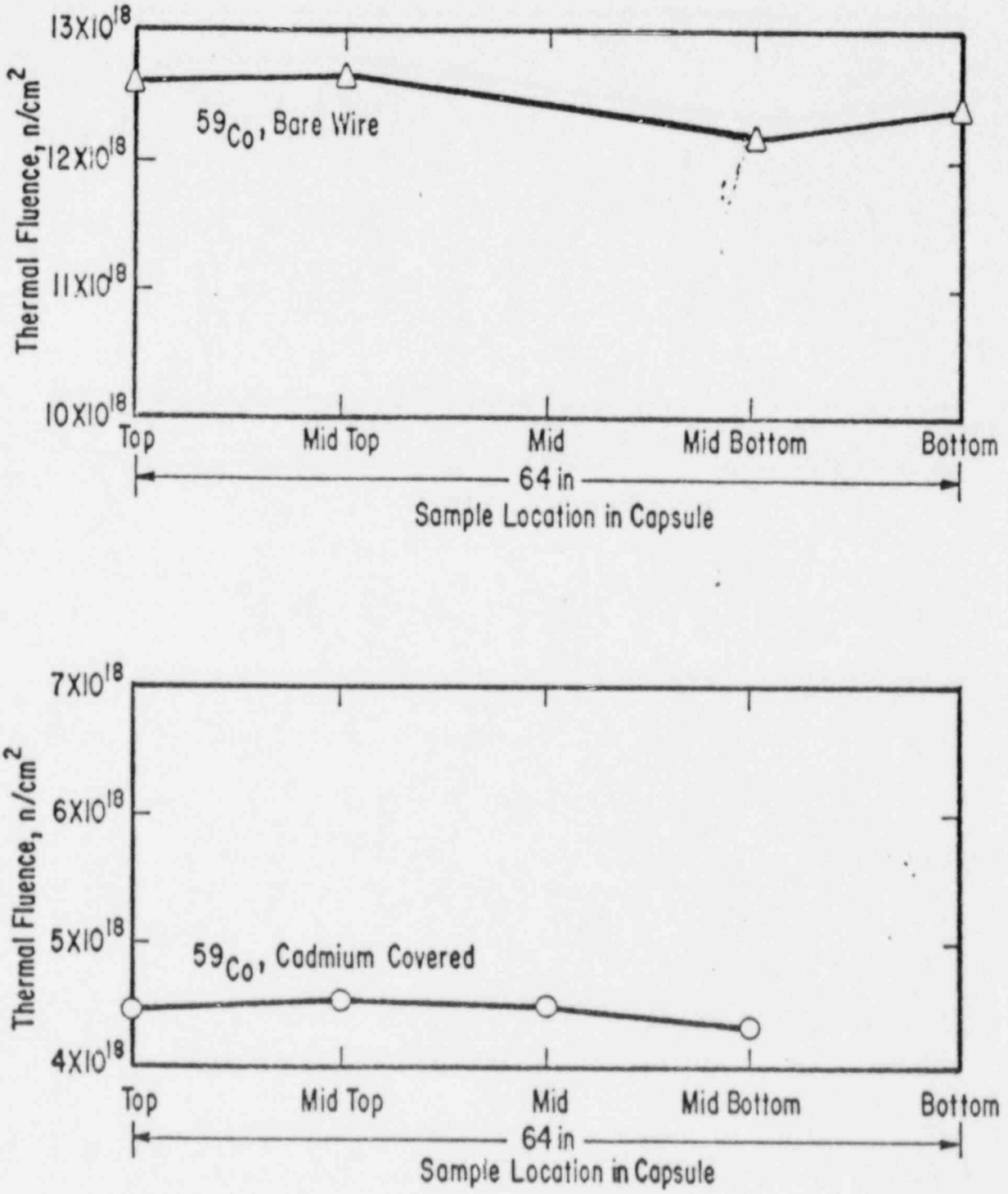

FIGURE 14. THERMAL NEUTRON FLUENCE PROFILE

TABLE 4. VALUES USED IN DOSIMETRY CALCULATIONS

Reaction	Target	Target Isotope % Abundance	$\bar{\sigma}$(1), barns	Threshold Energy Mev	Fission Yield %	Product Half-Life
$^{63}Cu(n,\alpha)^{60}Co$	100% Cu	69.17	0.00065	--	--	5.26y
$^{58}Ni(n,p)^{58}Co$	100% Ni	67.77	0.104	1.0	--	71.3d
$^{54}Fe(n,p)^{54}Mn$	Iron(3)	5.82	0.0838	1.5	--	314d
$^{238}U(n,f)^{137}Cs$	U_3O_8	>99.9	0.356	0.8	6.30 ±.27(2)	30.0y
$^{237}Np(n,f)^{137}Cs$	NpO_2	>99.9	2.63	0.4	6.44 ±.31(2)	30.0y
$^{59}Co(n,\gamma)^{60}Co$	Al-0.15% Co	100	37.1	--	--	5.26y

(1) For fast reactions, $\bar{\sigma}$ is for neutrons >1 Mev at capsule location.

(2) Private communication with Wm McElroy, HEDL, June 15, 1973.

(3) Two types of metal were analyzed. One was SA302 Grade B (97.6 percent Fe) and the other was weld metal (96.6 percent Fe).

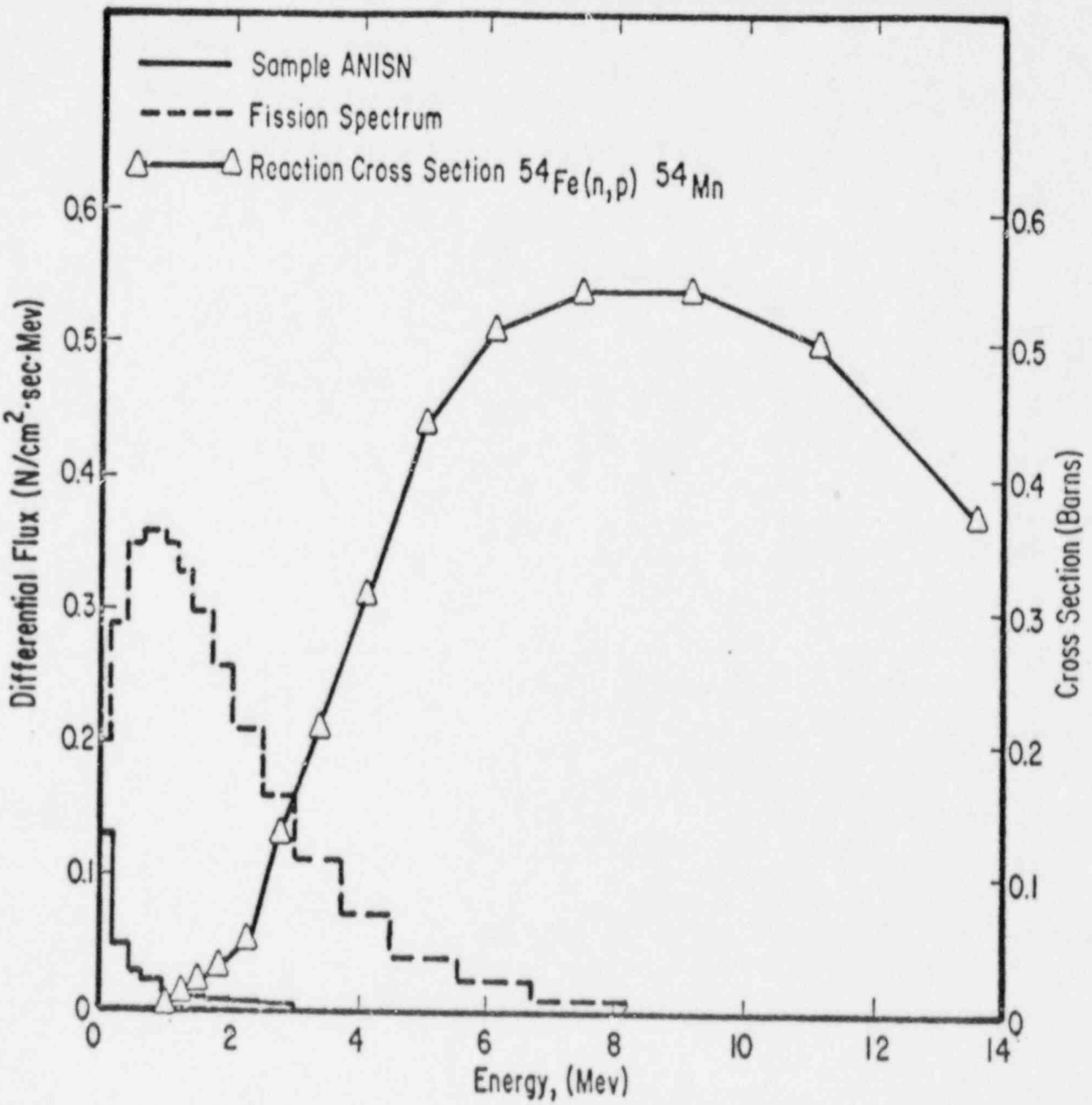

FIGURE 15. NEUTRON FLUX DISTRIBUTION AND ^{54}Fe CROSS SECTION

The value affected the most was that of ^{237}Np. In this case the effective cross section is larger than any cross section at an individual energy level because of the "weighting" effect of those cross sections below 1 Mev. The cross sections times the larger flux values below 1 Mev cause the effective cross section, $\bar{\sigma}_{>1\ Mev}$, to increase as shown by the equation

$$\bar{\sigma}_{>1\ Mev} = \frac{\int_{E=0}^{\infty} \phi(E)\ \sigma\ (E)dE}{\int_{E>1\ Mev}^{\infty} \phi(E)dE}$$

where σ and ϕ are calculated for each energy group. Only limited data was available on the $^{63}Cu\ (n,\alpha)\ ^{60}Co$ cross section so that a fission spectrum was assumed. The best value was considered to be calculated from

$$\bar{\sigma}^{f}_{>1\ Mev} = \bar{\sigma}^{f}_{TOT} \quad \frac{\int_{E=0}^{\infty} \phi_f(E)dE}{\int_{E>1\ Mev}^{\infty} \phi_f(E)dE}$$

where f = fission spectrum

$$\bar{\sigma}^{f}_{TOT} = 0.00045 \text{ barns from ASTM E261, Table 3.}$$

The ratio of the fission spectra was calculated using the 27 energy groups as follows:

$$\frac{\int_{E>1\ Mev}^{\infty} \phi_f(E)dE}{\int_{E=0}^{\infty} \phi_f(E)dE} = 0.688$$

Since the copper results were ~60 percent high, some of the error may occur in (1) uncertainty of the effective cross section and threshold, and/or (2) a small Co impurity. (It was calculated, using the thermal flux data in this report, that 1 ppm Co in the Cu dosimeter would result in a value

20 percent high.) Chemical analyses for this material at this low level were not available. The reason for the disagreement of the ^{238}U and ^{237}Np values with the ^{54}Fe results is unknown at this time. Probably the most significant factors affecting the calculations are the cross section at energies below 1 Mev, dependence on the neutron distribution at the precise sample location, and impurities. Considerable difficulty was encountered in handling the 10-20 mg of U_3O_8 and NpO_2 powders but it is thought that the experimental error is within ±10 percent. It is doubtful that foreign capsule material contaminated tne samples since this would lower the results.

In summary, the iron and nickel dosimeters have the best known physical constants and showed the most consistency resulting in a total fast neutron fluence (>1 Mev) of 3.58×10^{18} n/cm^2.

Impact Tests

The results of the tests of the Charpy impact specimens are listed in Tables 5 through 9. In addition to the impact energy values, the tables also list the measured values of lateral expansion and the estimated fracture-appearance values for each specimen. These two additional values are sometimes used in measurements of other transition-temperature shifts and are included here for the purpose of providing a complete test record for each specimen. The lateral expansion is a measure of the deformation produced by the striking edge of the impact machine when it impacts the specimen; that is, it is a change in thickness measurement of the section directly opposite that where the notch is located. The fracture appearance value is a visual estimate of the amount of shear or ductile type of fracture appearing on the fracture surface of the specimen.

The data listed in Tables 5 through 9 are also graphically shown in Figures 16 through 20. The shift in impact properties is clearly shown in these figures. Of primary interest to this program is the shift in the temperature corresponding to the impact energy of 30 ft-lb. This 30 ft-lb fix is that which was established as corresponding to the temperature defined as the nil ductility transition temperature.[19]

During the testing of these Charpy impact specimens, advanced instrumentation techniques were used to obtain valuable supplementary data. The results of these instrumented Charpy test evaluations are presented in Appendix C.

The curves for the irradiated pressure vessel material are well defined with little data scatter with only one exception. That exception is the curve for the irradiated HAZ metal. The reason for this is that it is difficult to cut specimens out of a heat-affected zone in a plate between base metal and weld metal, and be assured that the HAZ specimens all have the identical microstructure and thermal history. The main purpose of the Charpy impact tests was to determine the NDTT of the two base metal plates, the HAZ metal, and the weld metal of the pressure vessel. The results of these NDTT evaluations are summarized in Table 10. Also listed in the table are the results of the impact tests on the ASTM correlation monitor material.

TABLE 5. CHARPY V-NOTCH IMPACT TEST RESULTS FOR BASE METAL PLATE A9811

Specimen	Test Temperature, F	Impact Energy, ft lb	Lateral Expansion, mils	Fracture Appearance, Percent Shear	Specimen Fracture Surface
A2	-65	4.5	5	0	
A5	-25	5.5	5	2	
A7	5	8	8	15	
A3	26	22	21	15	
A9	33	26	26	25	
A6	51	41	38	35	
A11	79	46	45	40	

TABLE 5 (CONTINUED)

Specimen	Test Temperature, F	Impact Energy, ft lb	Lateral Expansion, mils	Fracture Appearance, Percent Shear	Specimen Fracture Surface
A12	104	55	51	70	
A10	119	71	64	70	
A8	162	87	76	95	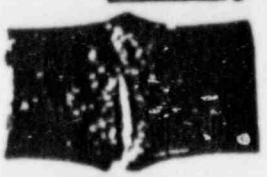
A4	208	88	79	99	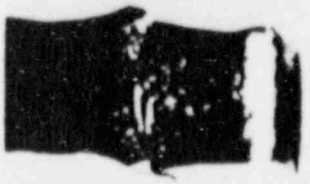
A1	290	90	76	95	

TABLE 6. CHARPY V-NOTCH IMPACT TEST RESULTS FOR BASE METAL PLATE C1423

Specimen	Test Temperature, F	Impact Energy, ft lb	Lateral Expansion, mils	Fracture Appearance, Percent Shear	Specimen Fracture Surface
C3	-102	3	4	0	
C1	-65	3	2	2	
C10	-24	11.5	10	10	
C5	0	18	16	10	
C7	5	37	31	15	
C12	26	35	30	15	
C11	33	38	31	40	

TABLE 6 (CONTINUED)

Specimen	Test Temperature, F	Impact Energy, ft lb	Lateral Expansion, mils	Fracture Appearance, Percent Shear	Specimen Fracture Surface
C8	52	55	45	25	
C2	79	76	63	55	
C4	120	101	73	80	
C9	208	119	88	100	
C6	300	121	79	98	

TABLE 7. CHARPY V-NOTCH IMPACT TEST RESULTS FOR HEAT-AFFECTED ZONE METAL

Specimen	Test Temperature, F	Impact Energy, ft lb	Lateral Expansion, mils	Fracture Appearance, Percent Shear	Specimen Fracture Surface
WH4	-87	5.5	3	5	
WH5	-26	31	28	25	
WH7	0	33	31	40	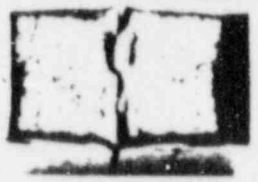
WH8	25	20	15	35	
WH3	36	99	70	90	
WH6	51	83	50	80	
WH1	79	110	81	95	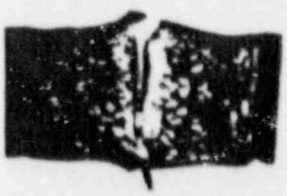
WH2	208	105	81	98	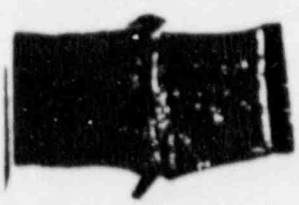

TABLE 8. CHARPY V-NOTCH IMPACT TEST RESULTS FOR WELD METAL

Specimen	Test Temperature, F	Impact Energy, ft lb	Lateral Expansion, mils	Fracture Appearance, Percent Shear	Specimen Fracture Surface
WW8	-87	2.5	1	5	
WW7	-31	6.5	5	15	
WW2	25	13	12	25	
WW4	50	27	22	40	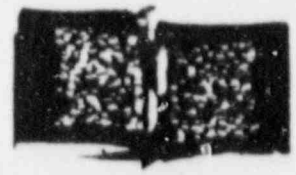
WW6	79	34	31	50	
WW5	123	46	43	70	
WW1	167	54	53	98	
WW3	208	52	53	99	

TABLE 9. CHARPY V-NOTCH IMPACT TEST RESULTS FOR ASTM CORRELATION MONITOR MATERIAL

Specimen	Test Temperature, F	Impact Energy, ft lb	Lateral Expansion, mils	Fracture Appearance, Percent Shear	Specimen Fracture Surface
R6	-25	3.5	2	2	
R1	50	10	8	10	
R7	78	22	19	15	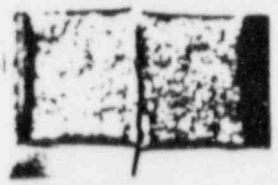
R5	122	20	21	30	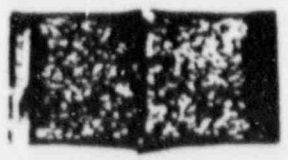
R4	127	27	26	40	
R2	161	40	36	55	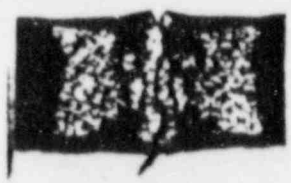
R3	188	56	51	75	
R8	236	64	54	98	

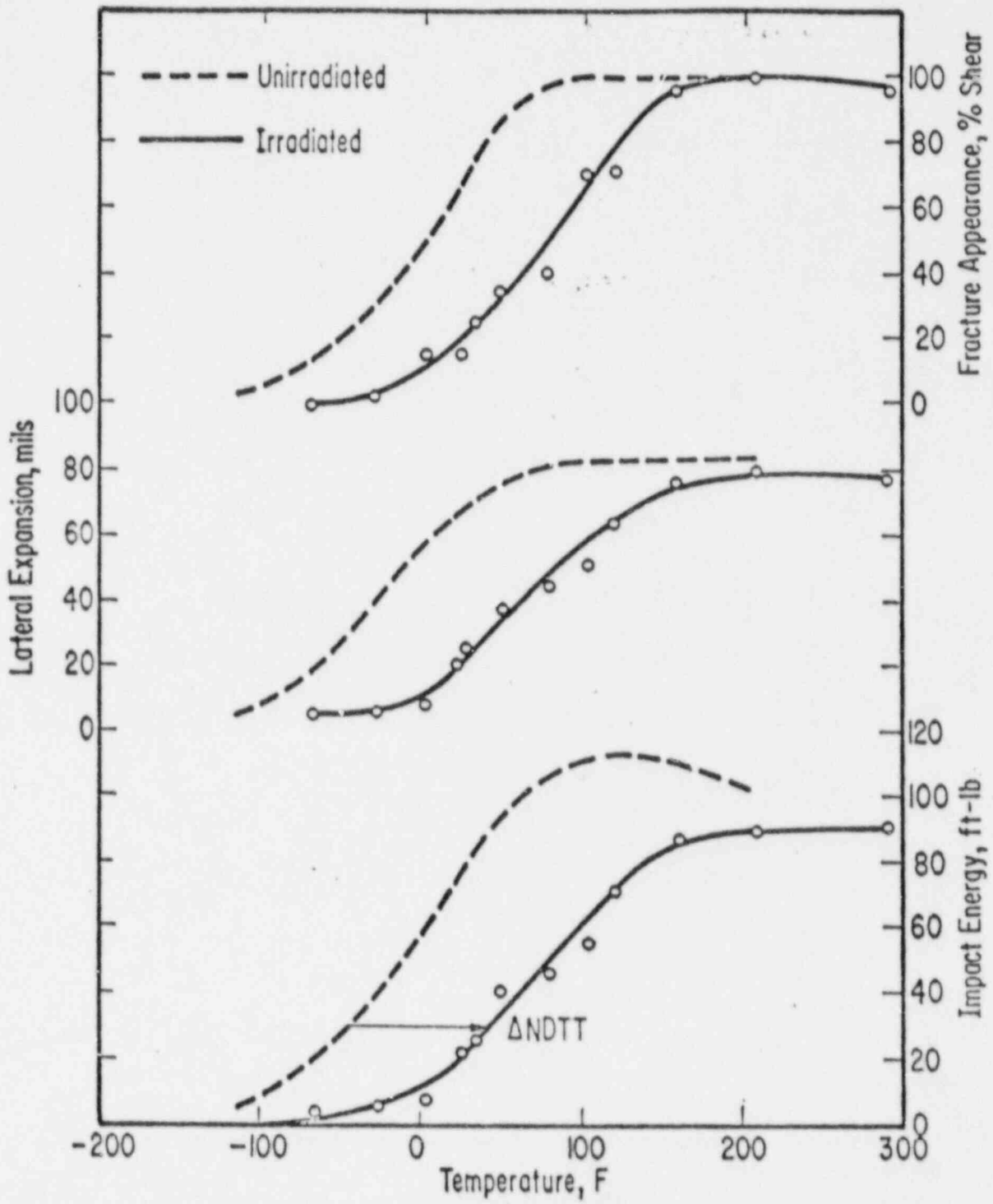

FIGURE 16. CHARPY IMPACT TEST RESULTS FOR BASE-METAL PLATE A9811

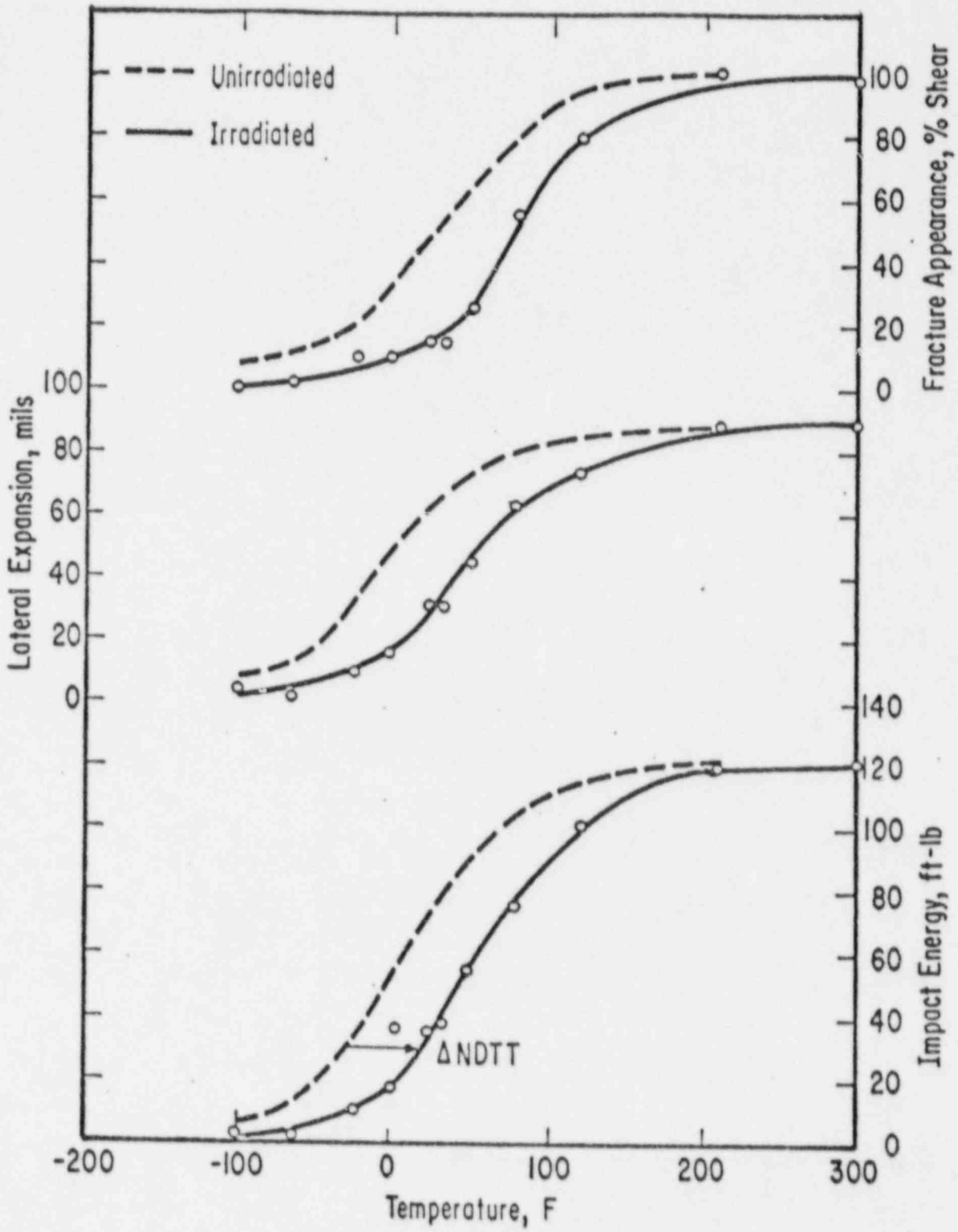

FIGURE 17. CHARPY IMPACT TEST RESULTS FOR BASE-METAL PLATE C1423

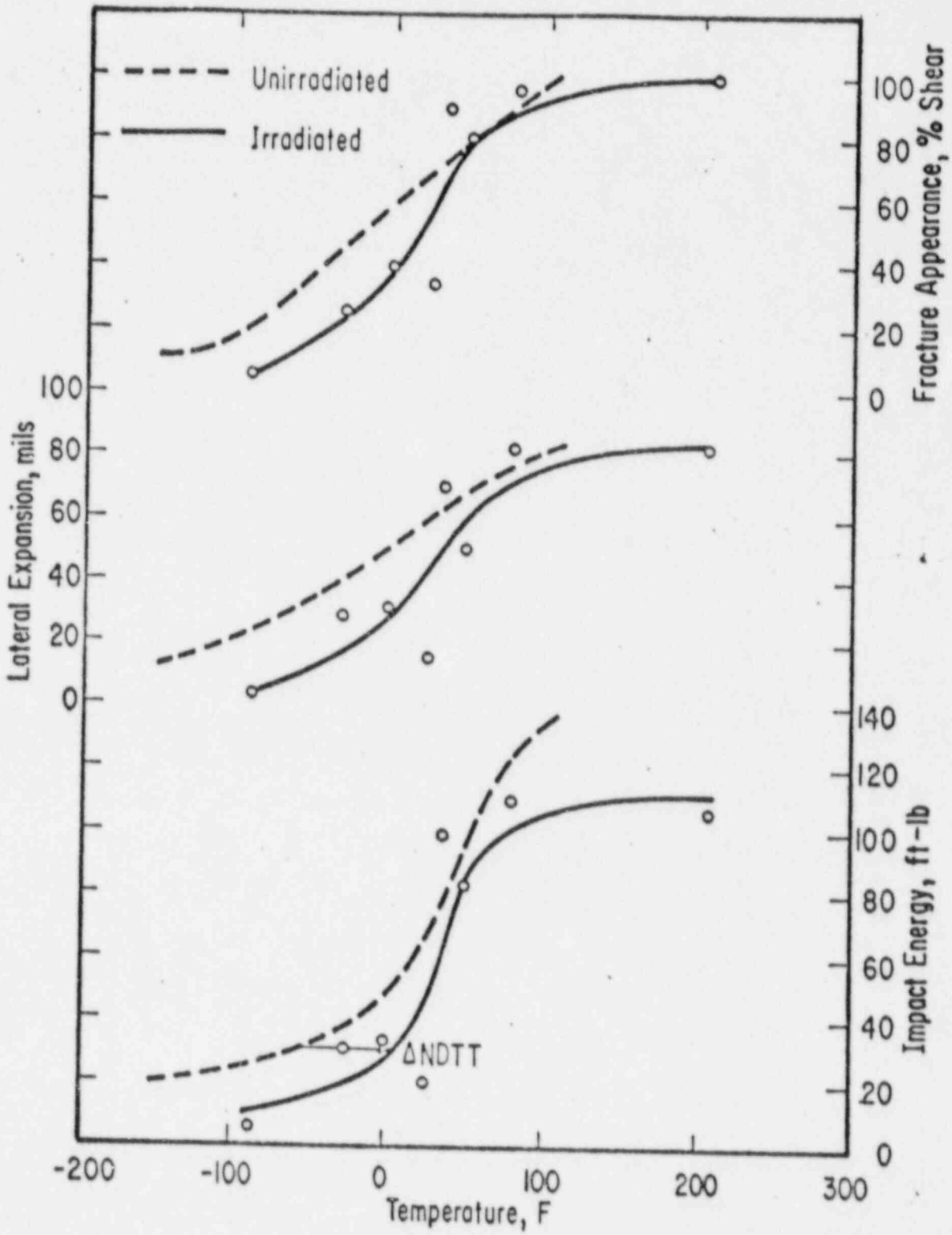

FIGURE 18. CHARPY IMPACT TEST RESULTS FOR HEAT-AFFECTED ZONE METAL

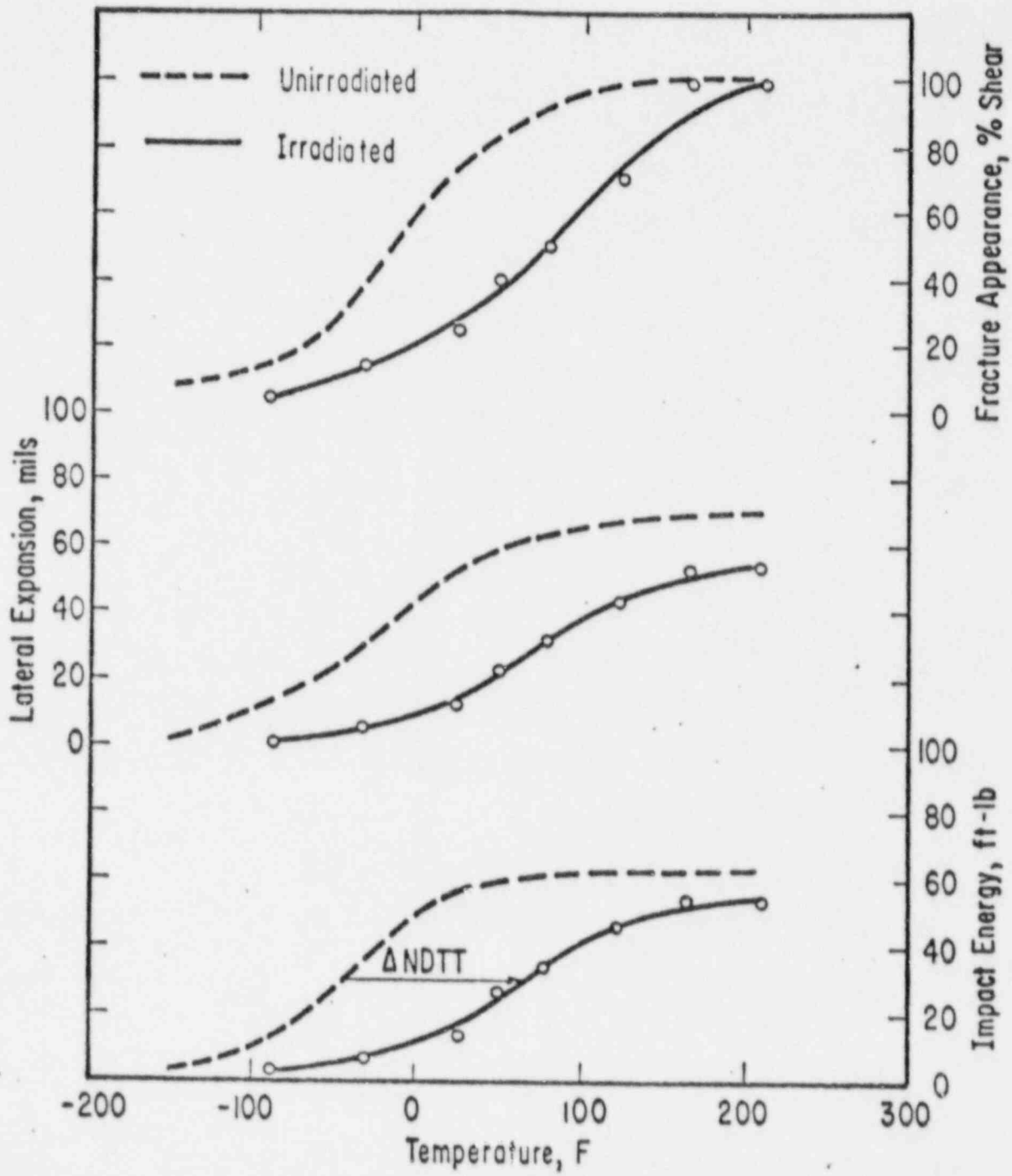

FIGURE 19. CHARPY IMPACT TEST RESULTS FOR WELD METAL

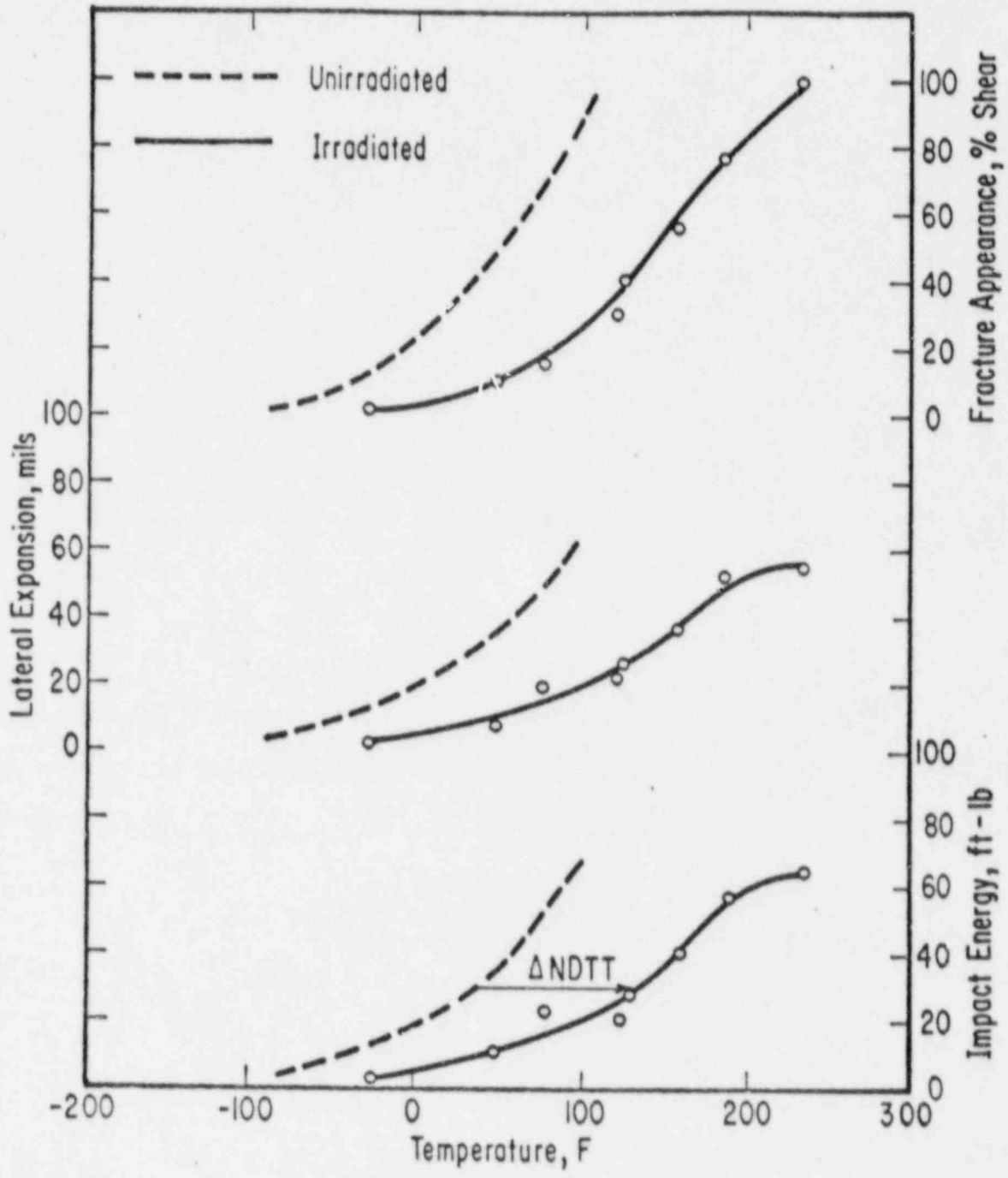

FIGURE 20. CHARPY IMPACT TEST RESULTS FOR CORRELATION-MONITOR MATERIAL

TABLE 10 SUMMARY OF CHARPY IMPACT TEST RESULTS

Material	Unirradiated NDTT, F	Irradiated NDTT, F	ΔNDTT, F
Plate A9811	-45	+45	+90
Plate C1423	-30	+20	+50
HAZ Metal	-60	+10	+70
Weld Metal	-45	+65	+110
Correlation Monitor	+40	+135	+95

Irradiation caused the NDTT to increase in all four of the pressure vessel materials. The base metal plate A9811 had an NDTT increase of 90 F, the base metal plate C1423 had an NDTT increase of 50 F, and the HAZ metal had an NDTT increase of 70 F. The weld metal had an NDTT increase of 110 F, the greatest of the four pressure vessel materials.

The highest NDTT of the unirradiated pressure vessel materials was -30 F for the base metal plate C1423. The highest NDTT of the irradiated pressure vessel materials is +65 F for the weld metal. Therefore, the limiting metal of the four pressure vessel materials at the present irradiation level is the weld metal.

The upper shelf energy of a Charpy impact curve is defined as the upper level of energy that curves exhibit at higher temperatures where increases in test temperature cause no further increase in impact energy. A general effect of irradiation is to lower the upper shelf energy. There is a sufficient amount of scatter in the actual data points for the preirradiation and postirradiation data to make the confirmation of this trend difficult in the present investigation in the case of the HAZ metal and the base metal plate C1423. (Data points for the preirradiation Charpy curves are not shown in Figures 16 through 20.) However, the base metal plate A9811 and the weld metal both show clear decreases in the upper shelf energy.

The upper shelf energy for all four irradiated materials is above 50 ft lb. However, the upper shelf energy for the weld metal is only slightly above, being about 53 ft lb. As discussed earlier, some investigators have stated that the NDTT concepts no longer apply when the upper shelf energy drops below 50 ft lb. When the impact specimens in the next surveillance capsule are tested, the test temperatures should be chosen such that the upper shelf energy is well established to determine if it has dropped below the 50 ft-lb level.

The capsule also contained ASTM correlation monitor Charpy impact specimens. The unirradiated and irradiated test results are shown plotted in Figure 20. As indicated in Table 10, the preirradiation NDTT was +40 F and the postirradiation NDTT is +135 F, resulting in a nil ductility transition temperature shift of +95 F.

The ΔNDTT values for the irradiated materials other than the ASTM correlation monitor material are shown plotted in Figure 21 as a function of fluence. Also shown in this figure are ΔNDTT values obtained in other surveillance programs[29-35]. The apparent large scatter in data among the various programs is not unusual. Note that the weld-metal values determine the upper bound of the trend band. The values used to form the trend band are those from programs where the irradiation temperature was between 550 and 590 F. It can be seen that the four ΔNDTT values for the pressure vessel materials of the present program fall well within the upper and lower bounds determined by materials of other investigations.

The ΔNDTT value for the irradiated correlation monitor material is shown in Figure 22. Also shown in this figure are ΔNDTT values obtained from other programs using this material. The ΔNDTT value determined in the present program is in good agreement with the other values shown.

The Figure 21 pressure vessel trend band for ΔNDTT charges can be used to estimate the ΔNDTT value of the pressure-vessel after various periods of reactor operation. These estimates assume that the surveillance capsule receives an accelerated fluence of 3.3 times that of the pressure vessel wall[36] and that the irradiation temperature of the pressure-vessel wall will continue to be equal to or greater than 550 F. The ΔNDTT estimates for 10, 20, and 32 years of effective full-power operation of the reactor are shown in Figure 23. The highest estimated values for the materials are represented by the upper bound of the trend band. The predicted ΔNDTT values for 10, 20, and 32 years of effective full power operation [1520 Mw(t)] are 210, 240, and 255 F. This is in reasonable agreement with the 32 years preirradiation prediction of 280 F for the reactor.[30] Subsequent examinations of specimens from future capsules will be used to substantiate the present 32 years NDTT shift estimate.

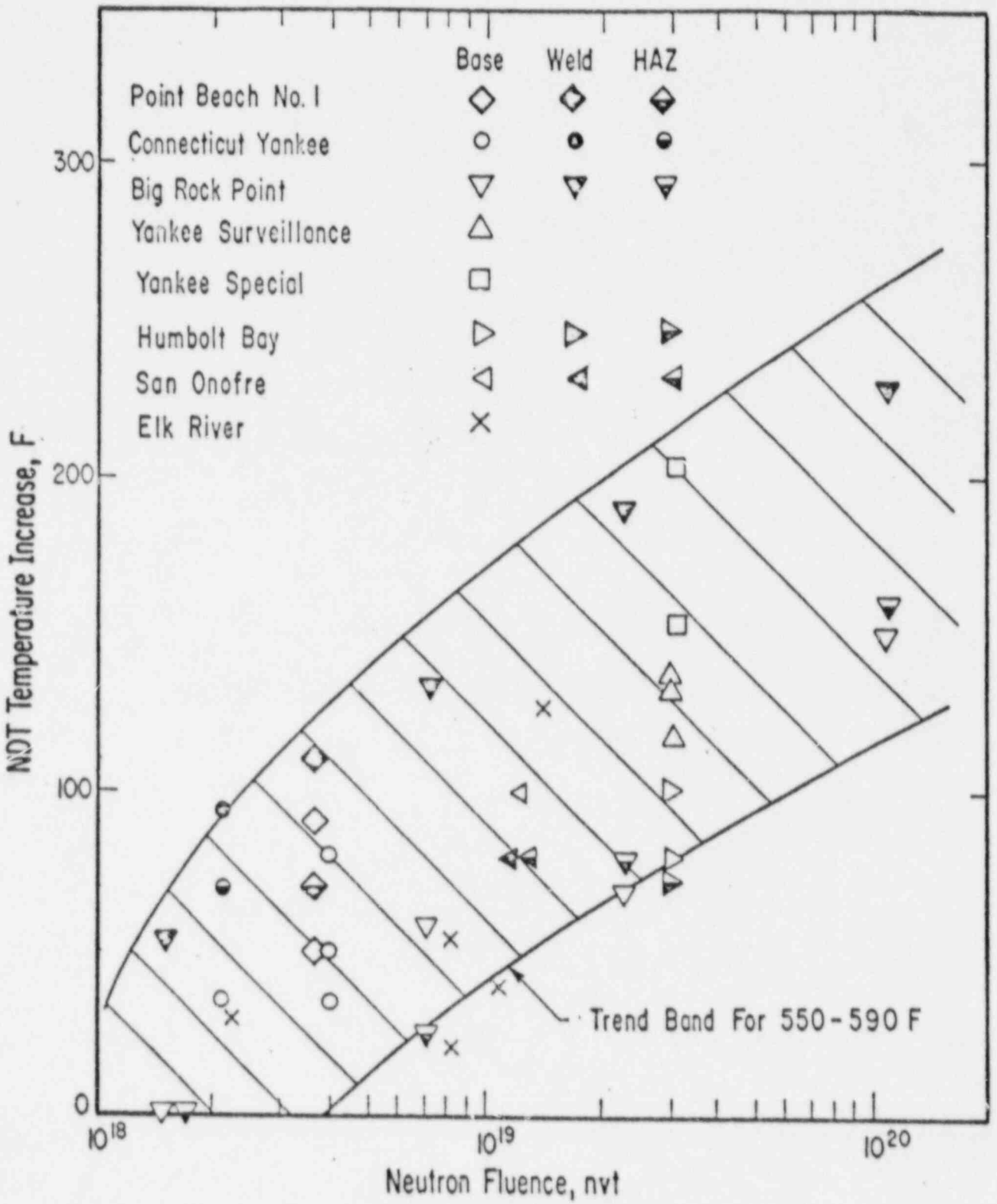

FIGURE 21. COMPARISON OF ΔNDTT VALUES FROM VARIOUS SURVEILLANCE PROGRAMS FOR SA302 GRADE B PRESSURE-VESSEL MATERIALS

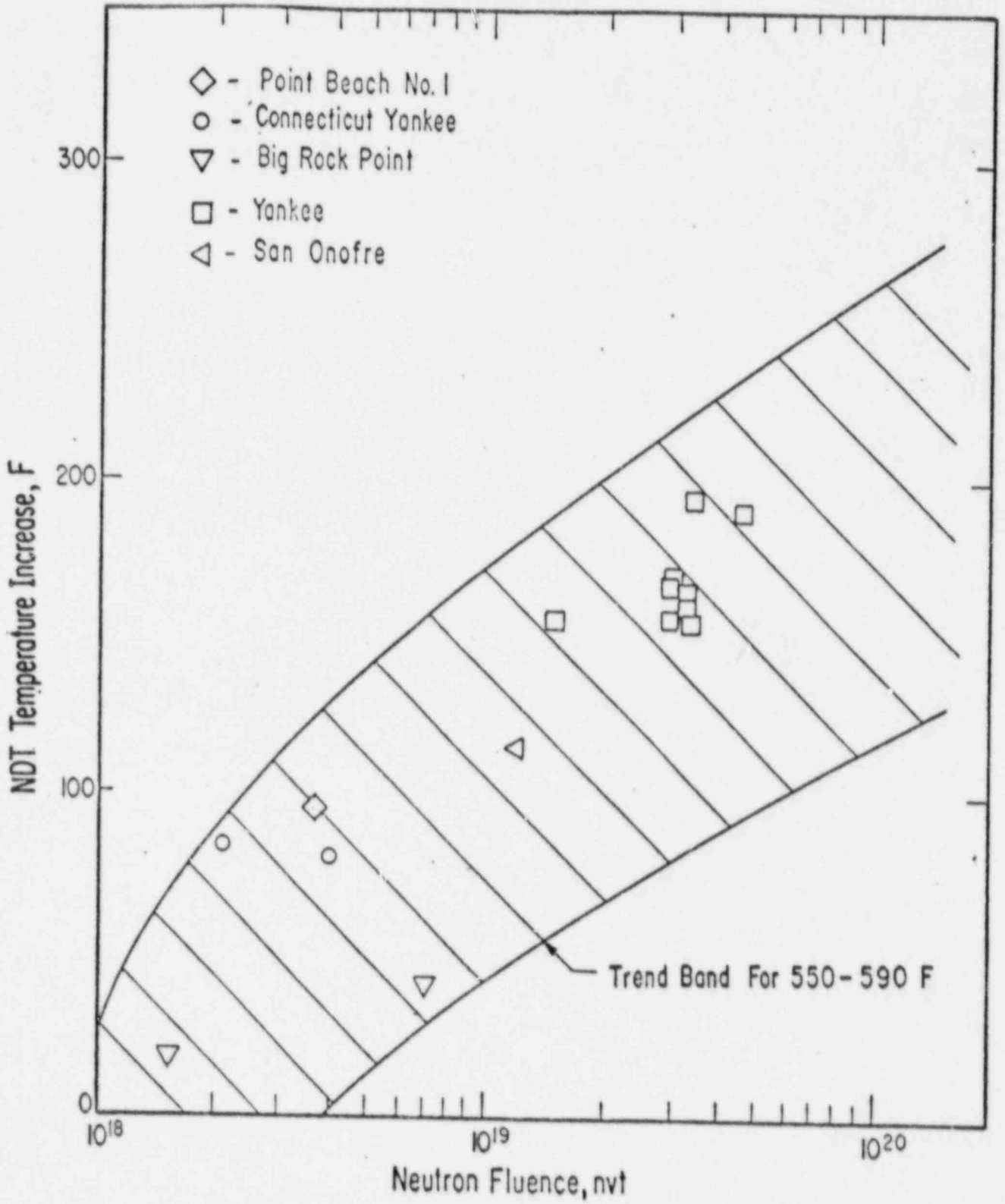

FIGURE 22. COMPARISON OF ΔNDTT VALUES FROM VARIOUS SURVEILLANCE PROGRAMS FOR SA302 GRADE B ASTM CORRELATION-MONITOR MATERIAL

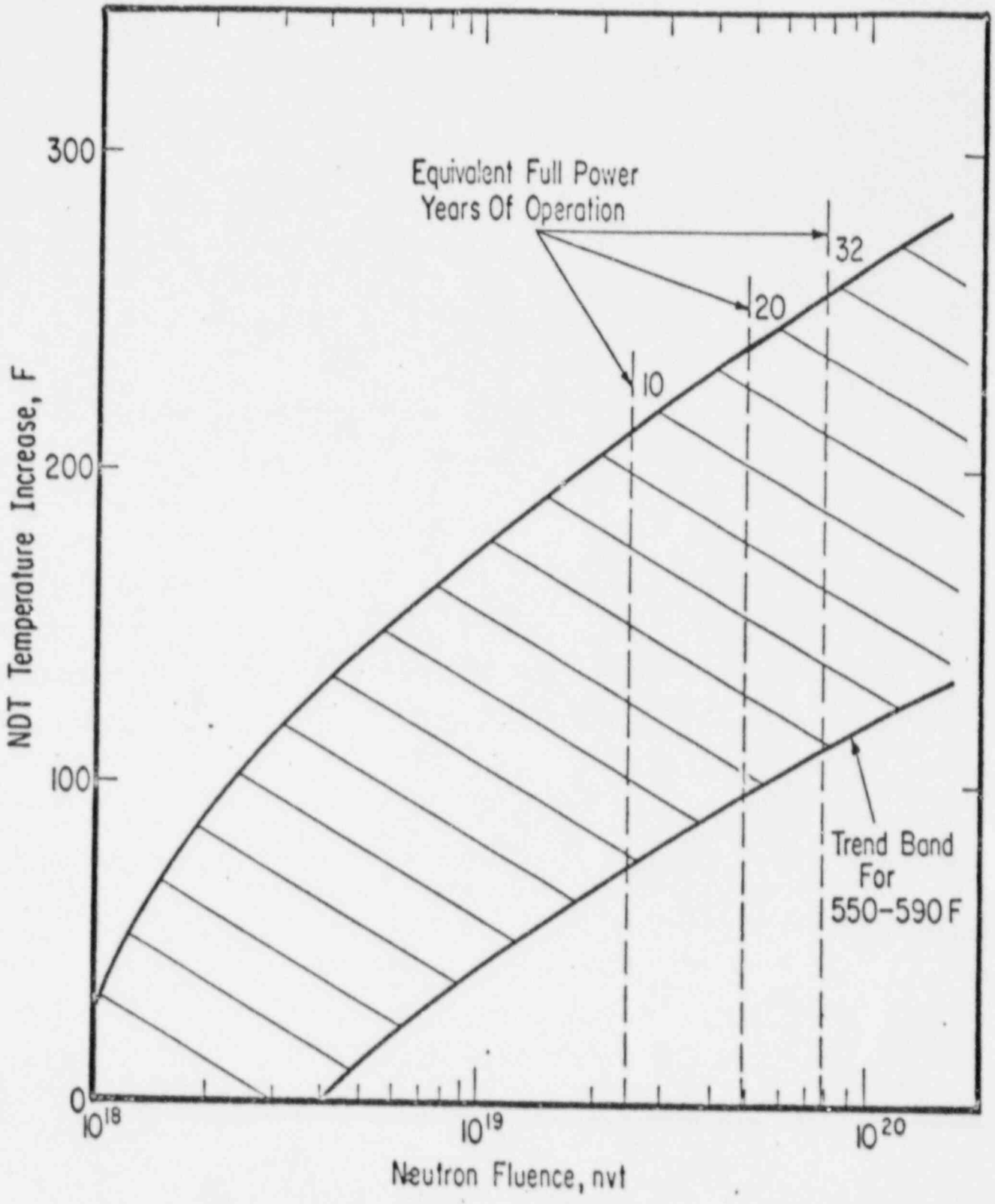

FIGURE 23. ΔNDTT ESTIMATES FOR 10, 20, AND 32 YEAR OF FULL-POWER OPERATION

The predicted maximum ΔNDTT values for 10, 20, and 32 years of effective full power operation are 210, 240, and 255 F, respectively.

Tensile Tests

The capsule contained tensile specimens from the base metal plate A9811, the base metal plate C1423, and the weld metal. Specimens were tested at temperatures ranging from -180 F to 550 F. The tensile data from these tests are listed in Table 11. The stress-strain curves are shown in Figures 24 through 30. In addition, photographs of the fractured specimens are given in Figures 31 through 37. These photographs show the necked down region of the gage length and the fractures.

Figures 38 through 40 show the unirradiated and irradiated values of elongation, reduction in area, 0.2 percent yield strength, and ultimate tensile strength for the three materials. The unirradiated values are from the report WCAP-7513.[9] The changes in tensile properties in general follow the expected behavior of irradiated metals such as the pressure vessel steel SA302 Grade B in the range 75 F to 550 F. There is no preirradiation low temperature data to which the -110 and -180 F irradiated tensile results can be compared. The elongation and reduction in area values generally have decreased as a result of irradiation, with the exception of plate C1423 in which the reduction in area at 75 F is unchanged and at 550 F is slightly increased. The 0.2 percent offset yield strength and ultimate tensile strength have increased in all cases. There is some scatter in the reduction in area values for base metal plate A9811, in that the 75 F value is moderately greater than the -110 and 550 F values.

TABLE 11. TENSILE PROPERTIES OF IRRADIATED PRESSURE-VESSEL SPECIMENS

Material	Specimen	Test Temperature, F	0.2 Percent Offset Yield Strength, psi	Ultimate Tensile Strength, psi	Total Elongation, Percent	Reduction in Area, Percent
Plate A9811	A3	-180	91,900	112,000	25.8	56.1
Plate A9811	A2	-110	79,800	102,700	24.1	48.6
Plate A9811	A4	75	67,800	89,100	18.9	58.5
Plate A9811	A1	550	59,500	88,400	11.9	44.6
Plate C1423	C2	75	76,000	96,200	17.0	65.0
Plate C1423	C1	550	66,800	93,800	13.1	59.0
Weld Metal	WW1	550	81,900	100,800	12.4	51.0

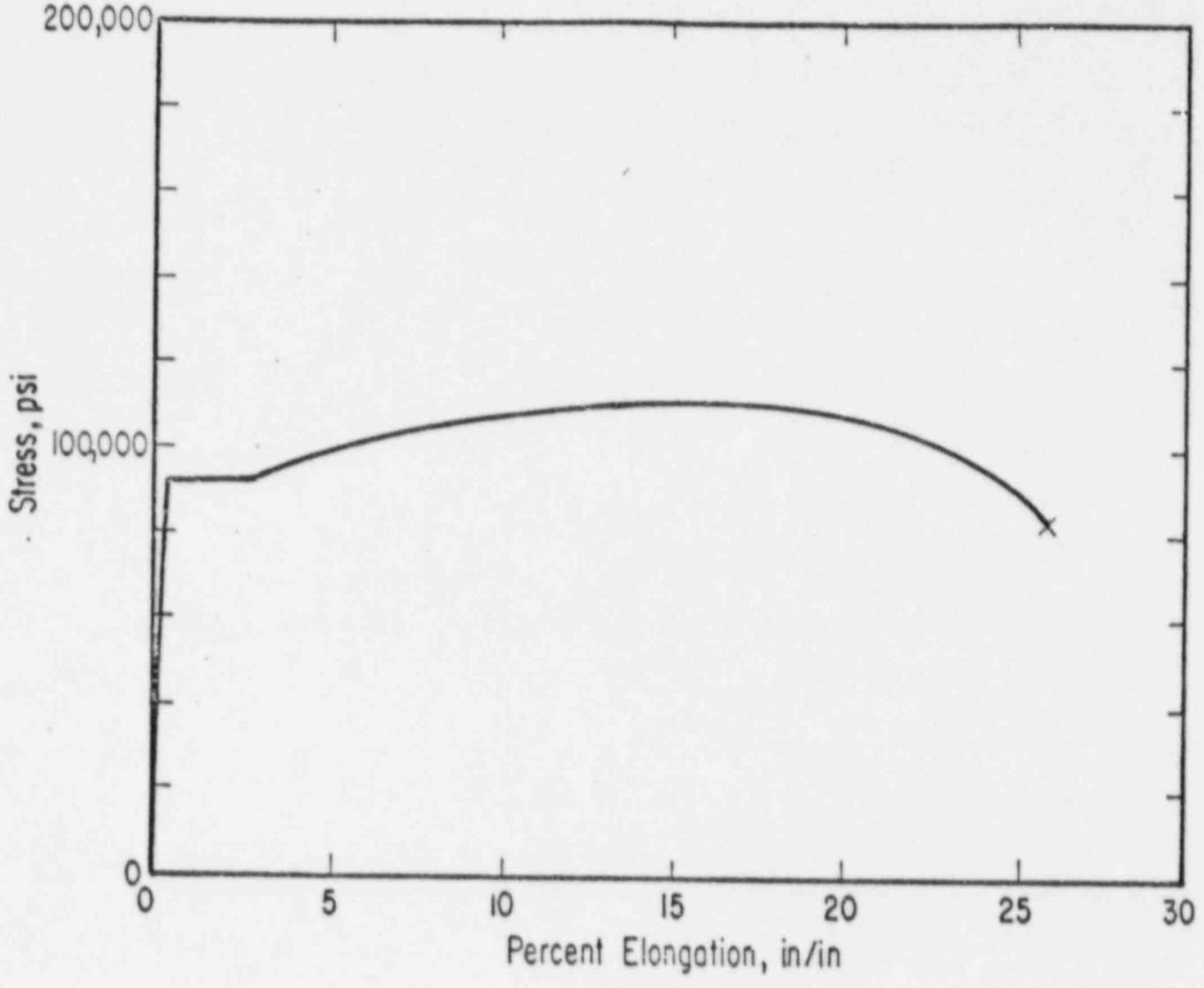

FIGURE 24. STRESS-STRAIN CURVE FOR IRRADIATED BASE-METAL PLATE A9811 (SPECIMEN A3) TESTED AT -180 F

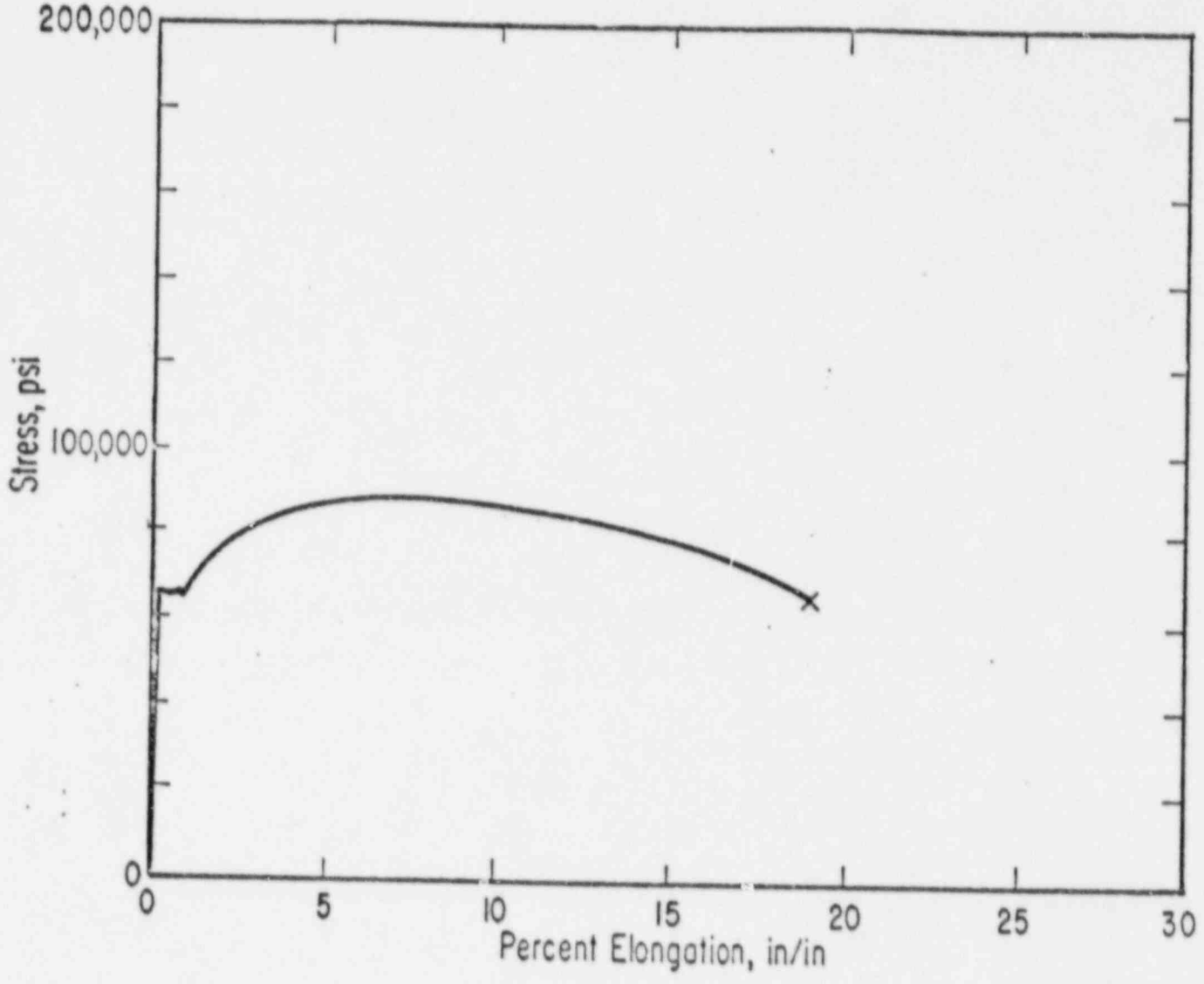

FIGURE 26. STRESS-STRAIN CURVE FOR IRRADIATED BASE METAL PLATE A9811 (SPECIMEN A4) TESTED AT 75 F

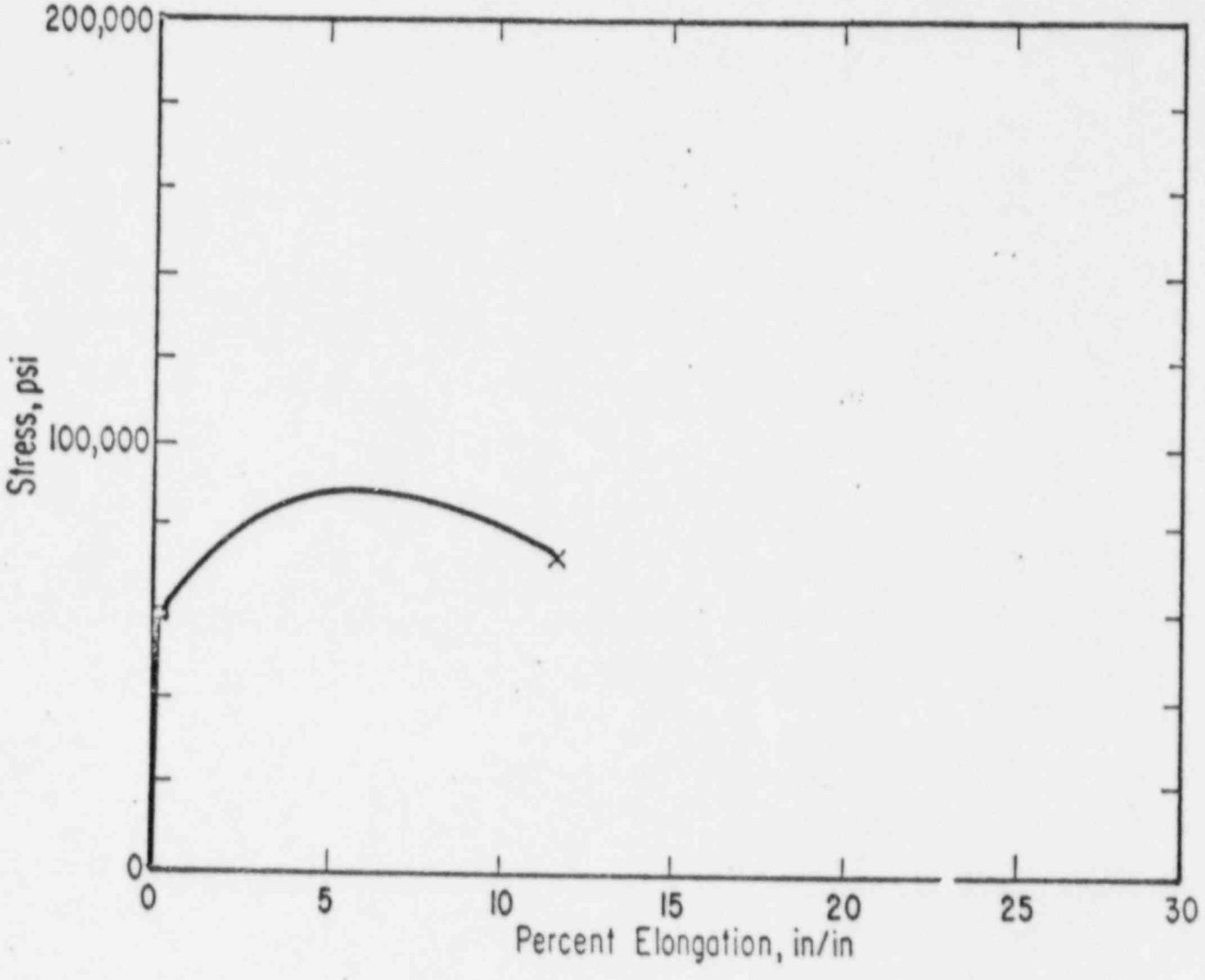

FIGURE 27. STRESS-STRAIN CURVE FOR IRRADIATED BASE-METAL PLATE A9811 (SPECIMEN A1) TESTED AT 550 F

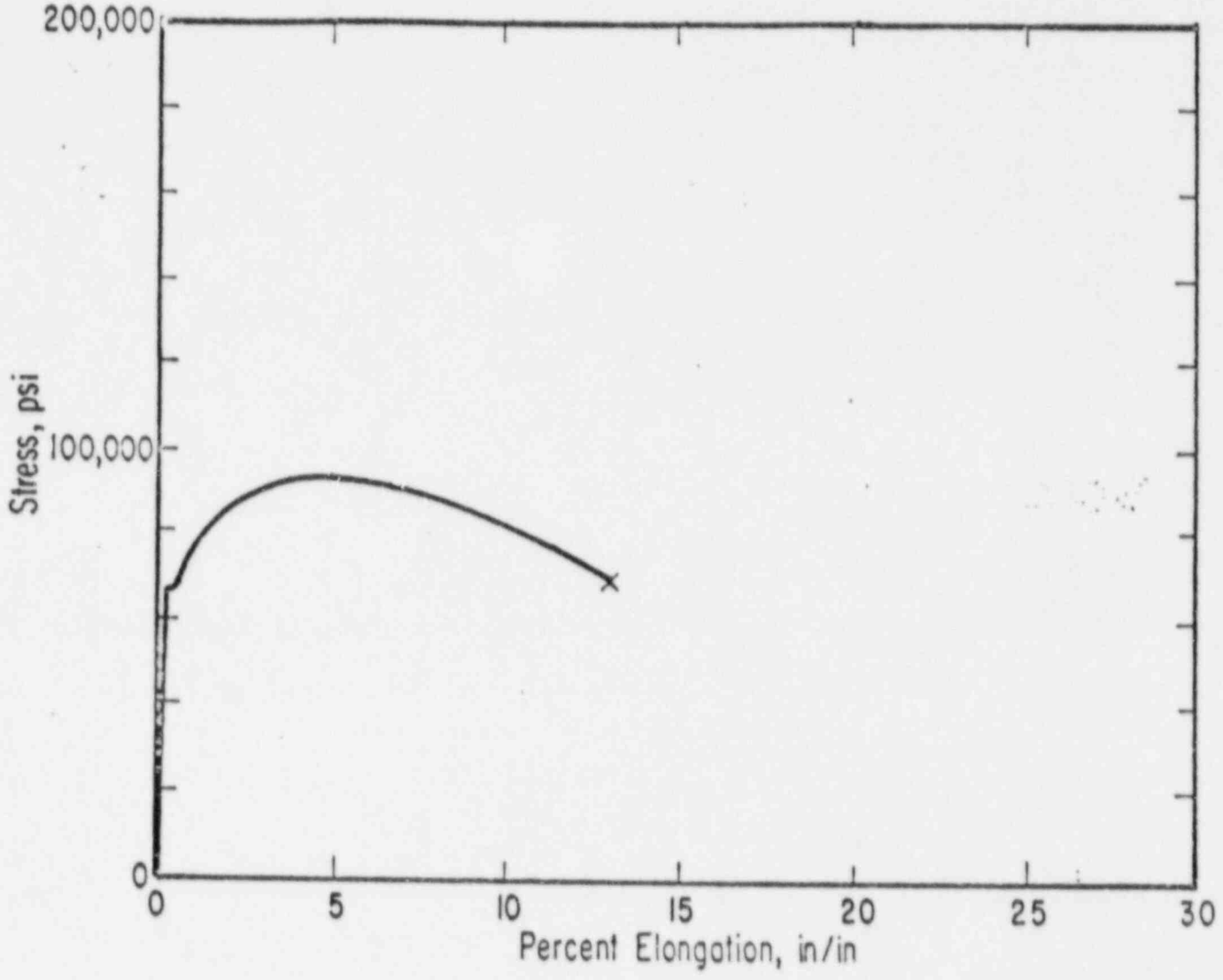

FIGURE 29. STRESS-STRAIN CURVE FOR IRRADIATED BASE-METAL PLATE C1423 (SPECIMEN C1) TESTED AT 550 F

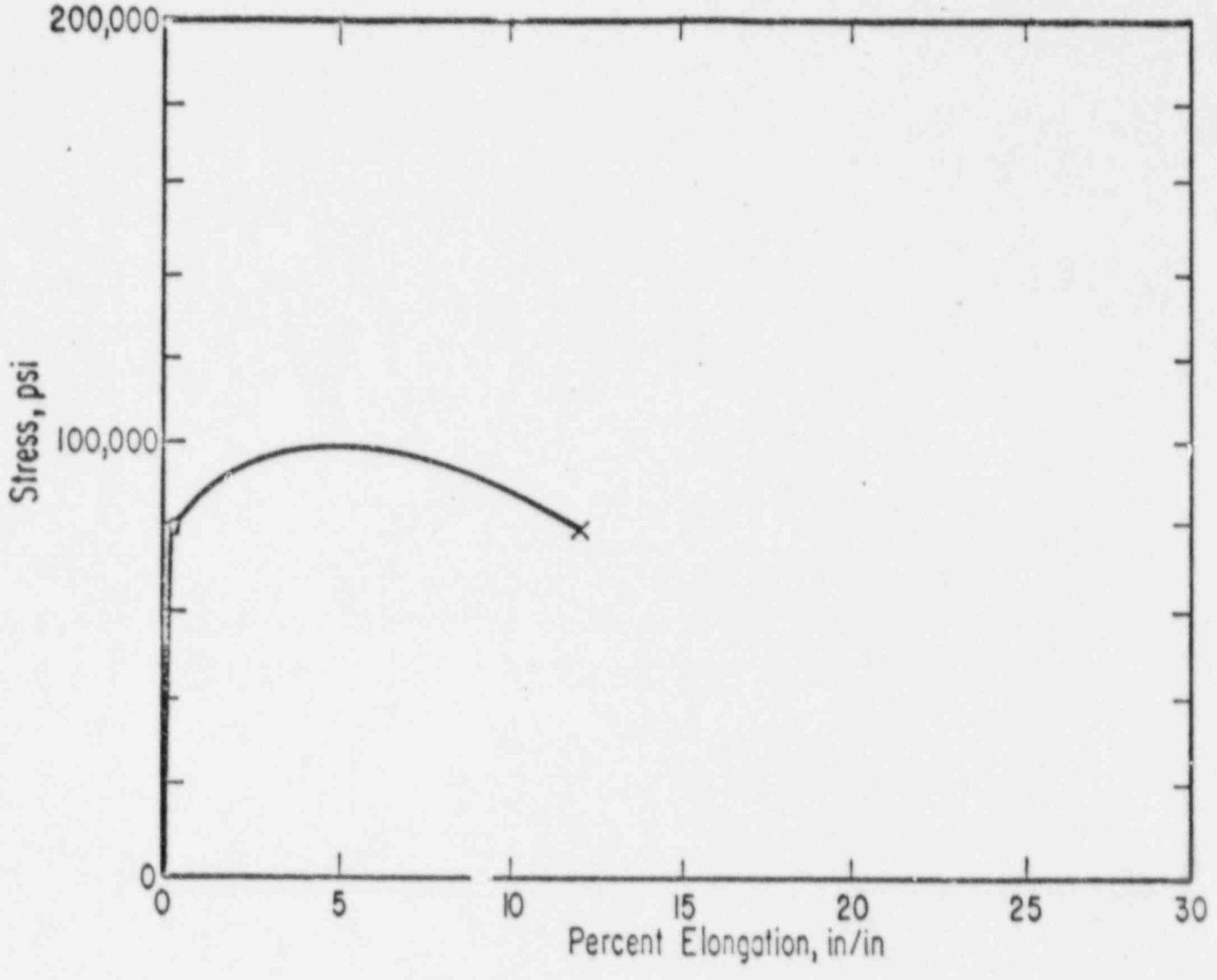

FIGURE 30. STRESS-STRAIN CURVE FOR WELD METAL (SPECIMEN WW1) TESTED AT 550 F

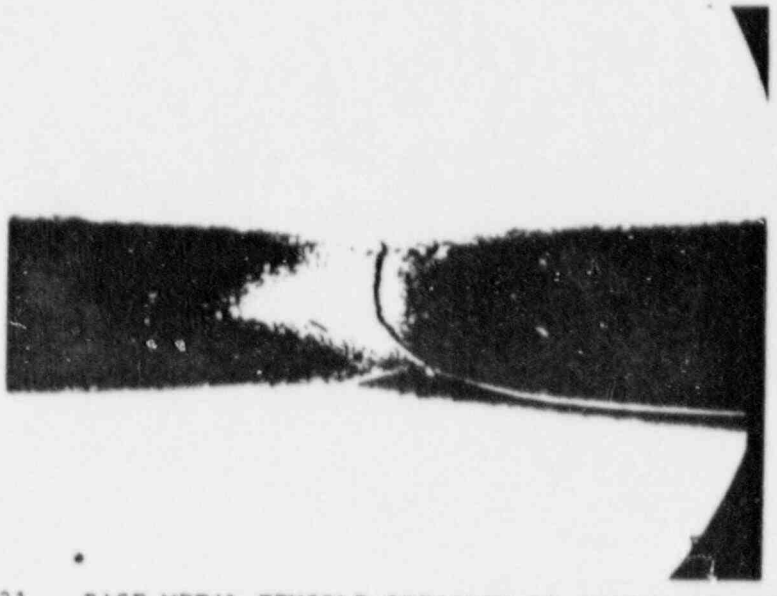

FIGURE 31. BASE METAL TENSILE SPECIMEN A3 TESTED AT -180 F

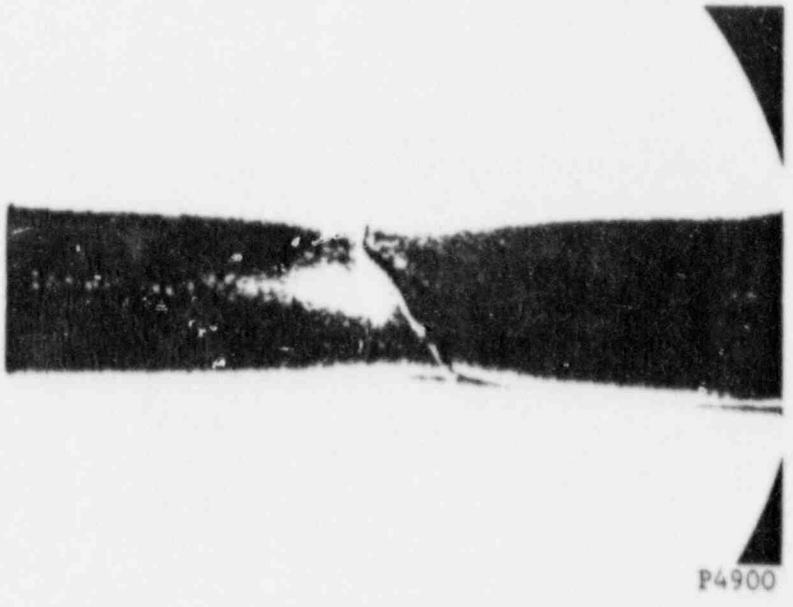

P4900

FIGURE 32. BASE METAL TENSILE SPECIMEN A2 TESTED AT -110 F

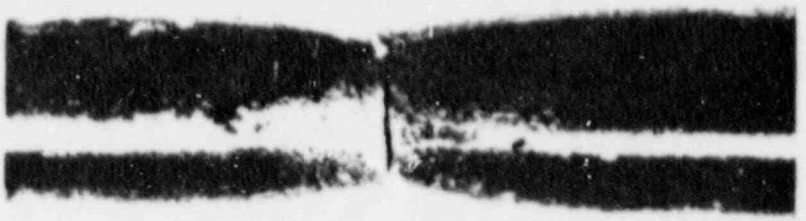

P4805

FIGURE 33. BASE METAL TENSILE SPECIMEN A4 TESTED AT 75 F

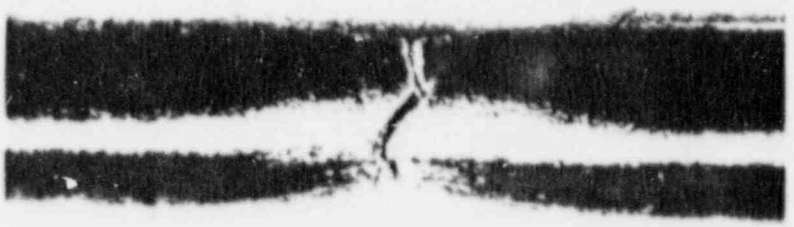

P4804

FIGURE 34. BASE METAL TENSILE SPECIMEN A1 TESTED AT 550 F

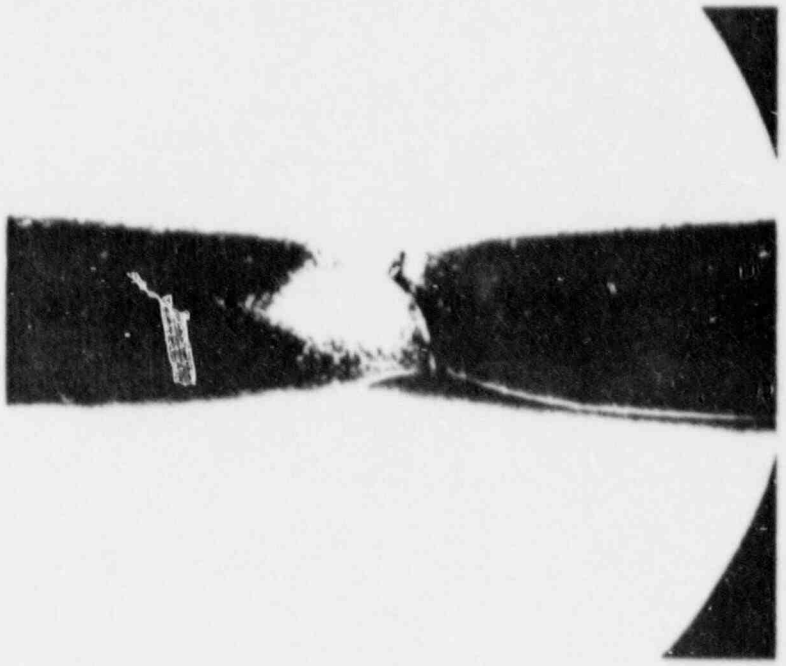

P4807

FIGURE 35. BASE METAL TENSILE SPECIMEN C2 TESTED AT 75 F

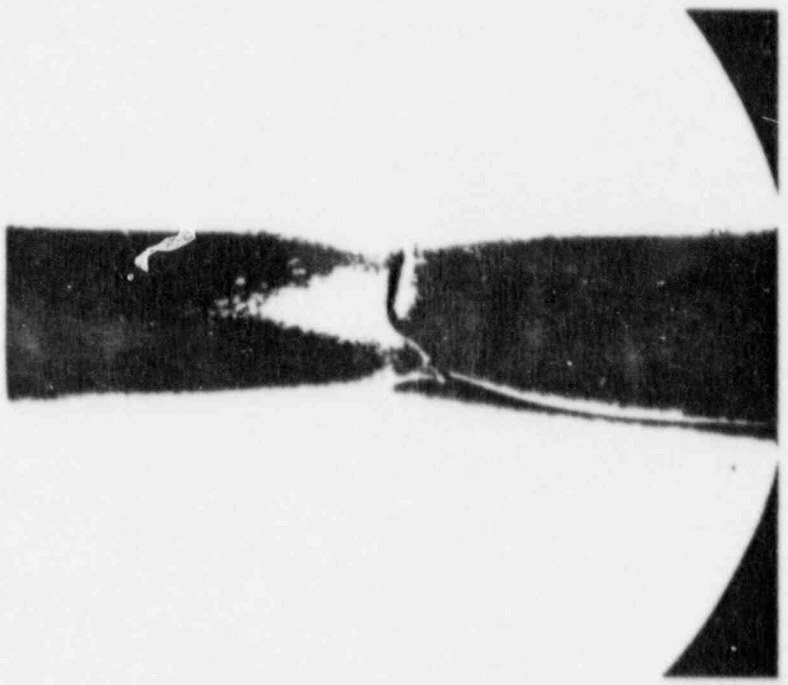

P4806

FIGURE 36. BASE METAL TENSILE SPECIMEN C1 TESTED AT 550 F

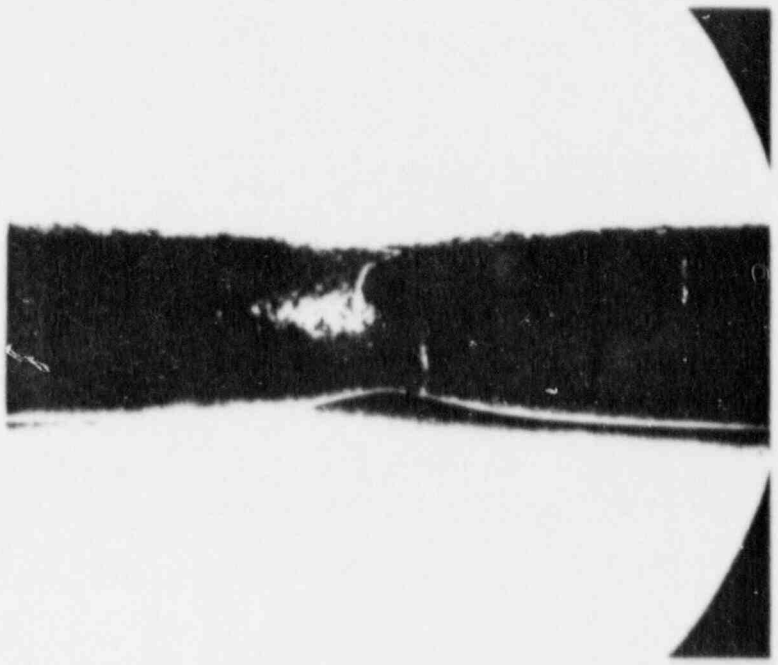

P4809

FIGURE 37. WELD METAL TENSILE SPECIMEN WW1 TESTED AT 550 F

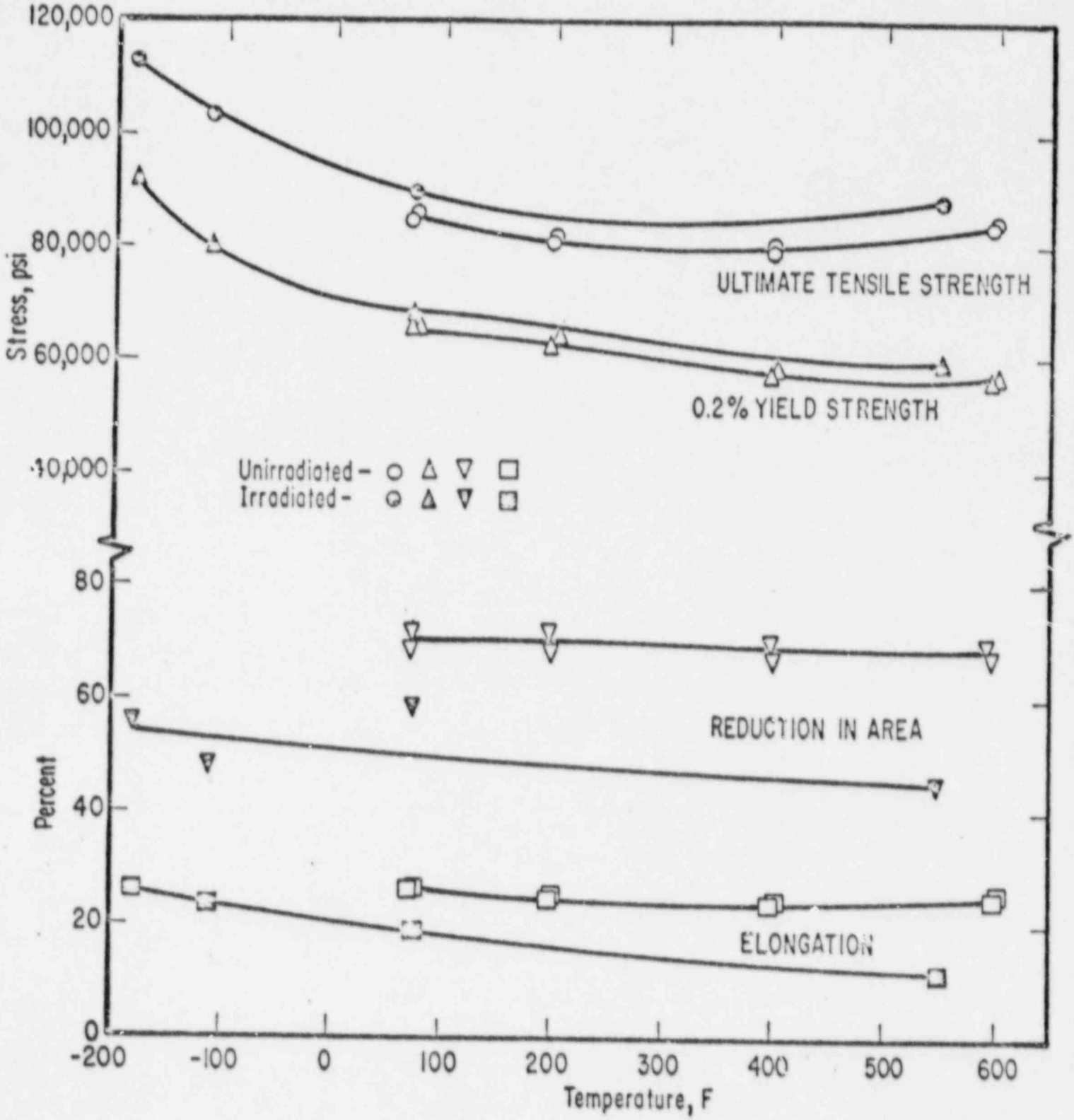

FIGURE 38. UNIRRADIATED AND IRRADIATED TENSILE PROPERTIES FOR THE WEP POINT BEACH UNIT NO. 1 REACTOR PRESSURE VESSEL SHELL PLATE A9811

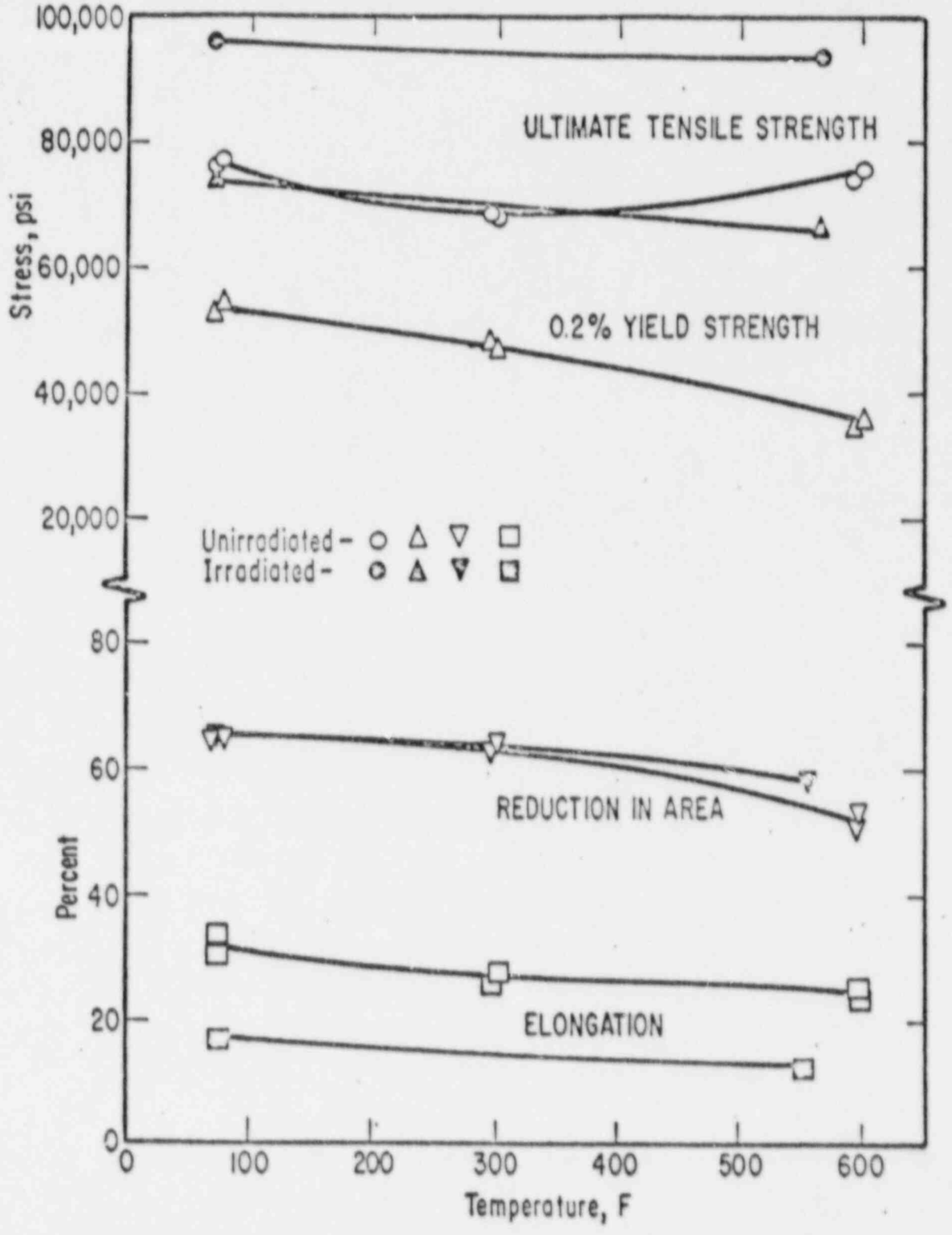

FIGURE 39. UNIRRADIATED AND IRRADIATED TENSILE PROPERTIES FOR THE WEP POINT BEACH UNIT NO. 1 REACTOR PRESSURE VESSEL SHELL PLATE C1423

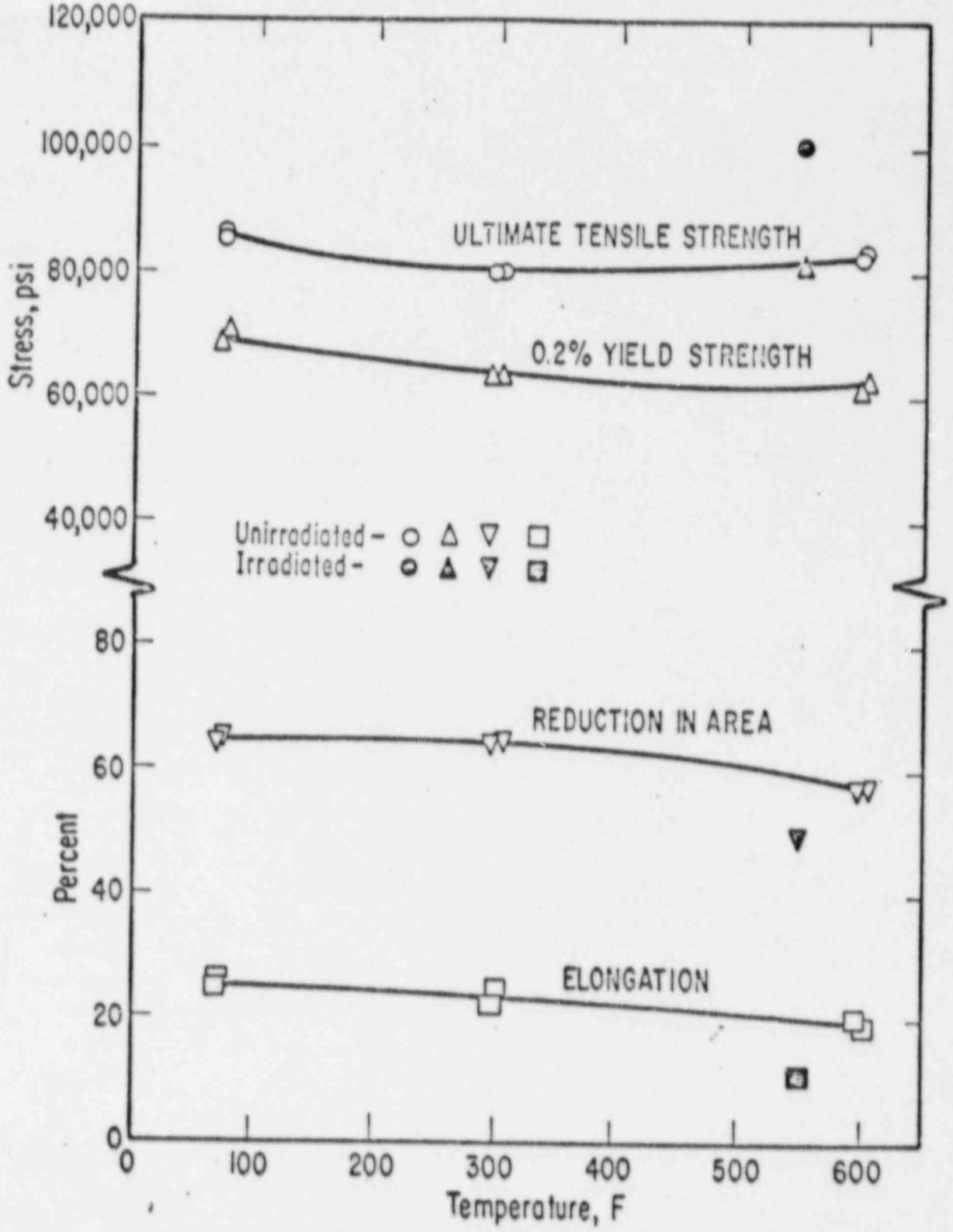

FIGURE 40. UNIRRADIATED AND IRRADIATED TENSILE PROPERTIES FOR THE WEP POINT BEACH UNIT NO. 1 REACTOR PRESSURE VESSEL WELD METAL

Fracture Toughness Tests

A typical WOL load-deflection curve is shown in Figure 41. The curve shown is for specimen C1 which was tested at -149 F. The curve meets the ASTM requirements for a valid fracture toughness test. If substantial plastic deformation had occurred before fracture, the plot would be curved rather than a straight line. The testing of the nine irradiated WOL specimens resulted in the determination of nine valid K_{Ic} fracture toughness values. The term "valid" refers to compliance with the ASTM E399-70T recommendation[19] that

$$B \geq 2.5 \left(\frac{K_{Ic}}{\sigma_{ys}}\right)^2 ,$$

where B is specimen thickness (1 in. for these specimens) and σ_{ys} is the tensile yield strength. The results of these WOL specimen tests are listed in Table 12. The crack length used in the K_{Ic} calculation was measured on the fracture surface after the test was completed. Three measurements were taken and averaged to determine the average crack length of each specimen. Views of the fracture surfaces of the irradiated specimens are shown in Figures 42 through 50. The curved line across each specimen half is the front of the crack introduced before irradiation by fatigue precracking.

The equation used to calculate K_{Ic} is

$$K_{Ic} = \frac{P}{B\sqrt{W}} \; f(a/W) ,$$

where

- a = the original crack length, from the load centerline to the average extent of the fatigue crack
- B = specimen thickness
- P = load at fracture,
- W = specimen depth, from load centerline to specimen end
- f(a/W) = dimensionless stress-intensity factor that empirically relates the applied load to the stress state at the fatigue crack.

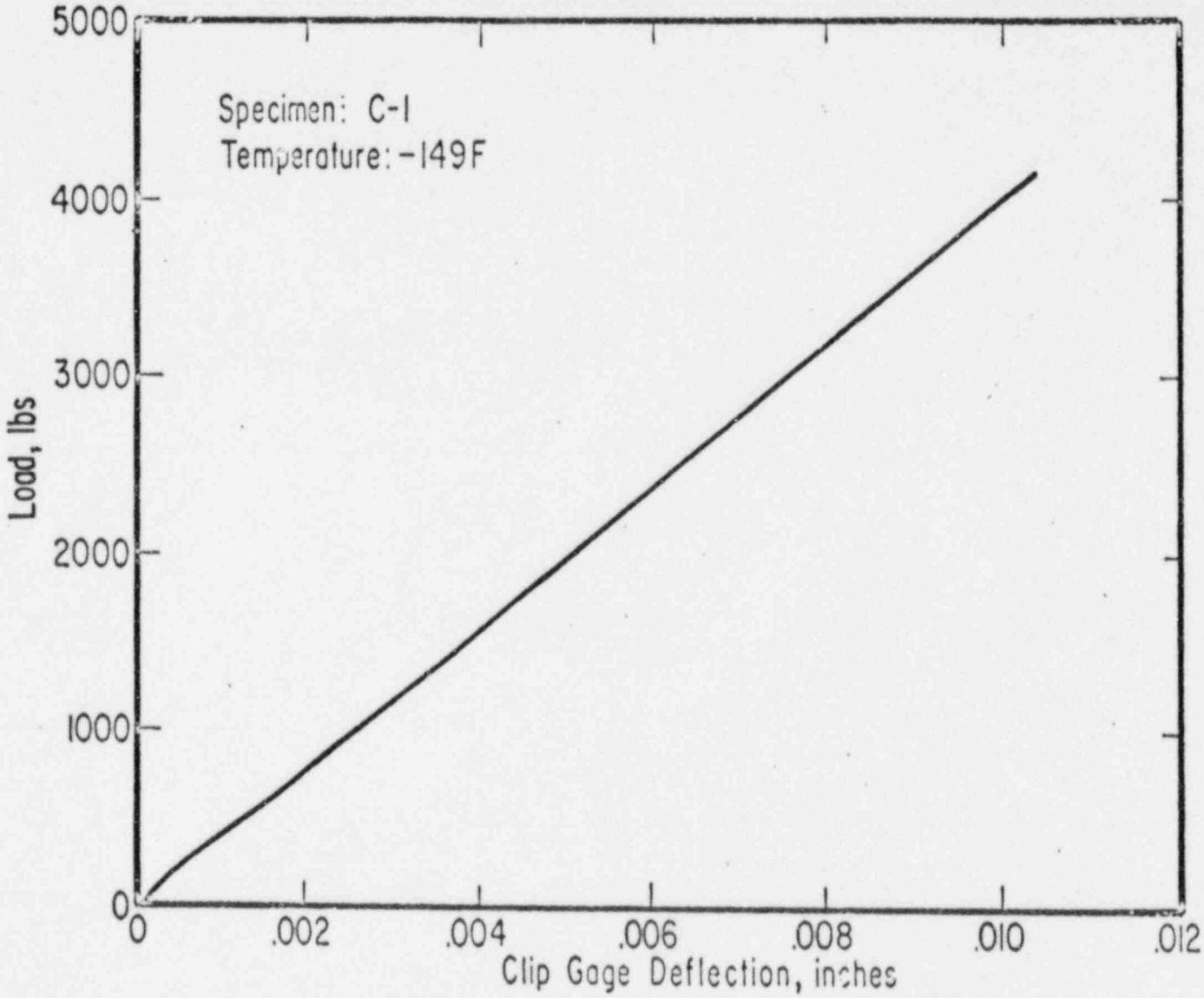

FIGURE 41. TYPICAL LOAD-DEFLECTION CURVE OBTAINED DURING A WOL TEST

TABLE 12. RESULTS OF WOL SPECIMEN TESTS OF BASE METAL AND WELD METAL

Specimen	Test Temperature, F	Average Crack Length (a), in.	Depth (W) in.	Fracture Load (P), lb	K_{Ic} psi $\sqrt{in.}$
A3	-180	0.543	1.135	3620	30,600
A1	-150	0.533	1.130	4690	39,100
A4	-150	0.540	1.128	4140	35,200
A2	-110	0.571	1.154	4680	41,200
C1	-149	0.546	1.129	4150	35,800
C3	-130	0.561	1.164	3980	33,600
C2	-108	0.536	1.136	5380	44,700
WW1	-90	0.563	1.150	3970	34,500
WW2	-45	0.549	1.126	4840	42,300

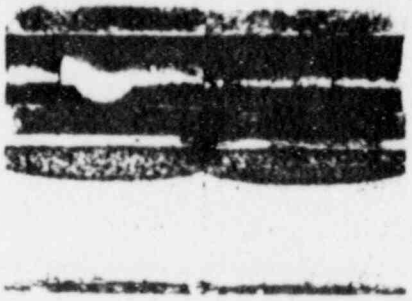

P4886

FIGURE 42. BASE METAL WOL SPECIMEN A3 TESTED AT -180 F

P4889

FIGURE 43. BASE METAL WOL SPECIMEN A1 TESTED AT -150 F

P4882

FIGURE 44. BASE METAL WOL SPECIMEN A4 TESTED AT -150 F

P4890

FIGURE 45. BASE METAL WOL SPECIMEN A2 TESTED AT -110 F

P4888

FIGURE 46. BASE METAL WOL SPECIMEN C1 TESTED AT -149 F

P4883

FIGURE 47. BASE METAL WOL SPECIMEN C3 TESTED AT -130 F

P4884

FIGURE 48. BASE METAL WOL SPECIMEN C2 TESTED AT -108 F

P4887

FIGURE 49. WELD METAL WOL SPECIMEN WW1 TESTED AT -90 F

P4885

FIGURE 50. WELD METAL SPECIMEN WW2 TESTED AT -45 F

The selection of test temperatures was based on the results of the impact specimen tests. In the surveillance program outlined in WCAP-7513 it is recommended that the first WOL specimen of each material be tested at a temperature of -200 F plus the nil ductility transition temperature shift that was measured by the impact specimen tests. For the A-series base metal the recommended temperature was therefore -110 F (-200 + 90); for the C series, -150 F; and for the weld metal series -90 F. The recommended temperatures were used as the initial test for each series.

The results of the WOL specimen tests of the three irradiated materials are shown in Figure 51 in the form of K_{Ic} versus temperature. The preirradiation values are not shown, as they are not reported in WCAP 7513. The fracture toughness in general increases as temperatures increases for each of the three materials. The fracture toughness values for the two base plate materials are in the same general range for a particular temperature, with the weld metal values lower than the two base plate materials. As can be seen in the figure, there is some scatter in the data. This is shown by the two tests for base metal plate A9811 at -150 F, which yielded fracture toughness values of 40,000 and 44,500 psi $\sqrt{in}$. This amount of scatter in the fracture toughness values for this type of pressure vessel steel is not unusual. However, it indicates that caution should be used in making conclusions based on a limited number of tests as in the case of the present program.

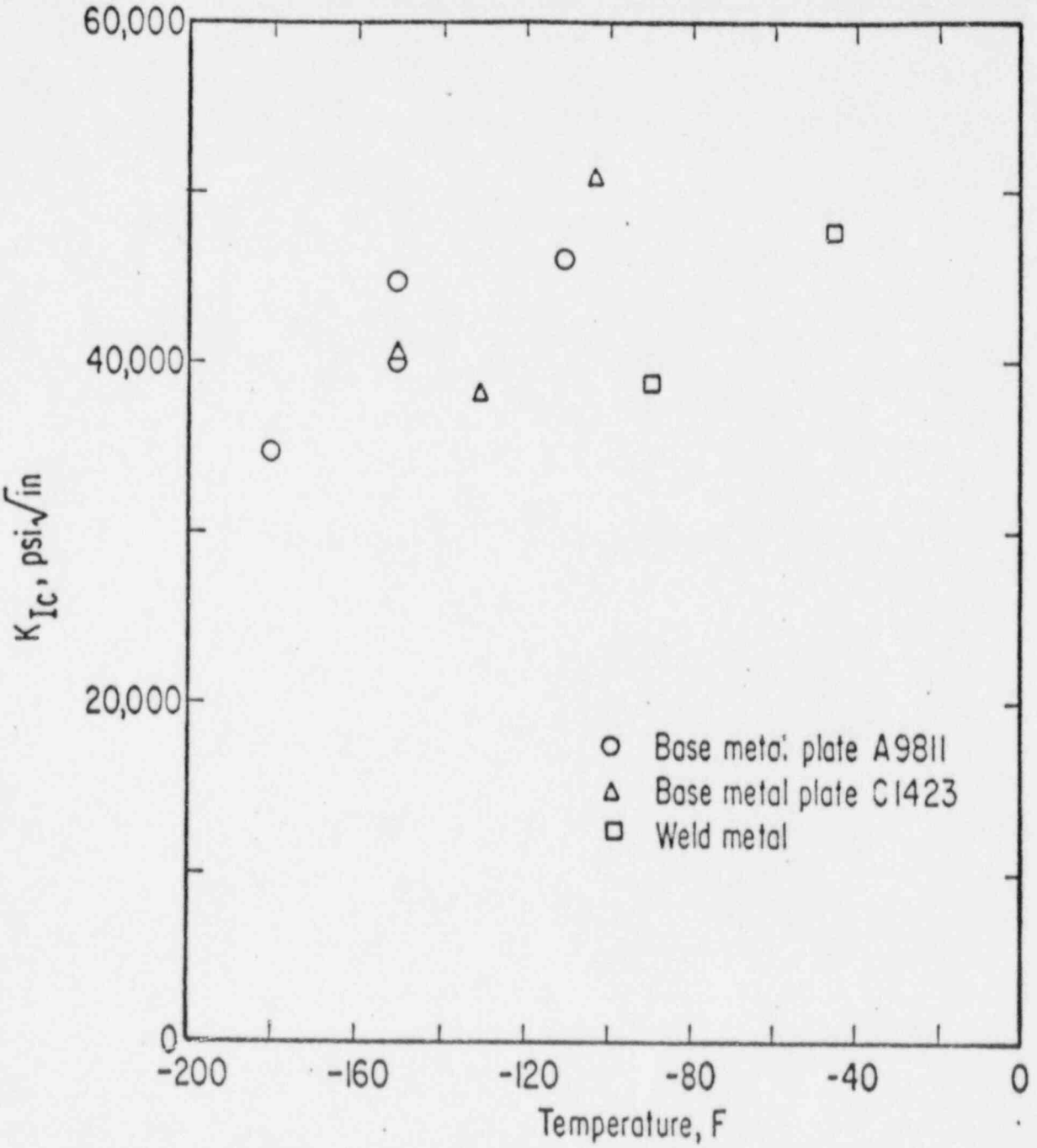

FIGURE 51. FRACTURE TOUGHNESS OF THREE IRRADIATED MATERIALS AS A FUNCTION OF TEMPERATURE

CONCLUSIONS

The maximum irradiation temperature of the surveillance capsule during irradiation did not exceed 590 F. The neutron fluence experienced by the capsule was 3.58×10^{18} nvt (>1 Mev) which was attained after 1.49 years equivalent full-power years of operation. This is equivalent to a maximum fluence of 1.11×10^{18} nvt (>1 Mev) for the pressure vessel after 1.49 equivalent full-power years. For a pressure-vessel life of 40 years operation at an 80 percent load factor (32 equivalent full-power years), the maximum fluence experienced by the pressure vessel would therefore be predicted to be 2.38×10^{19} nvt (>1 Mev).

Tensile tests were conducted on the two base metal plates and the weld metal. The yield strength and ultimate tensile strength of all three materials increased at 550 F due to irradiation. The corresponding ductilities (reduction in area and total elongation) decreased in all three materials at 550 F, except for the reduction in area of base metal plate C1423 which increased slightly.

Fracture toughness tests were conducted on the two base metal plates and the weld metal in the general temperature range of -180 F to -45 F. The plane strain fracture toughness for these materials was found to be in the general range of 30,600 to 44,700 psi $\sqrt{\text{in.}}$, with the fracture toughness genera'ly increasing with increasing temperature.

The shift in the nil ductility transition temperature (NDTT) was determined for the two base metal plates, heat-affected zone metal, and weld metal. The greatest NDTT shift due to irradiation was found to occur in the weld metal, which had a shift of +110 F. The highest NDTT after irradiation was the +65 F value determined for the weld metal. The NDTT shifts observed for the pressure vessel materials in the present investigation fit within a trend band for NDTT values from similar surveillance programs of other reactors using the same pressure-vessel material, SA302 Grade B.

The results obtained in this investigation show that the pressure vessel base metal, heat-affected zone metal, and weld metal mechanical properties are changing with irradiation in a manner consistent with the changes expected when the pressure vessel was fabricated and put into service.

REFERENCES

(1) Reuther, T. C., and Zwilsky, K. M., "The Effects of Neutron Irradiation on the Toughness and Ductility of Steels", in Proceedings of Toward Improved Ductility and Toughness Symposium, published by Iron and Steel Institute of Japan (October, 1971) pp 289-319.

(2) Steele, L. E., "Major Factors Affecting Neutron Irradiation Embrittlement of Pressure-Vessel Steels and Weldments", NRL Report 7176 (October 30, 1970).

(3) Berggren, R. G., "Critical Factors in the Interpretation of Radiation Effects on the Mechanical Properties of Structural Metals", Welding Research Council Bulletin 87, 1 (1963).

(4) Witt, F. J., "Heavy-Section Steel Technology Program Semiannual Progress Report for Period Ending February 29, 1972", ORNL Report 4816 (October, 1972).

(5) Alger, J. V., and Skupien, L. M., "Neutron Radiation Embrittlement at 500 and 650 F of Reactor Pressure Vessel Steels", in Materials in Nuclear Applications, American Society for Testing and Materials Special Technical Publication 276 (1960), pp 116-134.

(6) Porter, L. F., "Radiation Effects in Steel", in Materials in Nuclear Applications, American Society for Testing and Materials Special Technical Publication 276 (1960), pp 147-196.

(7) Steele, L. E., and Hawthorne, J. R., "New Information on Neutron Embrittlement and Embrittlement Relief of Reactor Pressure Vessel Steels", American Society for Testing and Materials, Special Technical Publication 381 (1964).

(8) ASTM Designation E185-70, "Surveillance Tests on Structural Materials in Nuclear Reactors", Book of ASTM Standards, Part 31 (1972), pp 565-569.

(9) Yanichko, S. E., "Wisconsin Michigan Power Co. Point Beach Unit No. 1 Reactor Vessel Radiation Surveillance Program, WCAP 7513 (June, 1970).

(10) Potapovs, U., and Hawthorne, J. R., "The Effect of Residual Elements on 550 F Irradiation Response of Selected Pressure Vessel Steels and Weldments", Nucl Appl, 6, 27-46 (1969).

(11) Hawthorne, J. R., and Fortner, E., "Radiation and Temper Embrittlement Processes in Advanced Reactor Weld Metals", J. Eng. Indus., Trans. ASME, 94, 807-814 (1972).

(12) Serpan, C. Z., et al., "Radiation Damage Surveillance of Power Reactor Pressure Vessels", NRL Report 6349 (1966).

(13) Barton, J. R., and Wylie, R. D., "Development of Nondestructive Testing Instrumentation for Reactor Pressure Vessels", SwRI-1243-14 (1964).

(14) Steele, L. E., et al., "Neutron Irradiation Embrittlement of Several Higher Strength Steels", NRL Report 6419 (September 7, 1966).

(15) ASTM Designation E208-69, "Conducting Drop-Weight Test to Determine Nil Ductility Transition Temperature of Ferritic Steels", Book of ASTM Standards, Part 31 (1972), pp 594-613.

(16) Pellini, W. S., and Puzak, P. P., "Fracture Analysis Diagram Procedures for the Fracture-Safe Engineering Design of Steel Structures", Bulletin 88, Welding Research Council (May, 1963).

(17) Loss, F. J., Hawthorne, J. R., and Serpan, C. Z., Jr., "A Reassessment of Fracture-Safe Operating Criteria for Reactor Vessel Steels Based on Charpy-V Performance", NRL Report 7152 (September 8, 1970).

(18) Sailors, R. H., and Corten, H. T., "Relationship Between Material Fracture Toughness Using Fracture Mechanics and Transition Temperature Tests", in Fracture Toughness, ASTM Special Technical Publication 514 (1972) pp 164-191.

(19) ASTM Designation E399-70T, "Plane-Strain Fracture Toughness of Metallic Materials", Book of ASTM Standards, Part 31 (1970), pp 911-927.

(20) ASTM Designation E320-69T, "Radiochemical Determination of Cesium-137 in Nuclear Fuel Solutions", Book of ASTM Standards, Part 30 (1970), pp 1004-1009.

(21) ASTM Designation E261-70, "Measuring Neutron Flux by Radioactivation Techniques", Book of ASTM Standards, Part 30 (1970), pp 762-772.

(22) ASTM Designation E262-70, "Measuring Thermal-Neutron Flux by Radioactivation Techniques", Book of ASTM Standards, Part 30 (1970), pp 773-780.

(23) ASTM Designation E263-70, "Measuring Fast-Neutron Flux by Radioactivation of Iron", Book of ASTM Standards, Part 30 (1970), pp 781-783.

(24) ASTM Designation E264-70, "Measuring Fast-Neutron Flux by Radioactivation of Nickel", Book of ASTM Standards, Part 30 (1970), pp 787-791.

(25) ASTM Designation E343-67T, "Fast-Neutron Flux by Activation of Molybdenum-99 Activity from Uranium-238 Fission", Book of ASTM Standards, Part 30 (1970), pp 1078-1084.

(26) ASTM Designation E393-69T, "Measuring Fast-Neutron Flux for Analysis for Barium-140 Produced by Uranium-238 Fission", Book of ASTM Standards, Part 30 (1970), pp 1174-1180.

(27) ASTM Designation E23-66, "Notched Bar Impact Testing of Metallic Materials", Book of ASTM Standards, Part 31 (1970), pp 271-285.

(28) ASTM Designation A370-71, "Mechanical Testing of Steel Products", Book of ASTM Standards, Part 31 (1971), p 45.

(29) Serpan, C. Z., Jr., and Watson, H. E., "Mechanical Property and Neutron Spectral Analyses of the Big Rock Point Reactor Pressure Vessel", Nucl. Eng. Design, 11, 393-415 (1970).

(30) Serpan, C. Z., Jr., and Hawthorne, J. R., "Yankee Reactor Pressure-Vessel Surveillance: Notch Ductility Performance of Vessel Steel and Maximum Service Fluence Determined from Exposure During Cores II, III, and IV", NRL Report 6616 (September 29, 1967).

(31) Brandt, F. A., "Humboldt Bay Power Plant Unit No. 3 Reactor Vessel Steel Surveillance Program", GECR-5492 (May, 1967).

(32) Ireland, D. R., and Norris, E. B., "Influence of Neutron Irradiation on the Properties of Steels and Weld Typical of the ERR Pressure Vessel After Two Power Years Operation", SwRI-1228-P-9-15 (March, 1968).

(33) Sterne, R. H., Jr., and Steele, L. E., "Steels for Commercial Nuclear Power Reactor Pressure Vessels", Nucl. Eng. Design, 10, 259-307 (1969).

(34) "Analysis of First Surveillance Material Capsule from San Onofre Unit I", Southern California Edison Company (July, 1971).

(35) Perrin, J. S., Sheckherd, J. W., and Scotti, V. G., "Examination and Evaluation of Capsule F for the Connecticut Yankee Reactor Pressure-Vessel Surveillance Program", Final Report to Connecticut Yankee Atomic Power Company (March 30, 1972).

(36) Private Communication from J. J. Zach and G. A. Reed, Point Beach Nuclear Power Plant (March 8, 1973).

APPENDIX A

PRESSURE VESSEL MATERIAL

APPENDIX A*

PRESSURE VESSEL MATERIAL

Babcock and Wilcox Co. supplied sections of SA302 Grade B steel plate to Westinghouse for the reactor vessel surveillance program. These sections represented material from the 6-3/4-inch-thick intermediate shell course plate A9811 and the 6-3/4-inch-thick lower shell course plate C1423 used in the WEP pressure vessel. In addition, a weldment made from sections of the two plates was also supplied by Babcock and Wilcox Co. The plates were produced for Babcock and Wilcox Co. by the Lukens Steel Co. The chemical analyses and heat treatment history of the plate material follows.

a. Chemical Analyses

	Percent		
Element	Plate A9811	Plate C1423	Weld Metal
C	0.19	0.21	0.09
Mn	1.42	1.37	1.47
P	0.010	0.014	0.019
S	0.020	0.019	0.024
Si	0.25	0.25	0.49
Mo	0.48	0.46	0.39
Cu	- -	- -	0.18
Ni	- -	- -	0.57
Cr	- -	- -	0.13
Al	- -	- -	0.035
N_2	- -	- -	0.016
V	- -	- -	0.001
Sn	- -	- -	0.004
Ti	- -	- -	0.001
As	- -	- -	0.004

*The information in this Appendix is from Yanichko, S.E., "Wisconsin Michigan Power Co. Point Beach Unit No. 1 Reactor Vessel Radiation Surveillance Program", WCAP-7513, Westinghouse Electric Corporation (June, 1970).

Co	- -	- -	0.001*
Zr	- -	- -	0.001*
Sb	- -	- -	0.001*
Zn	- -	- -	0.001*
B	- -	- -	0.003*

*Not detected. The number indicates the minimum limit of detection.

b. Heat Treatment

Plate A9811 Heated at 1650 F, 7 hours, water-quenched
Tempered at 1225 F, 7 hours, aircooled
Stress-relieved at 1125 F, 11-1/4 hours, furnace-cooled

Plate C1423 Heated at 1650 F, 7 hours, water-quenched
Tempered at 1225 F, 7 hours, aircooled
Stress-relieved at 1125 F, 10-1/2 hours, furnace-cooled

Weldment Stress-relieved at 1125 F, 11-1/4 hours, furnace-cooled

APPENDIX B

CORRELATION MONITOR MATERIAL

APPENDIX B*

CORRELATION MONITOR MATERIAL

The correlation monitor material SA302 Grade B was furnished by the U. S. Steel Corporation through Subcommittee II of ASTM Committee E10 on Radioisotopes and Radiation Effects. The specimens were machined from a 96-inch-wide by 72-inch-long by 6-inch-thick plate which was melted using a fine grain practice and a transverse-to-longitudinal rolling ratio of 1:1.

a. Chemical Analyses (percent)

C	Mn	P	S	Mo	Si
0.24	1.34	0.011	0.023	0.51	0.23

b. Heat Treatment

The U. S. Steel material was heat treated at the U. S. Steel Homestead District Works as follows:

The 6-inch-thick plate was charged into a furnace operating at 1100 F heated at a maximum rate of 63 F per hour, to 1650 F, held at temperature for four hours, and water-quenched to 300 F. The plate was then recharged into a furnace operating at 700 to 750 F and heated at a maximum rate of 63 F per hour to 1200 F for six hours.

---

*The information in this Appendix is from Yanichko, S. E., "Wisconsin Michigan Power Company Point Beach Unit No. 1 Reactor Vessel Radiation Surveillance Program", WCAP-7513, Westinghouse Electric Corporation (June, 1970).

APPENDIX C

INSTRUMENTED CHARPY EXAMINATION

APPENDIX C

INSTRUMENTED CHARPY EXAMINATION

SUMMARY

The instrumented Charpy technique was applied to the impact specimen evaluations of the following irradiated pressure vessel materials: two different base metal plates, weld metal, heat-affected zone (HAZ) metal, and ASTM correlation-monitor metal. Because of the limited number of specimens and their need in establishing other parameters such as the upper shelf energy and the NDTT, there were insufficient data available for a complete analysis of the effects of radiation on these materials. However, load-time traces were obtained for all 48 impact specimens. These traces show the change in impact behavior as a function of temperature for all five materials tested.

INTRODUCTION

The radiation embrittlement of an operating nuclear pressure vessel is determined by the accelerated irradiation of the original materials as part of a surveillance program. The lifetime of the pressure vessel will depend on the radiation-induced shift in the ductile-brittle transition temperature as measured by the Charpy V-notch impact test. Although a few fracture-toughness specimens are also included in some surveillance programs, their number is very limited and the present safety criteria are primarily based on Charpy impact behavior.

The value of irradiated Charpy impact specimens, particularly in present surveillance programs, can be considerably enhanced by the use of the instrumented Charpy test. The instrumented Charpy test provides a valuable link between the transition-temperature approach and the fracture-mechanics approach to fracture toughness. A knowledge of the effect of radiation on key metallurgical fracture parameters can be used to accurately predict (1) the radiation-induced shift in the ductile-brittle transition temperature, and (2) the radiation-induced change in the dynamic fracture toughness, K_{Id}. The results obtained by applying these techniques to the Charpy specimens contained in the first surveillance capsule of the Point Beach Unit No. 1 reactor are presented in this section of the report.

BACKGROUND

There are two approaches to determining the effect of radiation on the fracture toughness of pressure-vessel steels: (1) the shift in the ductile-brittle transition temperature (DBTT)*, and (2) the change in the fracture toughness (either the static fracture toughness K_{Ic} or the dynamic fracture toughness K_{Id}). The modern theories of the fracture define key metallurgical fracture parameters such as friction stress, grain size, grain-size dependence of the yield stress, and surface energy or plastic work of microcrack propagation. The effect of radiation on most of these metallurgical fracture parameters has been previously studied, but until recently, the results had not been directly linked with the radiation-induced change in fracture toughness. This recent work established the relationships between the key metallurgical fracture parameters and the DBTT and K_{Ic}[(1)]**.

The instrumented Charpy test is an excellent tool for determination of the effects of radiation on the key metallurgical fracture parameters. This test provides load-time information in addition to the energy absorbed. The loads involved during impact are obtained by instrumenting the Charpy striker with strain gages so that the striker is essentially a load cell. The details of this technique have been reported previously[(2)].

The additional information obtained from the instrumented Charpy test is the general yield load, P_{GY} (plastic yielding across the entire cross section of the Charpy specimen), the maximum load, P_{max}, the brittle fracture load, P_F, and the time to brittle fracture (see Figure C-1). Also, the area under the load-time curve corresponds to the total energy absorbed, which is the only data obtained in a normal uninstrumented Charpy test. The instrumented test, however, allows separation of the energy absorbed into (1) the energy required to initiate ductile or brittle fracture (premaximum load energy), (2) the energy required for ductile tearing (postmaximum load energy), and (3) the energy associated with shear lip formation (postbrittle fracture energy), as shown in Figure C-1.

---

* The DBTT should not be confused with the nil ductility transition temperature (NDTT), which is defined by a specific type of test as described in ASTM E208.

**References at the end of this Appendix.

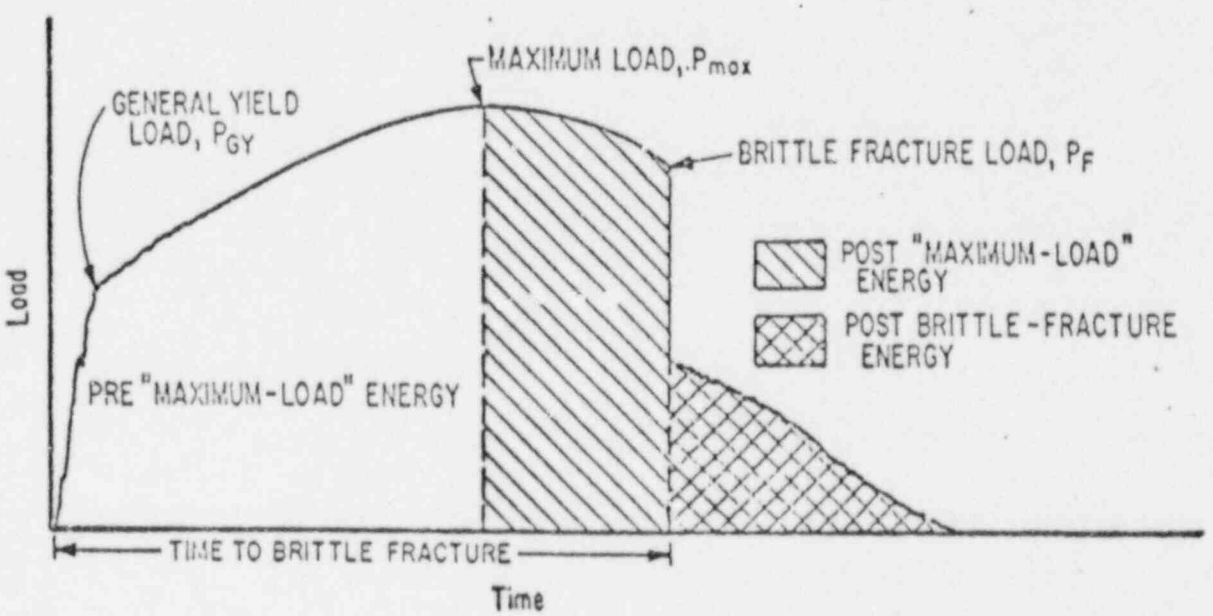

FIGURE C-1. AN IDEALIZED LOAD-TIME HISTORY FOR A CHARPY IMPACT TEST

In a normal Charpy impact study, the energy absorbed is determined as a function of temperature to obtain the Charpy impact curve and the ductile-brittle transition temperature (DBTT). The instrumented Charpy test also gives the information shown in Figure C-1 as a function of temperature, as shown by the example in Figure C-2. Various investigators[3-6] have developed theories that permit a detailed analysis of the load-temperature diagram. This diagram can be divided into four regions of fracture behavior, as shown in Figure C-2. In each region different fracture parameters are involved[2]. Extended discussions of these fracture parameters can be found in the references indicated above.

In general, the key metallurgical fracture parameters for radiation damage studies are the cleavage fracture stress, σ_f^*, and the yield strength σ_y. Both of these parameters and the temperature sensitivity of σ_y can be derived from the results of the instrumented Charpy tests. The determination of the cleavage fracture stress σ_f^*, requires an evaluation of P_{GY} at the temperature where P_F is 80 percent of P_{GY}. The yield strength, σ_y, is calculated from the general yield load, P_{GY}, and is related to the uniaxial tensile strength, σ_{YS}, by the relation[7]:

$$\sigma_{YS} = 33.3\ P_{GY}.$$

This relation is for a standard Charpy V-notch specimen, is dependent on the flank angle of the notch, and assumes Tresca yield criterion.

EXPERIMENTAL PROCEDURES

The general procedures for the instrumented Charpy test are the same as those for the conventional impact test, and are described in Part A of this report. The additional data are obtained through a fairly simple electronic configuration, as shown in the schematic diagram of Figure C-3.

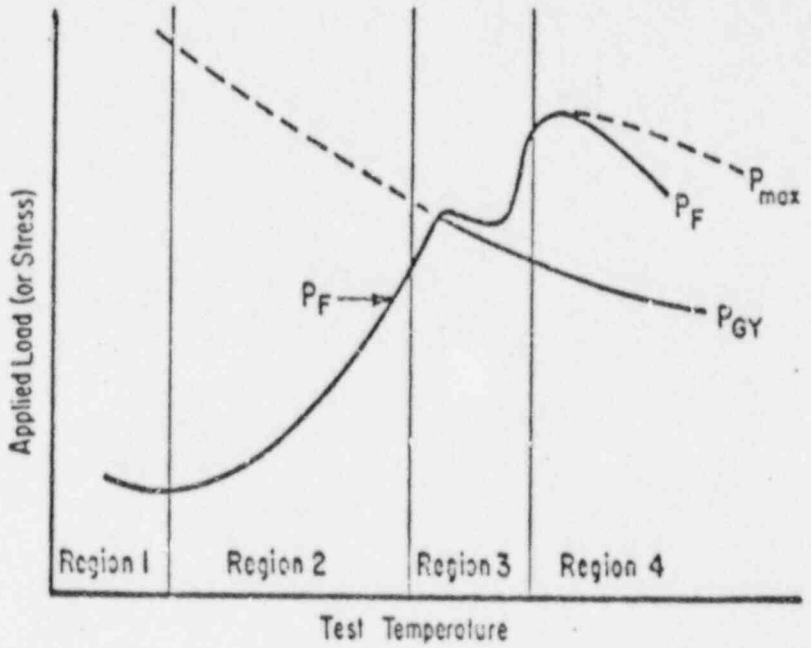

FIGURE C-2. GRAPHICAL ANALYSIS OF CHARPY IMPACT TEST DATA

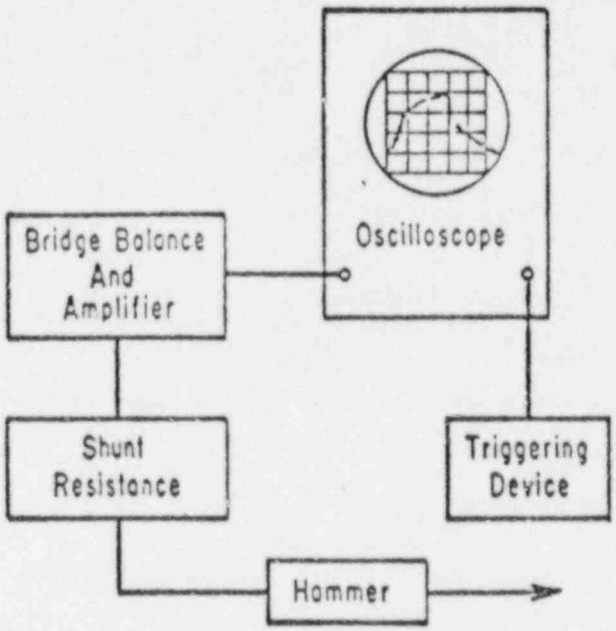

FIGURE C-3. DIAGRAM OF INSTRUMENTATION ASSOCIATED WITH INSTRUMENTED CHARPY TEST

The striker of the impact machine is modified to make it a dynamic load sensor. The modification consists of a four-arm resistance strain gage bridge positioned on the striker to detect the compression loading of the striker during the impact loading of the specimen. The compressive elastic strain signal resulting from the striker contacting the specimen is conditioned by a high-gain dynamic amplifier and the output is photographed as it develops on the cathode ray tube of an oscilloscope. A previously established calibration method[8] is used to convert the oscillograph into a time-load record. The time-load history as a function of test temperature forms the basis for further data analysis.

The oscilloscope is triggered by a solid-state device at the correct time to capture the amplifier output signal. This device consists of a regulated d-c power supply used to operate an incandescent lamp, which acts as a light source. When the Charpy hammer swings by the light source (which is located near the base of the impact tester), the light is reflected from a small metal mirror located on the side of the hammer. The reflected light is detected by a phototransitor which drives the trigger.

RESULTS AND DISCUSSION

The instrumented Charpy tests were conducted following the procedures discussed in Part A of this report. Specimens were tested from five irradiated materials. These were the pressure-vessel base-metal plates A9811, base metal plate C1423, heat-affected zone metal, weld metal, and ASTM correlation monitor material. The results of these tests and the corresponding load-time records are given in Tables C-1 through C-5. The tables list the specimen numbers, test temperature, impact energy, general yield load, and maximum load. It can readily be observed that the features of the load-time or load-deflection traces change as a function of temperature; however, all tests fall into one of the six distinctive notch-bar bending classifications shown in Figure C-4. The pertinent data used in the analysis of each record are the general yield load (P_{GY}), maximum load (P_{max}), and fracture load (P_F). The impact energy values listed in the tables are those normally obtained from the impact machine dial. These values are in excellent agreement with energy values calculated from the area under the load-time curves.

TABLE C-1. INSTRUMENTED CHARPY IMPACT DATA FOR BASE-METAL PLATE A9811

Specimen No.	A2
Test Temperature, F	-65
Impact Energy, ft-lb	4.5
General Yield Load, P_{GY}, lb	
Maximum Load, P_{max}, lb	3310

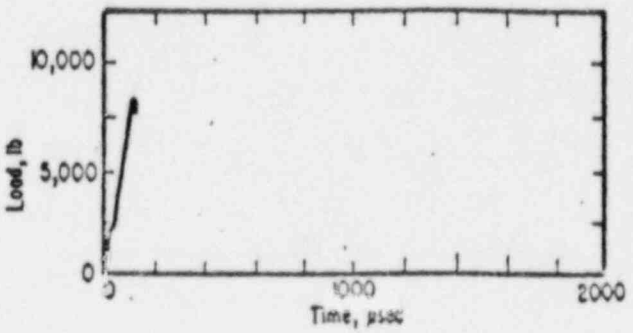

Specimen No.	A5
Test Temperature, F	-25
Impact Energy, ft-lb	5.5
General Yield Load, P_{GY}, lb	
Maximum Load, P_{max}, lb	3360

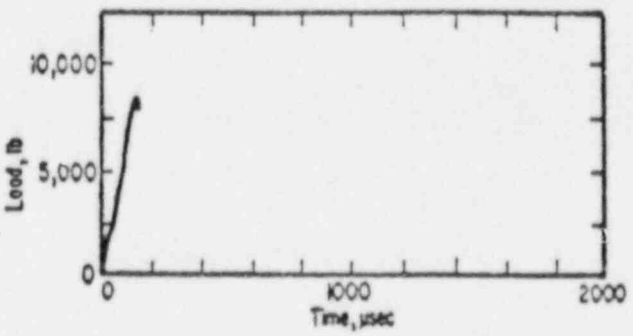

Specimen No.	A7
Test Temperature, F	5
Impact Energy, ft-lb	8
General Yield Load, P_{GY}, lb	
Maximum Load, P_{max}, lb	3310

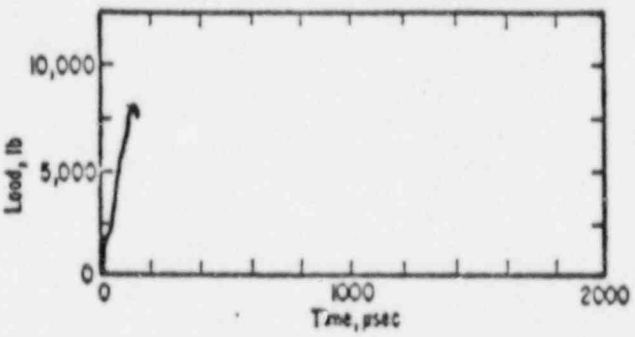

Specimen No.	A3
Test Temperature, F	26
Impact Energy, ft-lb	22
General Yield Load, P_{GY}, lb	3100
Maximum Load, P_{max}, lb	3540

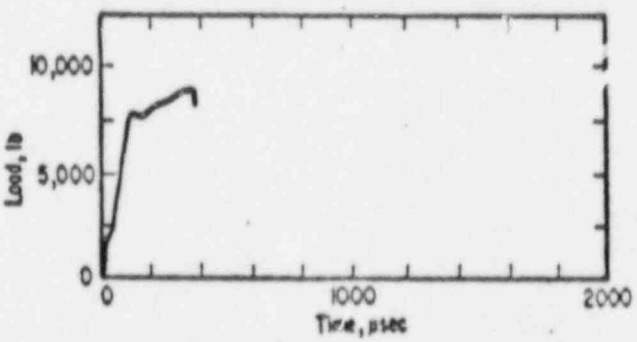

FOR BASE-METAL

TABLE C-1 (Continued)

	A10	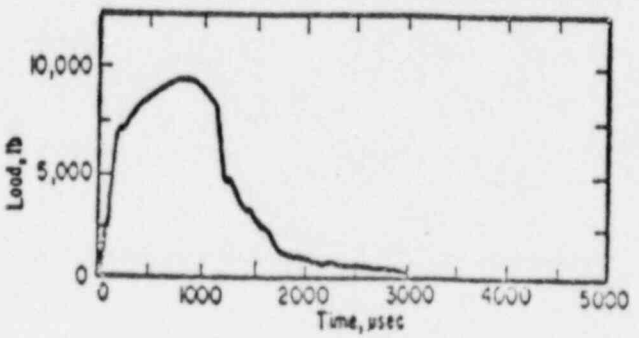	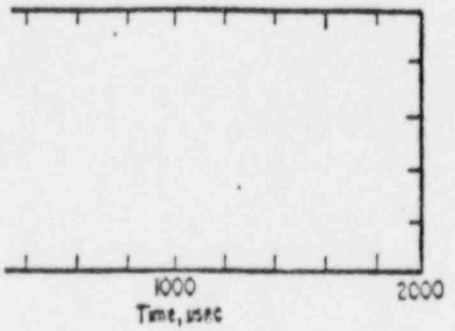
	119		
	71		
1b	2810		
	3810		
	A8	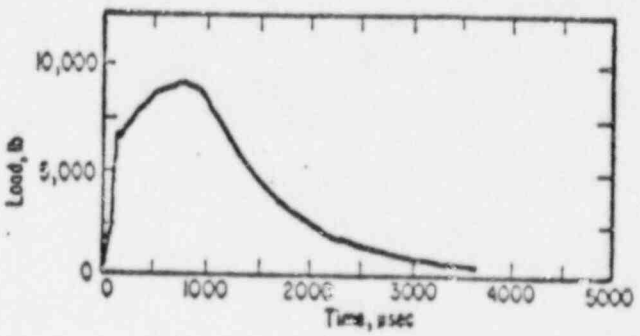	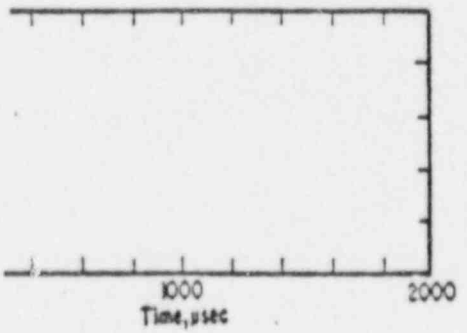
	162		
	87		
1b	2690		
	3690		
	A4	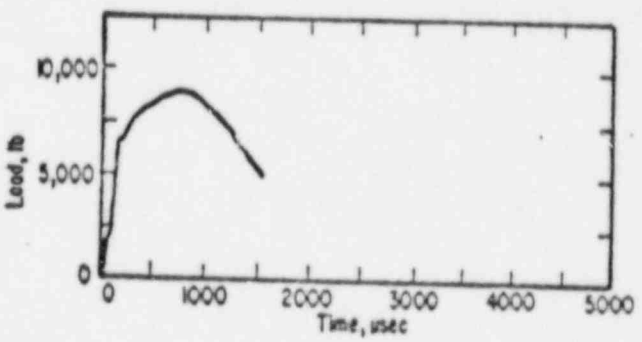	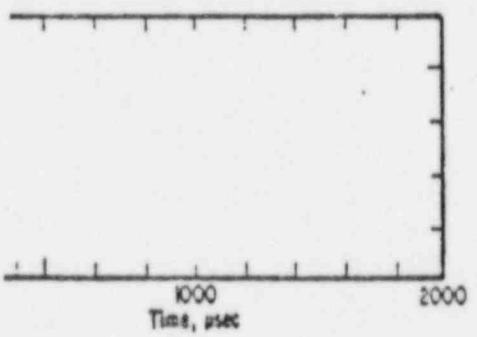
	208		
	88		
b	2600		
	3640		
	A1	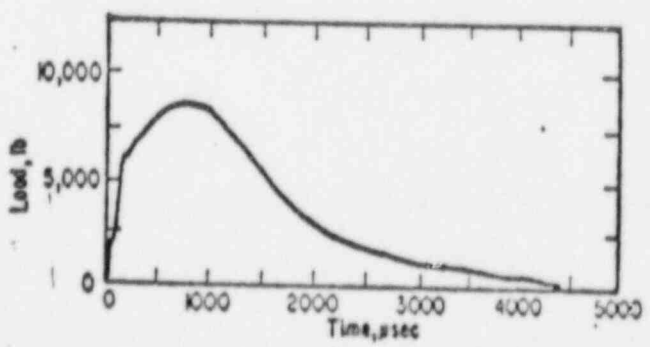	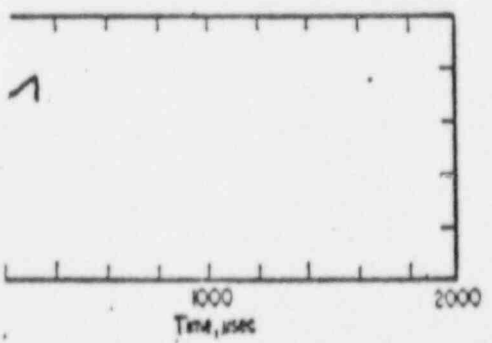
	290		
	90		
	2460		
	3480		

TABLE C-2 (Continued)

Specimen No.	C7
Test Temperature, F	5
Impact Energy, ft-lb	37
General Yield Load, P_{GY}, lb	3400
Maximum Load, P_{max}, lb	4260

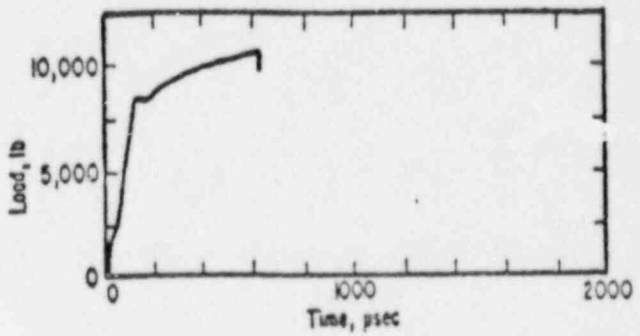

Specimen No.	C12
Test Temperature, F	26
Impact Energy, ft-lb	35
General Yield Load, P_{GY}, lb	3320
Maximum Load, P_{max}, lb	4200

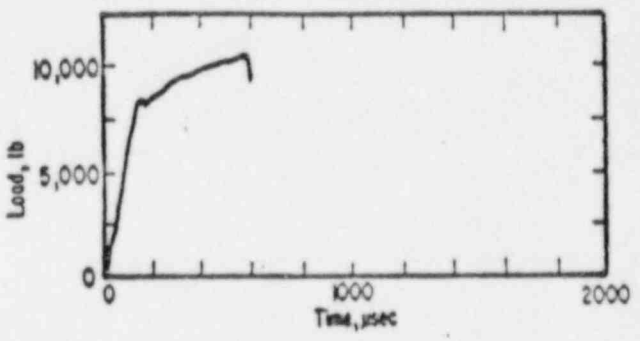

Specimen No.	C11
Test Temperature, F	33
Impact Energy, ft-lb	38
General Yield Load, P_{GY}, lb	3280
Maximum Load, P_{max}, lb	4180

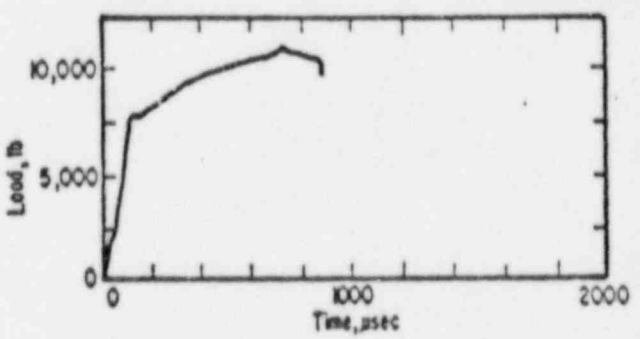

Specimen No.	C8
Test Temperature, F	52
Impact Energy, ft-lb	55
General Yield Load, P_{GY}, lb	3230
Maximum Load, P_{max}, lb	4270

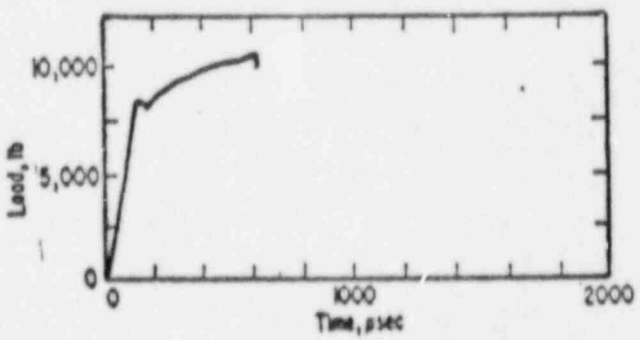

TABLE C-2 (Continued)

Specimen No.	C2
Test Temperature, F	79
Impact Energy, ft-lb	76
General Yield Load, P_{GY}, lb	3110
Maximum Load, P_{max}, lb	4200

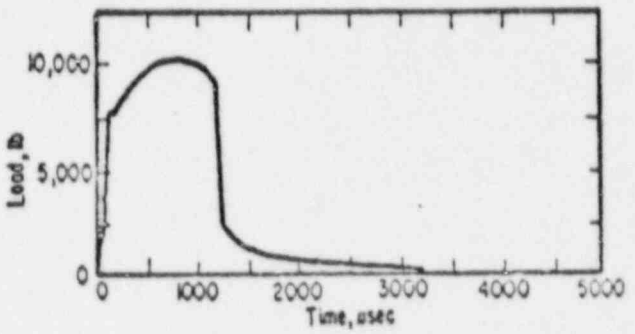

Specimen No.	C4
Test Temperature, F	120
Impact Energy, ft-lb	101
General Yield Load, P_{GY}, lb	3030
Maximum Load, P_{max}, lb	4140

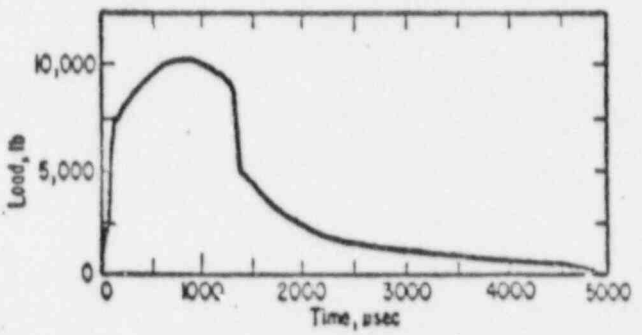

Specimen No.	C9
Test Temperature, F	208
Impact Energy, ft-lb	119
General Yield Load, P_{GY}, lb	2810
Maximum Load, P_{max}, lb	3940

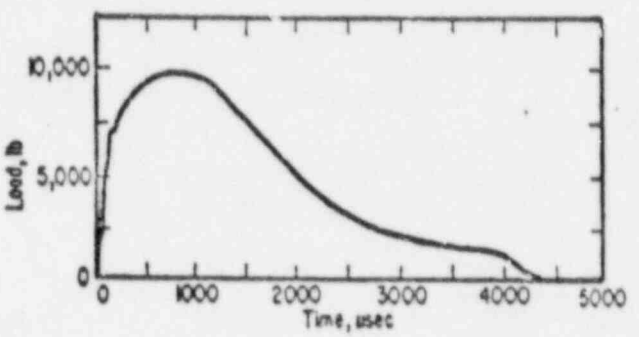

Specimen No.	C6
Test Temperature, F	300
Impact Energy, ft-lb	121
General Yield Load, P_{GY}, lb	2560
Maximum Load, P_{max}, lb	3790

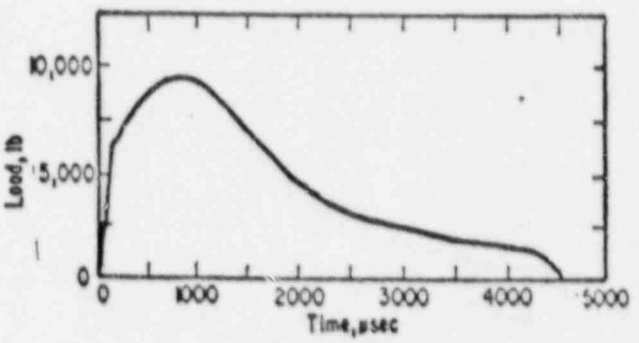

TABLE C-3. INSTRUMENTED CHARPY IMPACT DATA FOR HEAT-AFFECTED ZONE METAL

Specimen No.	WH4
Test Temperature, F	-87
Impact Energy, ft-lb	5.5
General Yield Load, P_{GY}, lb	
Maximum Load, P_{max}, lb	3740

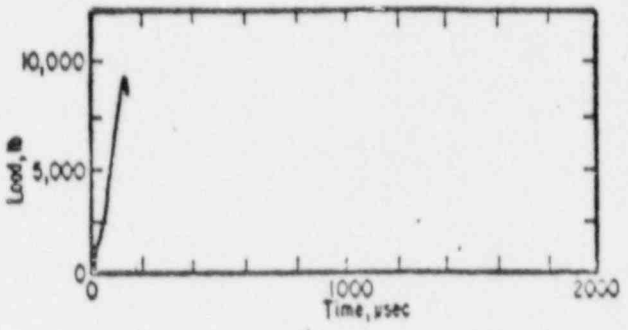

Specimen No.	WH5
Test Temperature, F	-26
Impact Energy, ft-lb	31
General Yield Load, P_{GY}, lb	3600
Maximum Load, P_{max}, lb	4320

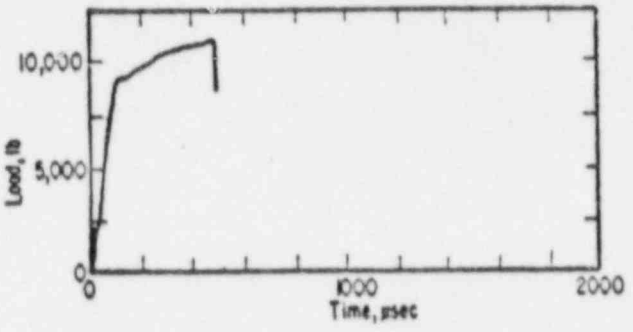

Specimen No.	WH7
Test Temperature, F	0
Impact Energy, ft-lb	33
General Yield Load, P_{GY}, lb	3550
Maximum Load, P_{max}, lb	4220

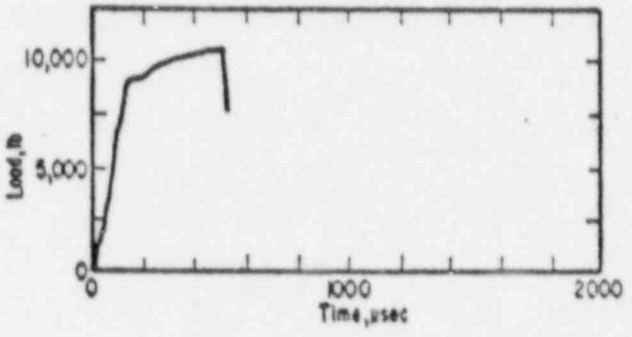

Specimen No.	WH8
Test Temperature, F	25
Impact Energy, ft-lb	20
General Yield Load, P_{GY}, lb	3520
Maximum Load, P_{max}, lb	3830

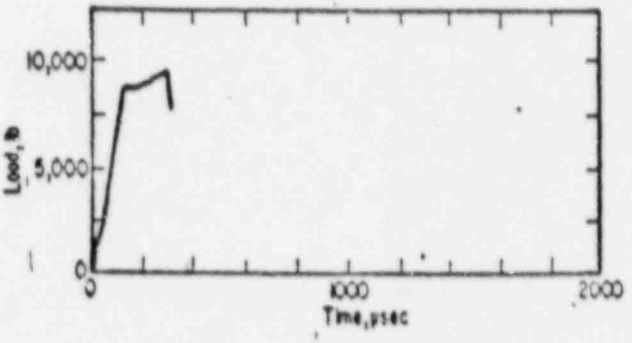

TABLE C-3 (Continued)

Specimen No.	WH3
Test Temperature, F	36
Impact Energy, ft-lb	99
General Yield Load, P_{GY}, lb	3340
Maximum Load, P_{max}, lb	4330

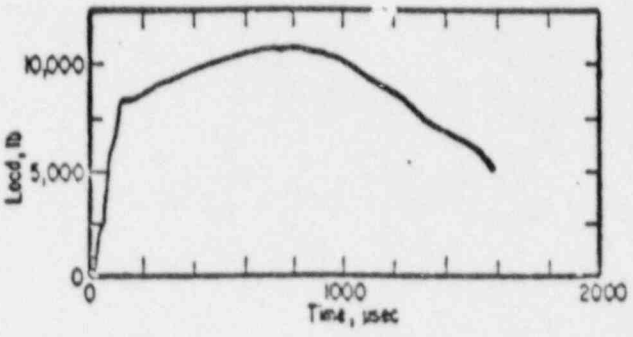

Specimen No.	WH6
Test Temperature, F	51
Impact Energy, ft-lb	83
General Yield Load, P_{GY}, lb	3420
Maximum Load, P_{max}, lb	4470

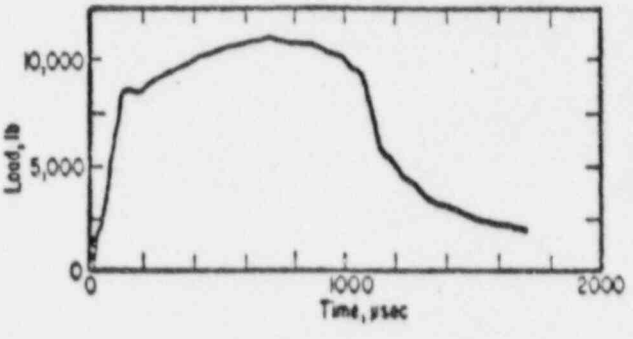

Specimen No.	WH1
Test Temperature, F	79
Impact Energy, ft-lb	110
General Yield Load, P_{GY}, lb	3280
Maximum Load, P_{max}, lb	4270

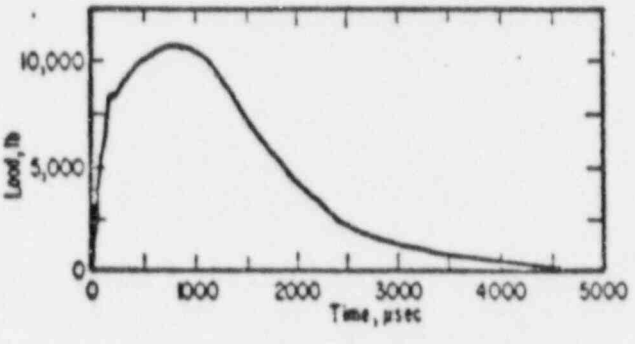

Specimen No.	WH2
Test Temperature, F	208
Impact Energy, ft-lb	105
General Yield Load, P_{GY}, lb	2840
Maximum Load, P_{max}, lb	3790

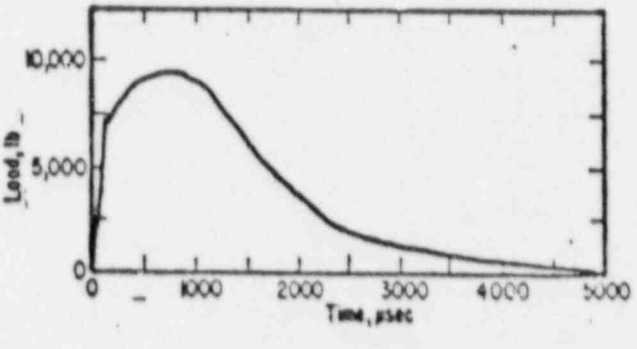

TABLE C-4. INSTRUMENTED CHARPY IMPACT DATA FOR WELD METAL

Specimen No.	WW8
Test Temperature, F	-87
Impact Energy, ft-lb	2.5
General Yield Load, P_{GY}, lb	
Maximum Load, P_{max}, lb	2180

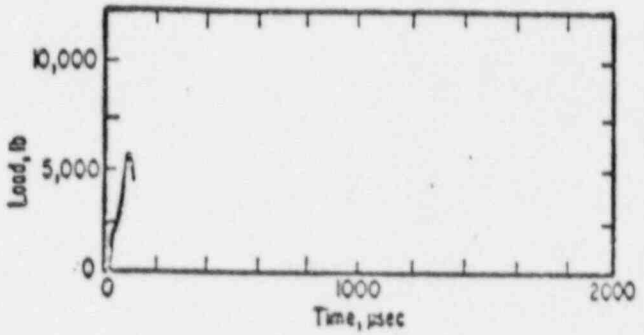

Specimen No.	WW7
Test Temperature, F	-31
Impact Energy, ft-lb	6.5
General Yield Load, P_{GY}, lb	
Maximum Load, P_{max}, lb	3540

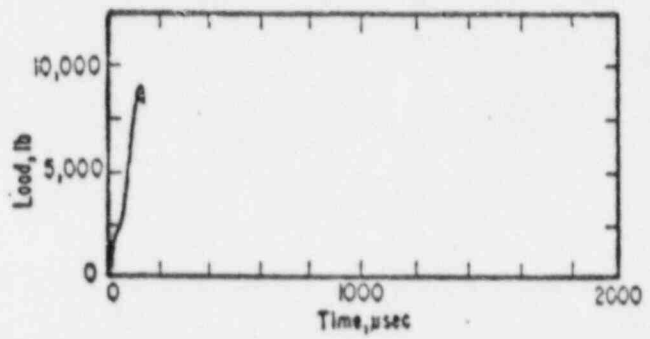

Specimen No.	WW2
Test Temperature, F	25
Impact Energy, ft-lb	13
General Yield Load, P_{GY}, lb	3460
Maximum Load, P_{max}, lb	3620

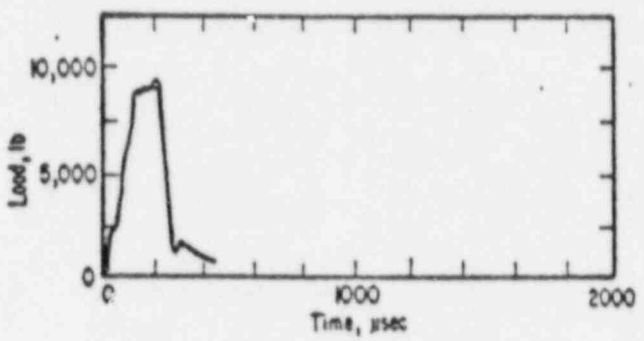

Specimen No.	WW4
Test Temperature, F	50
Impact Energy, ft-lb	27
General Yield Load, P_{GY}, lb	3390
Maximum Load, P_{max}, lb	3920

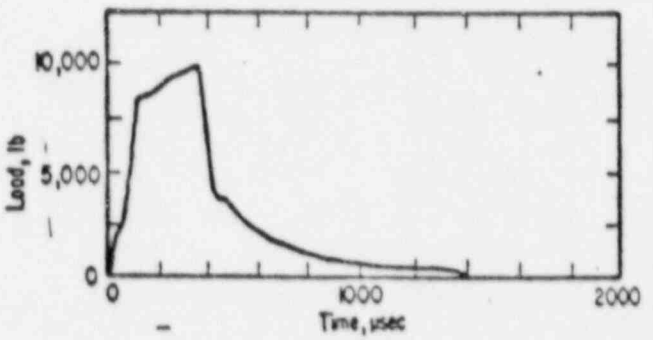

TABLE C-4 (Continued)

Specimen No.	WW6
Test Temperature, F	79
Impact Energy, ft-lb	34
General Yield Load, P_{GY}, lb	3320
Maximum Load, P_{max}, lb	3980

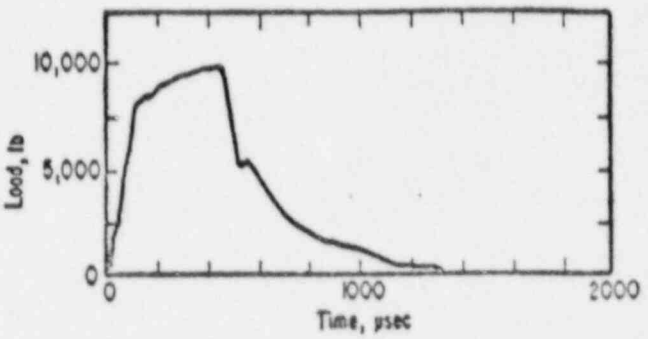

Specimen No.	WW5
Test Temperature, F	123
Impact Energy, ft-lb	46
General Yield Load, P_{GY}, lb	3200
Maximum Load, P_{max}, lb	3940

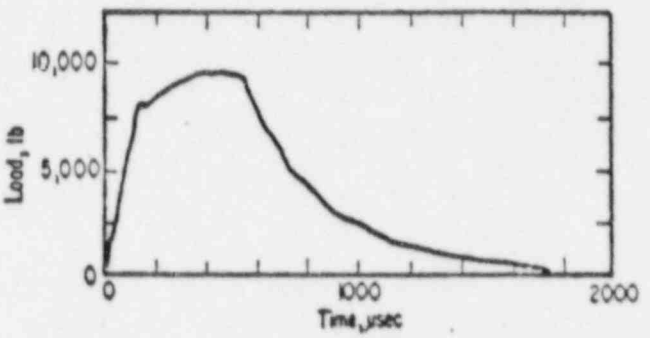

Specimen No.	WW1
Test Temperature, F	167
Impact Energy, ft-lb	54
General Yield Load, P_{GY}, lb	3100
Maximum Load, P_{max}, lb	3850

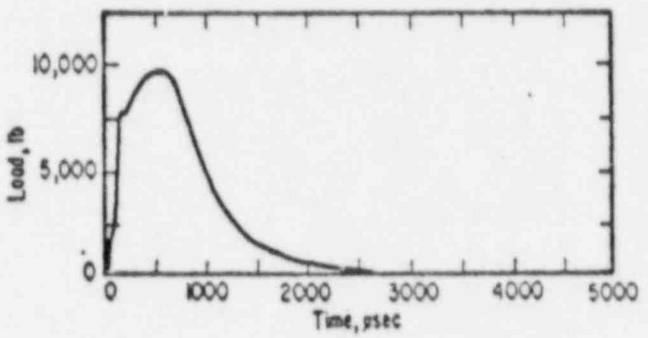

Specimen No.	WW3
Test Temperature, F	208
Impact Energy, ft-lb	52
General Yield Load, P_{GY}, lb	3050
Maximum Load, P_{max}, lb	3770

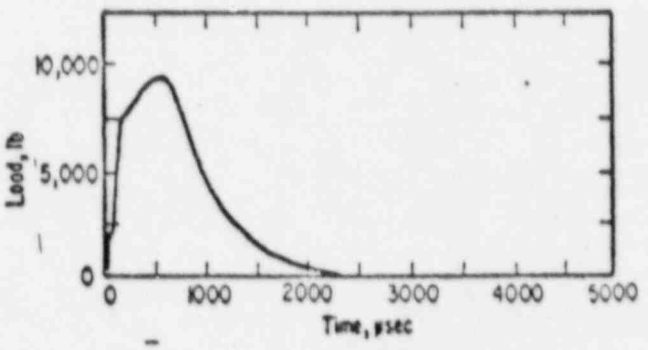

TABLE C-4 (Continued)

Specimen No.	WW6
Test Temperature, F	79
Impact Energy, ft-lb	34
General Yield Load, P_{GY}, lb	3320
Maximum Load, P_{max}, lb	3980

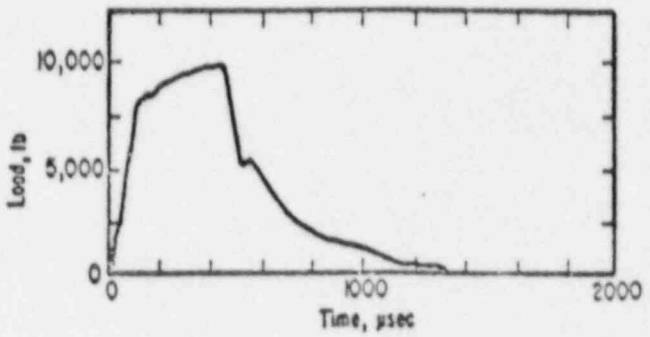

Specimen No.	WW5
Test Temperature, F	123
Impact Energy, ft-lb	46
General Yield Load, P_{GY}, lb	3200
Maximum Load, P_{max}, lb	3940

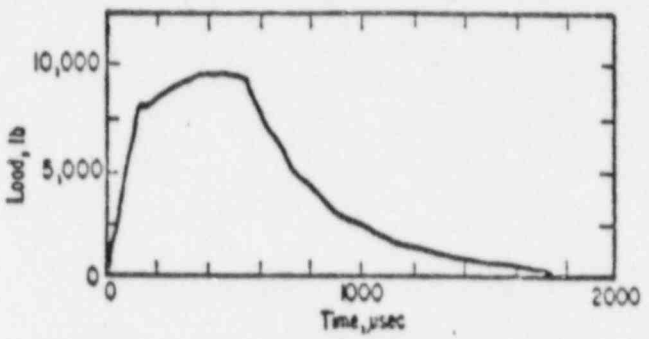

Specimen No.	WW1
Test Temperature, F	167
Impact Energy, ft-lb	54
General Yield Load, P_{GY}, lb	3100
Maximum Load, P_{max}, lb	3850

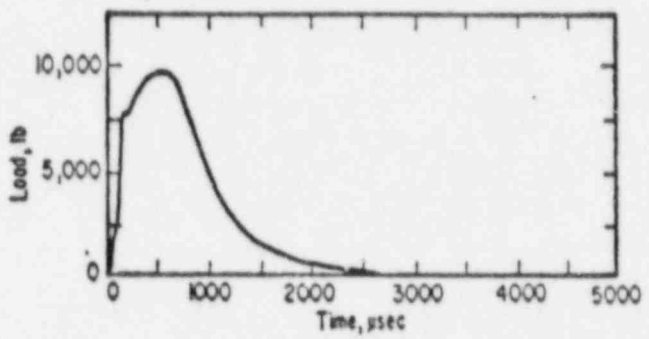

Specimen No.	WW3
Test Temperature, F	208
Impact Energy, ft-lb	52
General Yield Load, P_{GY}, lb	3050
Maximum Load, P_{max}, lb	3770

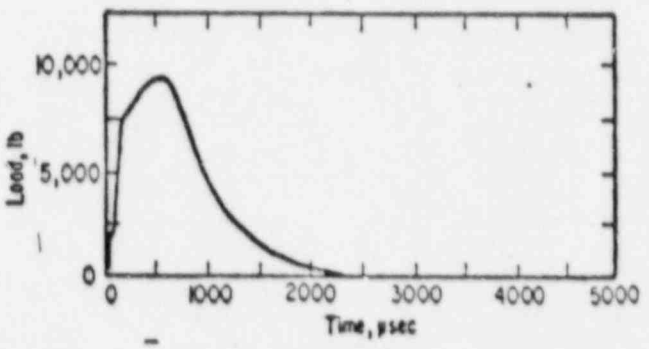

TABLE C-5. INSTRUMENTED CHARPY IMPACT DATA FOR CORRELATION MONITOR MATERIAL

Specimen No.	R6
Test Temperature, F	-25
Impact Energy, ft-lb	3.5
General Yield Load, P_{GY}, lb	
Maximum Load, P_{max}, lb	2650

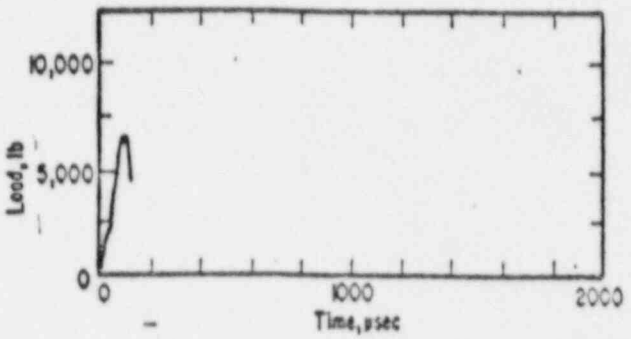

Specimen No.	R1
Test Temperature, F	50
Impact Energy, ft-lb	10
General Yield Load, P_{GY}, lb	3420
Maximum Load, P_{max}, lb	3480

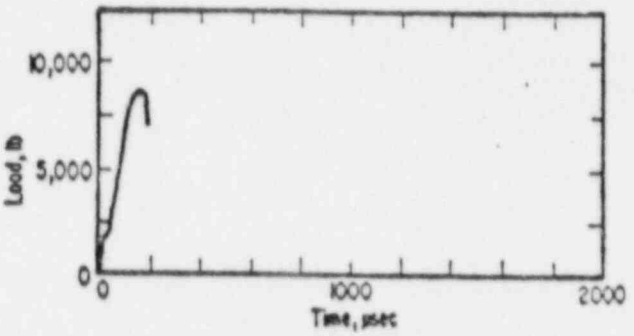

Specimen No.	R7
Test Temperature, F	78
Impact Energy, ft-lb	22
General Yield Load, P_{GY}, lb	3310
Maximum Load, P_{max}, lb	3920

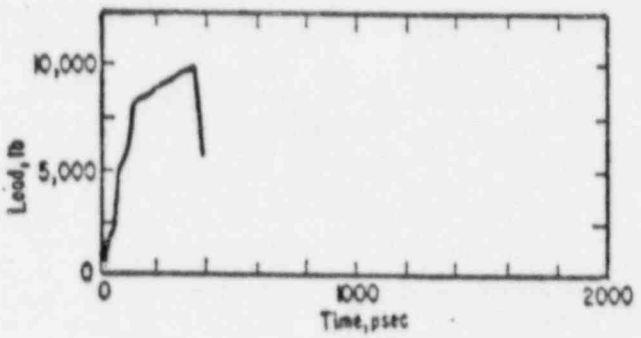

Specimen No.	R5
Test Temperature, F	122
Impact Energy, ft-lb	20
General Yield Load, P_{GY}, lb	3200
Maximum Load, P_{max}, lb	3630

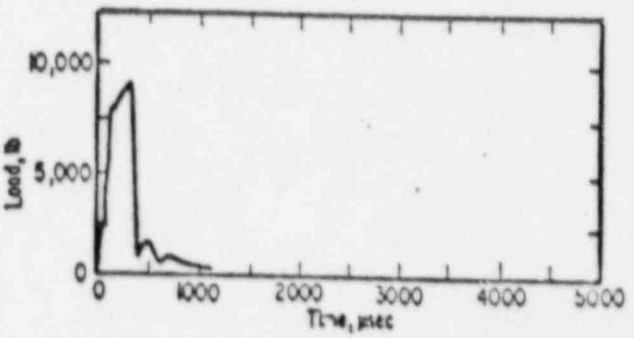

TABLE C-5 (Continued)

Specimen No.	R4
Test Temperature, F	127
Impact Energy, ft-lb	27
General Yield Load, P_{GY}, lb	3130
Maximum Load, P_{max}, lb	3790

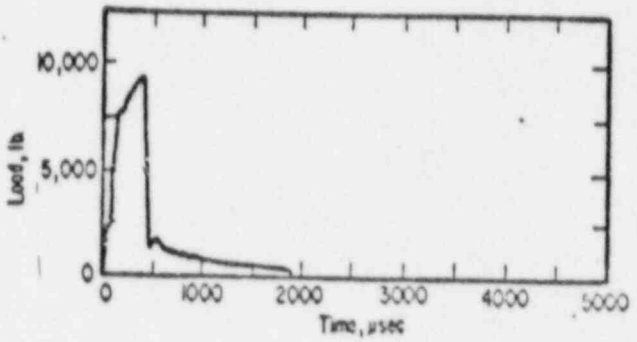

Specimen No.	R2
Test Temperature, F	161
Impact Energy, ft-lb	40
General Yield Load, P_{GY}, lb	3100
Maximum Load, P_{max}, lb	3920

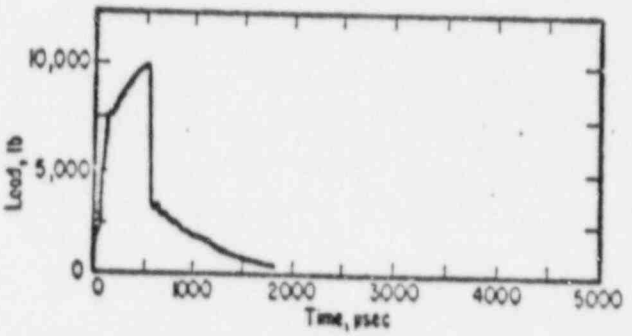

Specimen No.	R3
Test Temperature, F	188
Impact Energy, ft-lb	56
General Yield Load, P_{GY}, lb	3070
Maximum Load, P_{max}, lb	4010

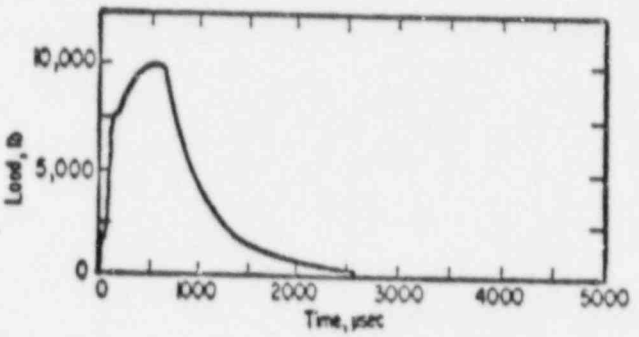

Specimen No.	R8
Test Temperature, F	236
Impact Energy, ft-lb	64
General Yield Load, P_{GY}, LB	2880
Maximum Load, P_{max}, lb	3890

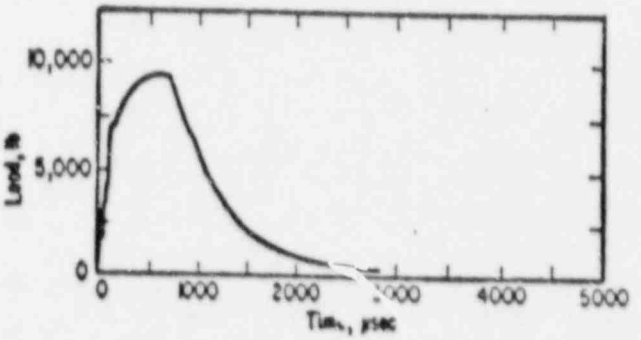

FRACTURE TYPE	LOAD-DISPLACEMENT CURVES	RAW DATA	REMARKS
I	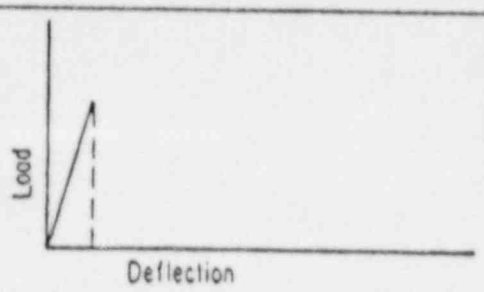	P_F	Brittle fracture
II	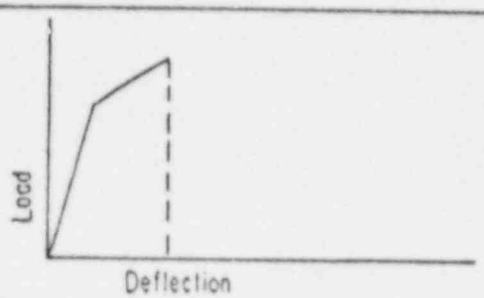	P_{GY}	Brittle fracture
III	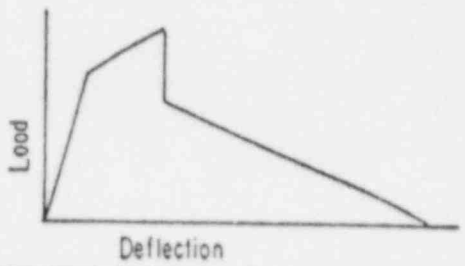	P_{GY}	Brittle fracture followed by fracture indicative of shear lip formation
IV	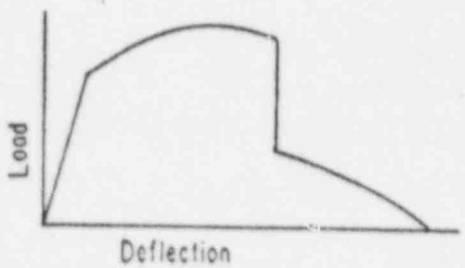	P_{GY} , P_{max}	Stable crack propagation followed by unstable brittle fracture and fracture indicative of shear lip formation
V	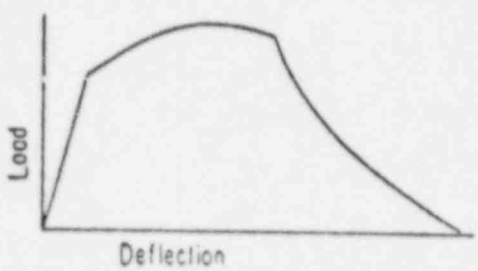	P_{GY} , P_{max}	Stable crack propagation followed by fracture indicative of shear lip formation
VI	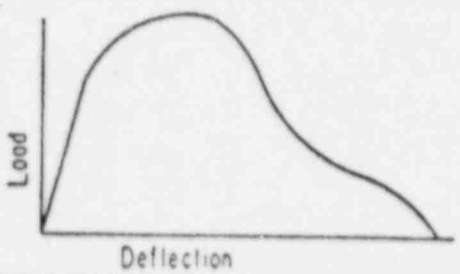	P_{GY} , P_{max}	Stable crack propagation followed by gross deformation

FIGURE C-4. THE SIX TYPES OF FRACTURE FOR NOTCHED BAR BENDING

The Charpy energy curves and the load-temperature information obtained from the instrumented Charpy tests are shown in Figures C-5 through C-9. These figures illustrate a unique feature of this type of analysis; that is, the determination of a definitive fracture transition temperature by discrimination between fractures occurring below and above general yield (P_{GY}). This transition is a clear indication of the mechanical properties of the material and does not depend on empirical correlations, as the nil-ductility transition temperature (NDTT) determined by the 30 ft-lb fix temperature does. It is interesting to note that impact fracture at the 30 ft-lb level corresponds to ductile specimen behavior, where considerable work hardening is required to raise the stress at the notch to a value sufficiently above the yield stress for fracture to result. This is dramatically shown for Specimen WH5 in the plot of load versus time in Table C-3. This specimen was tested at -26 F, which is right at the 30 ft-lb fix (the actual value for Specimen WH5 is 31 ft-lb). The plot shows appreciable work hardening after yielding rather than a completely brittle failure.

The determination of cleavage fracture stress, σ_f^*, required evaluation of P_{GY} at the temperature where P_F is 80 percent of P_{GY}. Because of the limited number of specimens and the requirements for determination of the NDTT and upper shelf energies, there were insufficient specimens to perform enough tests in the brittle range to well define values of σ_f^*. However, a cleavage fracture stress of approximately 270,000 psi was determined for base-metal plate C1423 and the weld material. The cleavage fracture stress was determined for the correlation monitor material as being approximately 260,000 psi.

CONCLUSIONS

The instrumented Charpy impact test technique was used to study the impact behavior of irradiated pressure-vessel materials and irradiated ASTM correlation-monitor material. Because of the limited number of Charpy specimens, it was not possible to do a complete analysis of the effects of irradiation on these five materials. However, it was shown that in all four materials the nil-ductility transition temperature as determined by the 30 ft-lb fix corresponds to specimen behavior where there is some ductile behavior rather than completely brittle behavior.

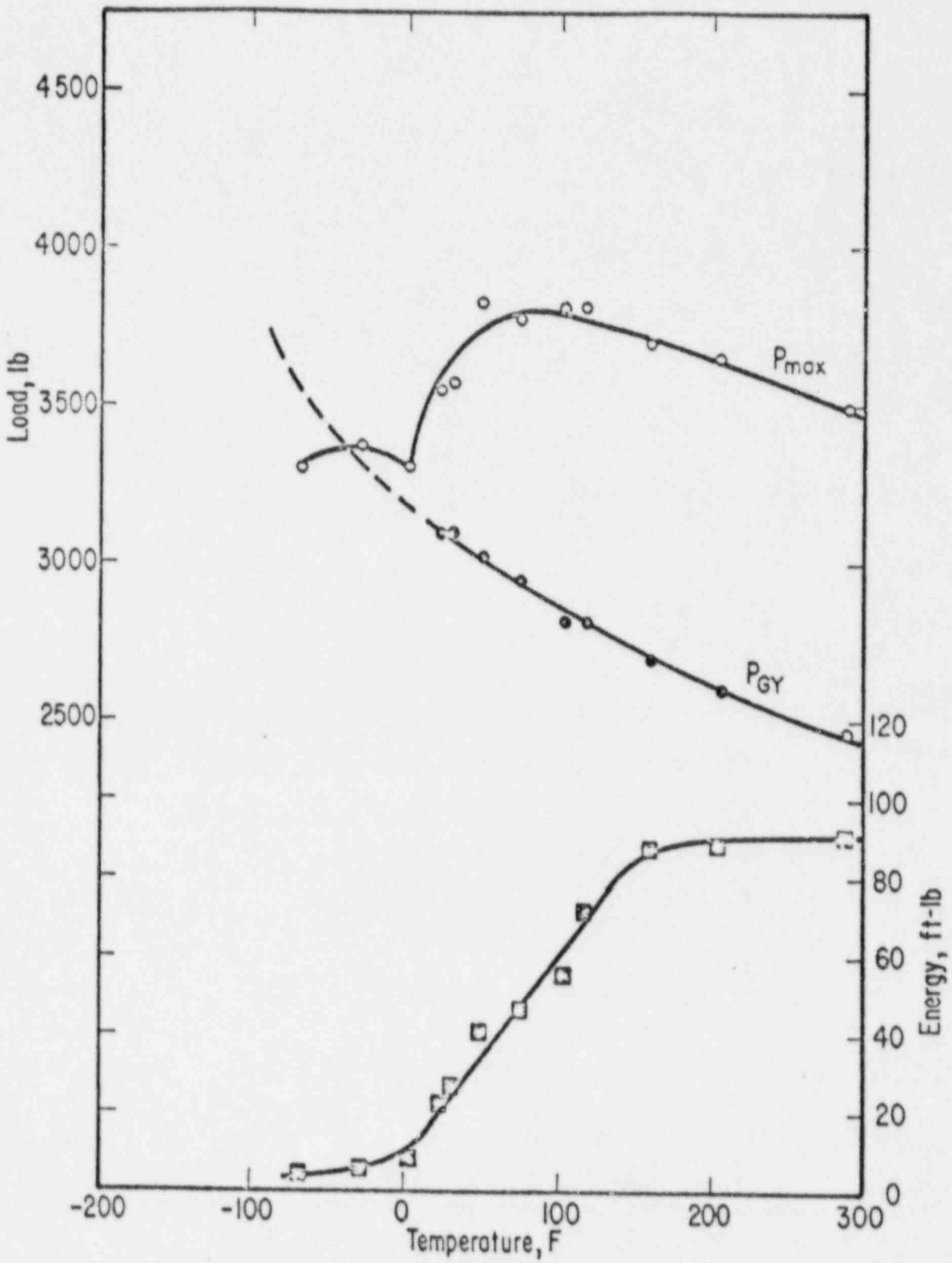

FIGURE C-5. INSTRUMENTED CHARPY LOAD-TEMPERATURE AND IMPACT ENERGY-TEMPERATURE CURVES FOR BASE-METAL PLATE A9811

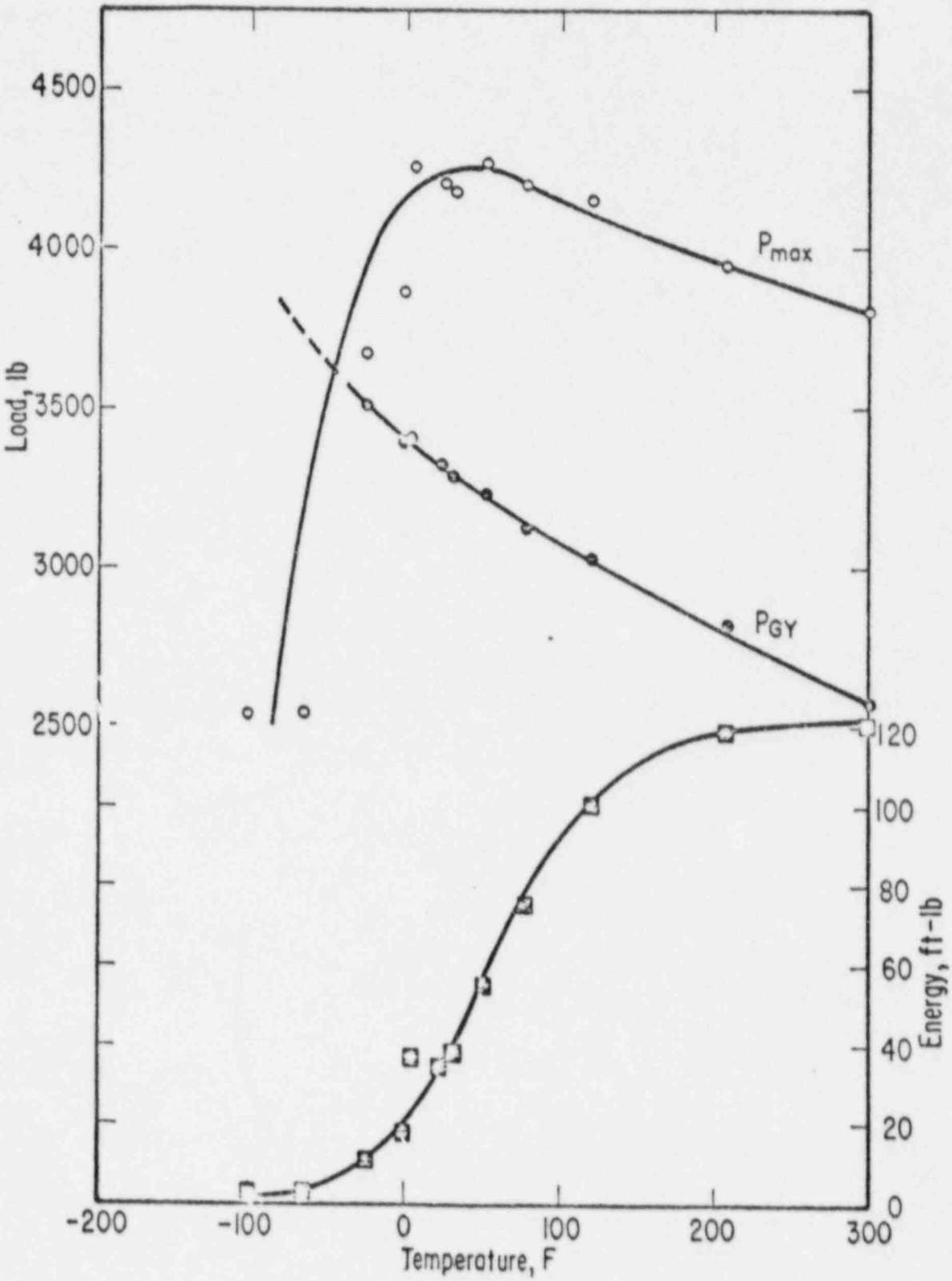

FIGURE C-6. INSTRUMENTED CHARPY LOAD-TEMPERATURE AND IMPACT ENERGY-TEMPERATURE CURVES FOR BASE-METAL PLATE C1423

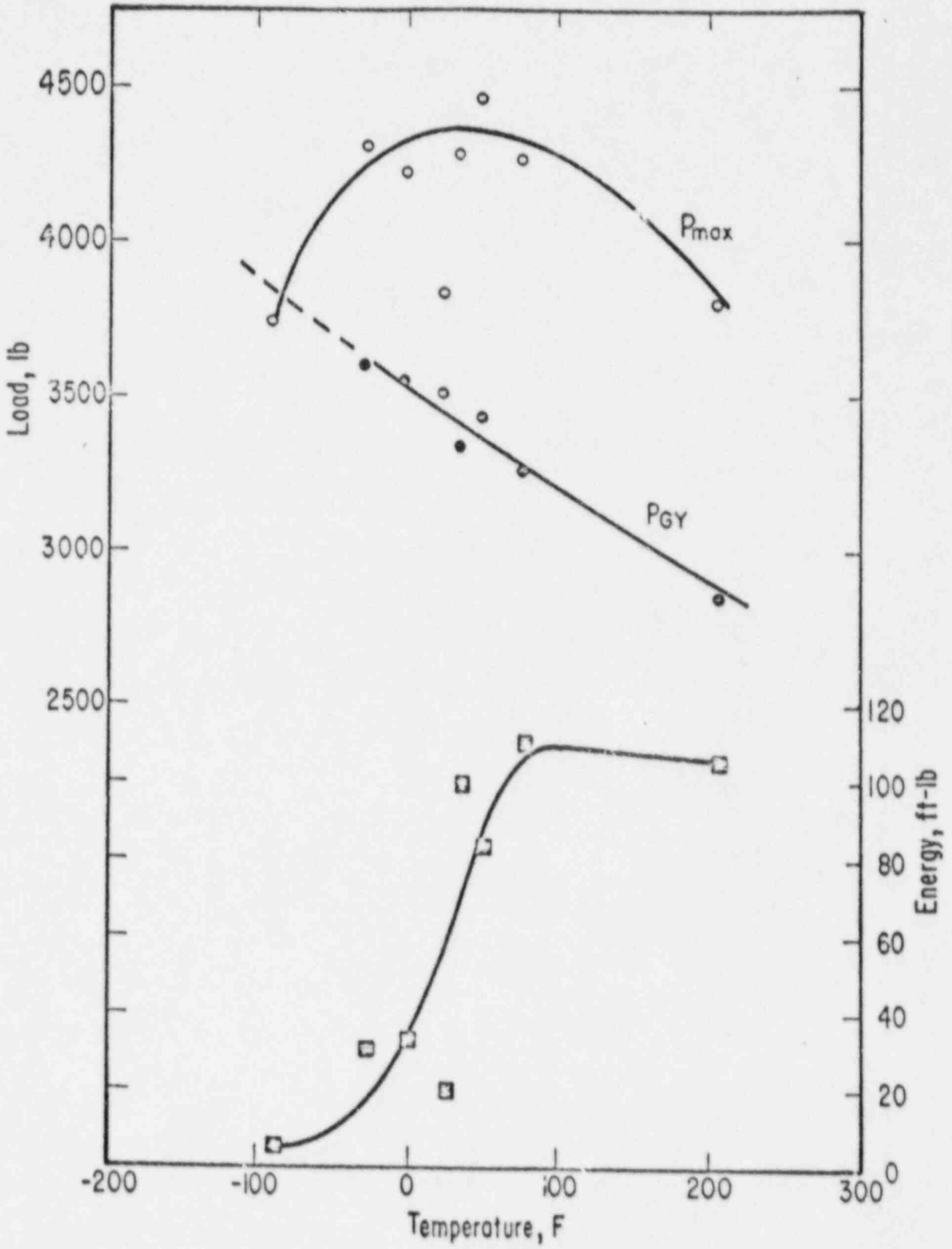

FIGURE C-7. INSTRUMENTED CHARPY LOAD-TEMPERATURE AND IMPACT ENERGY-TEMPERATURE CURVES FOR HEAT-AFFECTED ZONE METAL

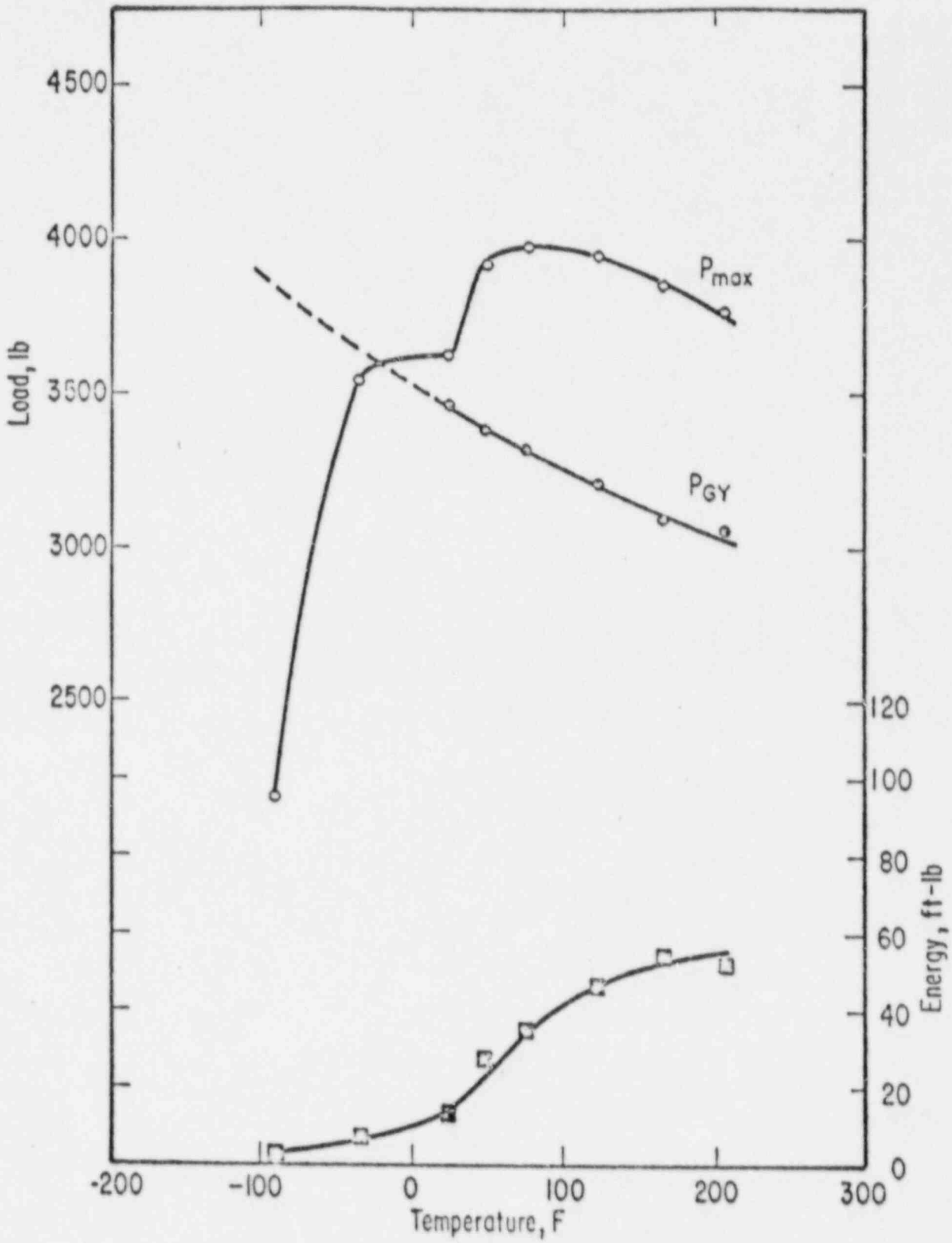

FIGURE C-8. INSTRUMENTED CHARPY LOAD-TEMPERATURE AND IMPACT ENERGY-TEMPERATURE CURVES FOR WELD METAL

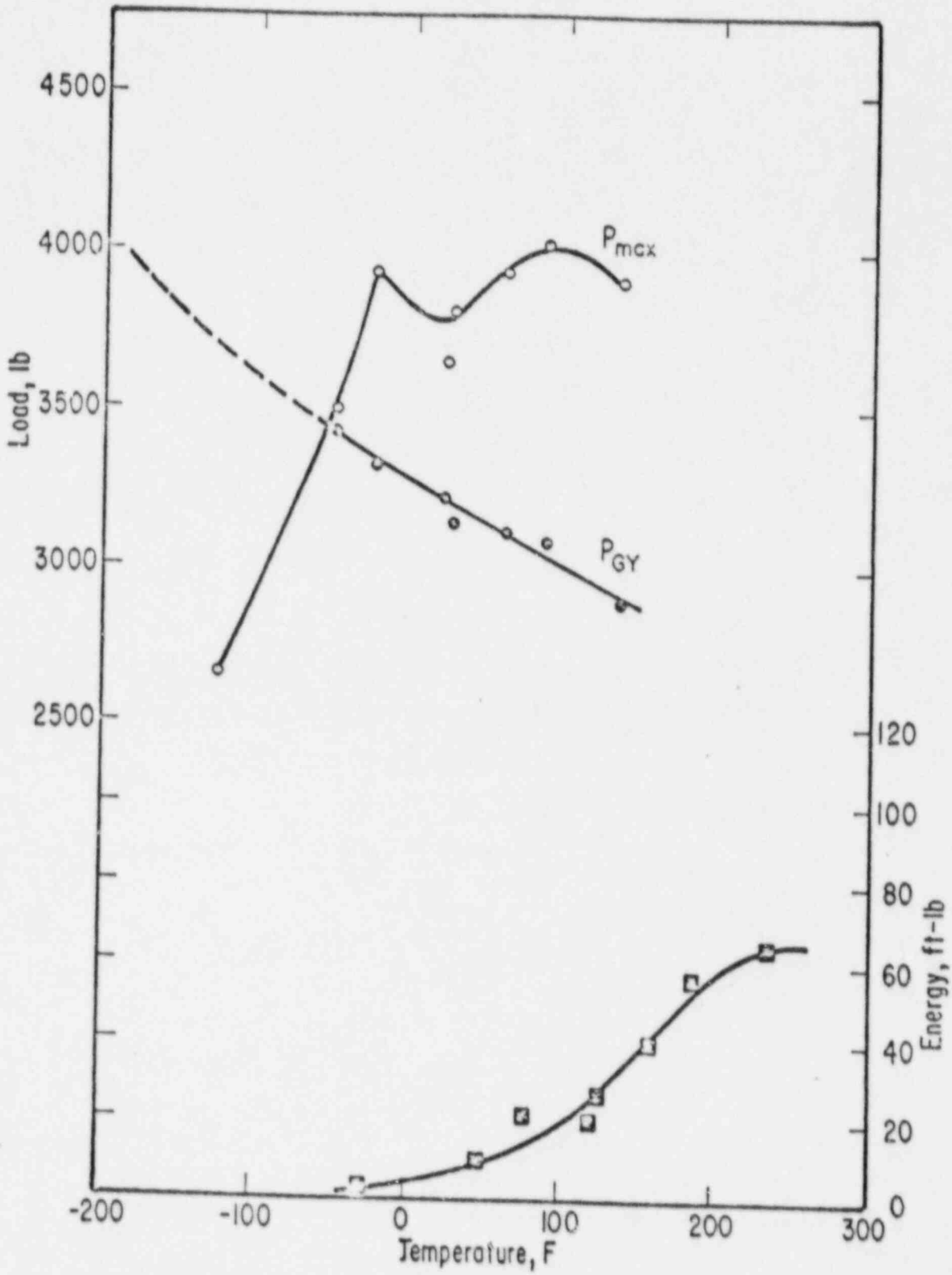

FIGURE C-9. INSTRUMENTED CHARPY LOAD-TEMPERATURE AND IMPACT ENERGY-TEMPERATURE CURVES FOR ASTM CORRELATION-MONITOR MATERIAL

Appendix C References

(1) Wullaert, R. A., Ireland, D.R., and Tetelman, A. S., "Radiation Effects on the Metallurgical Fracture Parameters and Fracture Toughness of Pressure Vessel Steels", paper presented at the ASTM Annual Meeting, Niagara Falls, New York, June 29, 1970.

(2) Wullaert, R. A., "Applications of the Instrumented Charpy Impact Test", in Impact Testing of Metals, American Society for Testing and Materials Special Technical Publication 466, p 148 (1970).

(3) Wilshaw, T. R., and Pratt, P. O., "The Effect of Temperature and Strain Rate on the Deformation and Fracture of Mild-Steel Charpy Specimens", in Proceedings of the First International Conference on Fracture, Sendai, Japan, September, 1965, 2, p 973.

(4) Tetelman, A. S., and McEvily, A. J. R., Fracture of Structural Materials, John Wiley and Sons, Inc., New York (1967).

(5) Knott, J. F., "Some Effects of Hydrostatic Tension on the Fracture Behavior of Mild Steel", Ph.D. dissertation, University of Cambridge, Cambridge, England (1962).

(6) Fearnehough, G. D., and Hoy, C. J., "Mechanism of Deformation and Fracture in the Charpy Test as Revealed by Dynamic Recording of Impact Loads", Iron Steel Inst., 202, 912 (1964).

(7) Green, A. P., and Hundy, B. B., J. Mech. Phys. Solids, 4, 128 (1956).

(8) Server, W. L., and Tetelman, A. S., "The Use of Precracked Charpy Specimens to Determine Dynamic Fracture Toughness", UCLA-ENG-7153 (July, 1971).